Technical Report

Adelaide Coastal Waters Study

Stage 2 *Research Program 2003 - 2005*

Technical Report No. 20 May 2007

Physical oceanographic studies of Adelaide coastal waters using high-resolution modelling, in-situ observations and satellite techniques

Sub Task 2 - Final Technical Report

Government of South Australia

WaterCare
It's in your hands

CSIRO

Physical oceanographic studies of Adelaide coastal waters using high-resolution modelling, in-situ observations and satellite techniques

Sub Task 2 – Final Technical Report

Authors

Charitha Pattiaratchi, John Newgard and Ben Hollings

School of Environmental Systems Engineering
The University of Western Australia
Crawley, Australia, 6009

Disclaimer

This report has been prepared by consultants for the Environment Protection Authority (EPA) and the views expressed do not necessarily reflect those of the EPA. The EPA cannot guarantee the accuracy of the report, and does not accept liability for any loss or damage incurred as a result of relying on its accuracy.

ISBN 1 92112518 7

May 2007

Reference

This report can be cited as:

Pattiaratchi, C. Newgard, J. and B. Hollings (2007) *"Physical oceanographic studies of Adelaide coastal waters using high resolution modelling, in-situ observations and satellite techniques – Sub Task 2 Final Technical Report".* ACWS Technical Report No. 20 prepared for the Adelaide Coastal Waters Study Steering Committee. School of Environmental Systems Engineering, The University of Western Australia.

Acknowledgement

This report is a product of the Adelaide Coastal Waters Study. In preparing this report, the authors acknowledge the financial and other support provided by the ACWS Steering Committee including the South Australian Environment Protection Authority, SA Water Corporation, the Torrens Patawalonga and Onkaparinga Catchment Water Management Boards, Department for Transport Energy and Infrastructure, Mobil Refining Australia Pty Ltd, TRUenergy, Coast Protection Board and PIRSA. Non-funding ACWS Steering Committee members include the Conservation Council of SA, SA Fishing Industry Council Inc, Local Government Association, Department of Water Land and Biodiversity Conservation and Planning SA.

Acknowledgements

The authors would like to acknowledge the following people who helped with the provision of various data sets used for the model forcing: Steve Marvanek (bathymetry and habitat maps), Jeremy Wilkinson (point source discharges to the Adelaide coastal waters), Peter Christie (discharges to the Port River/Barker Inlet system), and Jochen Kaempf (current data). Chris Dallimore and Emma Gale helped with the set-up and running of ELCOM. Ruth Gongora-Mesas did an excellent job proofreading and formatting the text.

Executive Summary

This report details the numerical modelling of circulation and transport of suspended sediments and nutrients using several modules undertaken as part of Project PPM2 of the Adelaide Coastal Waters Study (ACWS). Details of each module are described together with the model validation and results of the model application to the ACWS region.

The circulation model ELCOM (Estuary and Lake COmputer Model) was used to predict circulation and mixing within the ACWS region. ELCOM is a finite-difference model that allows the specification of rectangular grids. The model was forced using tides, meteorology (winds and air–sea fluxes), and point source discharges (rivers, industrial and wastewater outfalls, and stormwater drains). The numerical wave model SWAN (Simulating WAves Nearshore) was used to simulate the propagation of swell and wind-generated waves in the study region. It was forced using offshore swell waves, local winds, and water levels. ELCOM and SWAN were validated through comparison of field data obtained from the study region. Different model scenarios were undertaken to determine the transport of freshwater, suspended sediment concentration, and nutrients under past, present, and future discharge scenarios, including their seasonal variability.

The results indicated that, within the study region, tidal currents dominated the circulation pattern and the wind was a secondary effect, which influenced the mean circulation pattern, particularly at the surface. The current patterns were oriented parallel to the coastline. The seasonally varying wind climate results in a reversal in the mean circulation pattern. In summer, the net movement of water is northwards, whereas during winter the direction is reversed towards the south; however, as the southerly and south-westerly winds are stronger and more prevalent, the annual movement of water is northward. In the nearshore zone, because of the dominance of wave-induced currents, the net flow is towards the north. Because of the predominantly alongshore movement of water, land-based discharges are mainly transported in a north-south direction, parallel to the coastline, with minimal offshore extent. The nearshore waters, inshore of the 5 m depth contour, had higher residence times than those farther offshore and varied between 1 and 10 days depending on weather conditions. During the summer, the mean residence times were lower (1 to 1.5 days), whereas during winter the mean residence times were slightly higher (up to 2.5 days).

The Port River/Barker Inlet system has a major influence on nutrient and suspended sediment concentrations within the study region. This is through a combination of industrial (Penrice), wastewater, and stormwater discharges. In summer, the discharges were transported northwards from the Port River entrance, whereas during winter there was southerly transport with discernable impact along the Adelaide coastal strip. Discharges from the Bolivar outfall did not appear to have a direct influence on the Adelaide coastal strip. The relative importance of stormwater and wastewater (industrial and municipal) discharges depended on the nutrient (nitrogen or phosphorous) and also on season. During the summer, discharges from wastewater outfalls (which included Penrice) had more influence on the magnitude and extent of the SSC concentrations, whereas in winter the stormwater discharges had a larger influence. For nitrogen concentrations, stormwater discharges resulted in higher concentrations during the summer, whereas wastewater discharges were dominant in winter. For phosphorous concentrations, stormwater discharges had concentrations along the metropolitan coastal strip during both summer and winter, whereas the wastewater discharge from Bolivar was dominant along the northern section.

CONTENTS

1. Introduction

The Adelaide Coastal Waters Study (ACWS) is aimed at examining the coastal strip between Port Gawler and Sellicks Beach. It is recognised that this narrow coastal strip (defined as the region from the high water mark to a depth of ~5m) is under considerable stress due to human activity. Particular concerns include the addition of nutrients through freshwater inputs from (1) river systems where the catchments have been cleared and are currently used for farming; (2) wastewater discharges; and, (3) stormwater (both urban and rural) discharges. The main aim of the Adelaide Coastal Waters Study is to determine the transport and fate of these nutrients and other pollutants through their impact on coastal ecosystems.

Within the ACWS, there are several study tasks. Study task PPM 2: *Physical oceanographic studies of Adelaide coastal waters using high-resolution modelling, in-situ observations and satellite techniques* has four main objectives as follows:

- To understand the water circulation, flushing, and exchange characteristics along Adelaide's costal strip, its seasonal variability, and its impact on the dispersion of nutrients, suspended matter, and other pollutants
- To understand sediment movement from its sources, its fate, transport and re-suspension processes along the coastal strip, and its impact on seagrass distributions
- To understand seasonal variability of suspended matter in relation to key benthic features as a function of land-based discharge, oceanographic, and meteorological factors

To achieve the above objectives, four subtasks were defined and this report is concerned with the following subtask:

Subtask 2: Application of a numerical model to Adelaide's metropolitan coastal strip to predict dispersion patterns of freshwater, nutrient, and suspended particulate matter. The numerical model will use realistic initial and forcing conditions, provided by subtask 1, to simulate seasonal variations of hydrodynamics and dispersion patterns, including flushing and exchange characteristics in the study region. This will include analysis of effects arising from historical, present, and future discharge scenarios of freshwater, nutrient, and sediment inputs.

This report presents the results of the numerical modelling of hydrodynamic processes undertaken as part of the Adelaide Coastal Waters Study addressing the above two tasks. Figure 1.1 defines the location of the ACWS and the modelling boundaries.

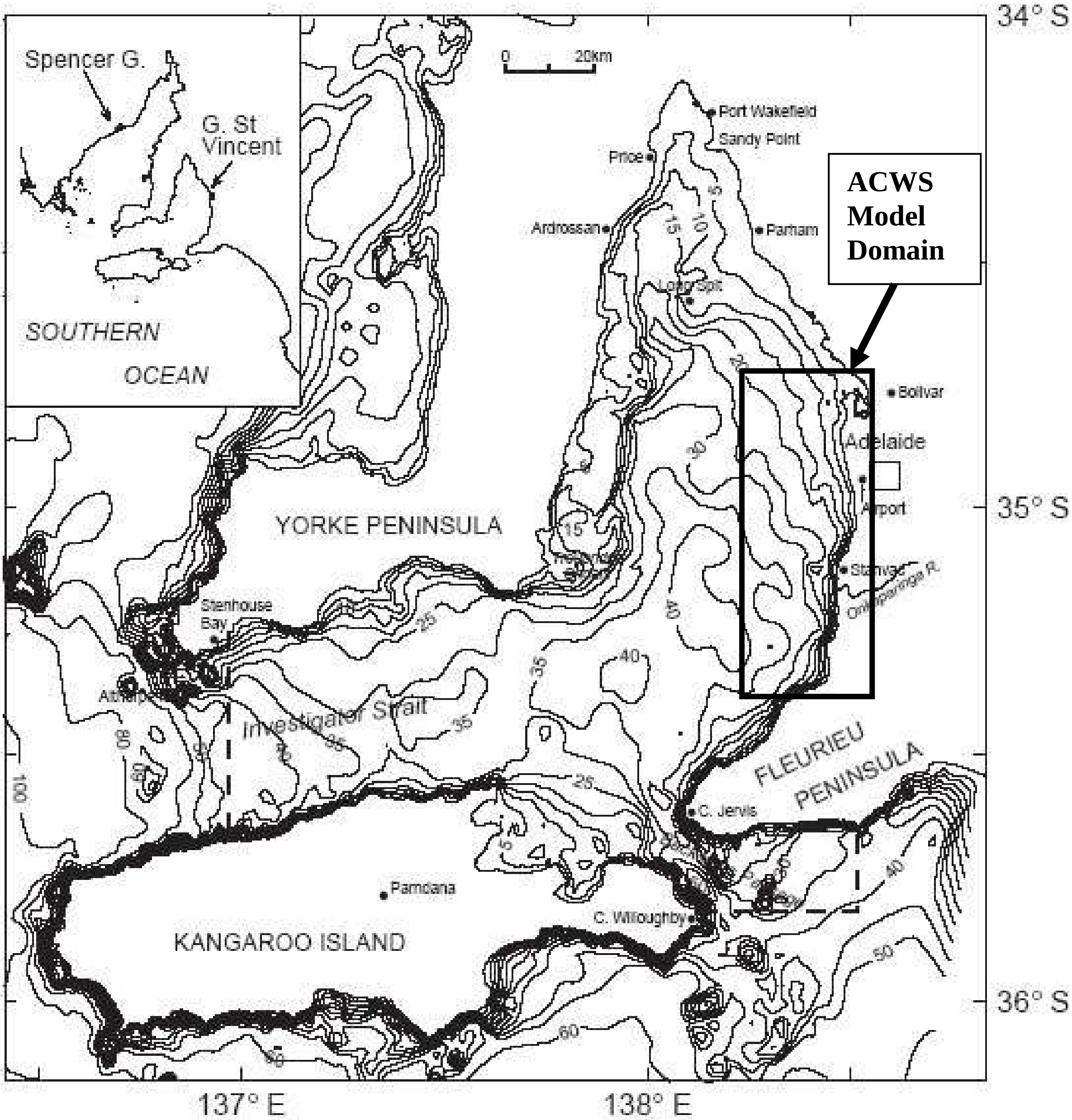

Figure 1.1: Location of the study area and the model for the Adelaide Coastal Waters Study

1.1. Model flowchart

The modelling 'system' adopted for simulating the Adelaide coastal waters can be schematically described in a flowchart (Figure 1.2). Each model had some independent inputs, and the outputs were input into other models to reach the final model output.

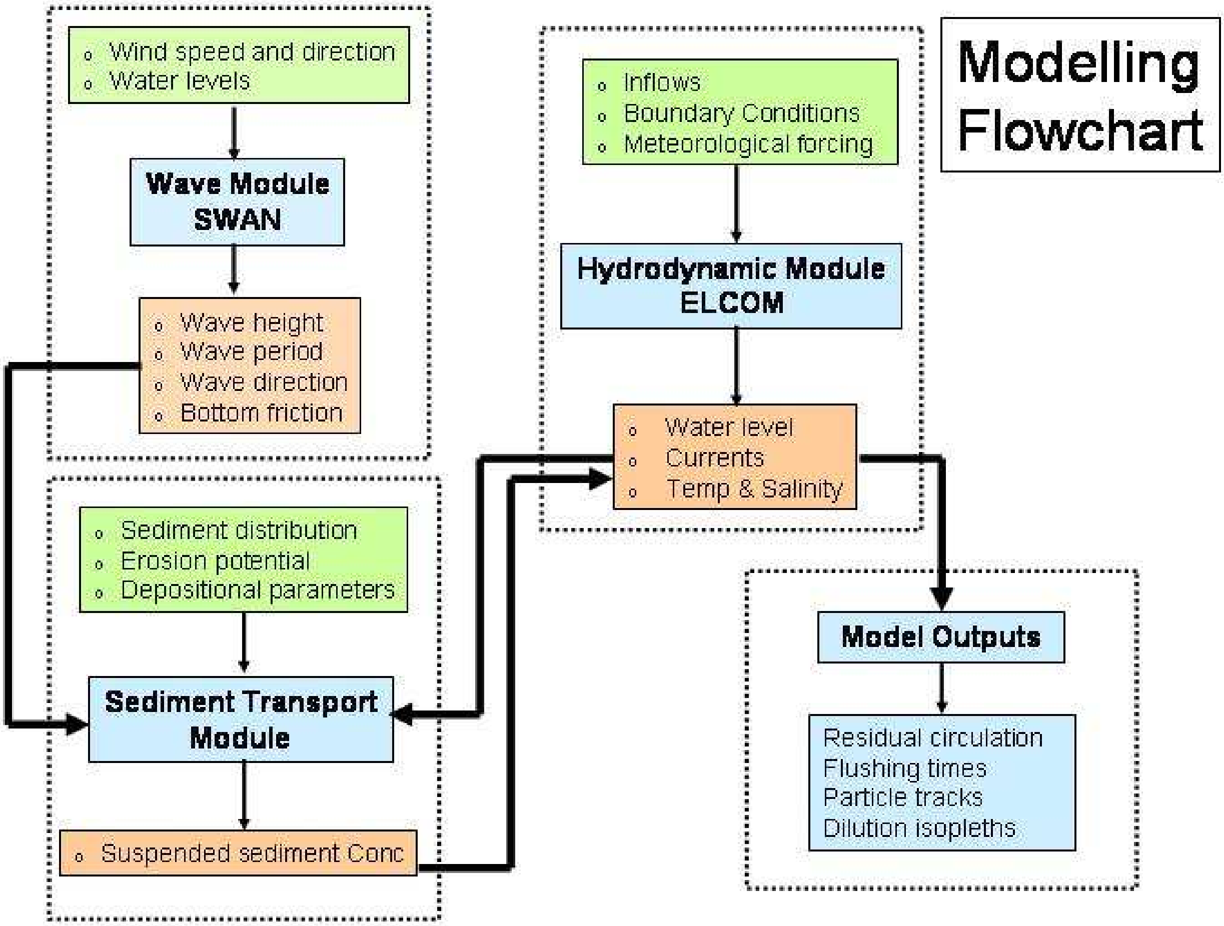

Figure 1.2: Modelling structure for the Adelaide Coastal Waters Study

Each module and its interrelationships is summarised below; Section 4 presents each module in detail.

Wave module
The numerical wave model SWAN (Simulating WAves Nearshore) was implemented as the wave input model. SWAN is a third-generation wave model that computes random, short-crested, wind-generated waves in coastal regions. The model inputs were bathymetry, wind speed and direction, and water levels. Wind speed and direction were obtained from the Bureau of Meteorology station at Adelaide Airport, and water levels were prescribed from tidal variations. The model outputs were significant wave height, wave period, wave direction, and bottom friction. These parameters were used as input values to the sediment transport module, circulation model for generation of longshore currents and to estimate bottom shear stress within the model domain.

Sediment re-suspension module
Along the Adelaide coastal waters, sediment transport occurs due to the combined action of waves and tidal currents. The relative importance of the waves and tidal currents in the transport of sediment is generally related to the water depth. For example, inside the surf zone, the influence of tidal currents is diminished and the sediment transport is dominated by the action of waves, and in particular, the wave- induced currents in the longshore and cross-shore directions. In the longshore direction, it is generally accepted that the longshore transport of sediment is related to some proportion of the longshore component of wave

power incident on the beach and such methods are mainly used to examine beach stability. In the Adelaide coastal water region the predominant wave direction is from the south-west which results in a northward transport of sediment along the beach. Also, the effects of swell waves diminish northward as the waves are attenuated due to the shallower water. Outside the surf zone, as the depth increases, the influence of waves of is generally diminished. Here, the combination of waves and currents (through a non-linear process) results in shear stress being exerted on the sea bed leading to sediment transport when a critical shear stress is exceeded. The rate at which sediment is transported is proportional to the excess shear stress (defined as the difference between the applied shear stress and the critical value), sediment grain size and density.

In general, coastal regions consist of non-cohesive inorganic sediments where the gravitational forces dominate and sand grains exist as individual particles. In contrast, estuarine regions consist of the mainly cohesive sediments where the electrostatic forces act ('flocculation') to bind individual grains to form larger composite particles defined as 'flocs'. The non-cohesive sediments consists of grain sizes generally > 10µm and are mainly quartz or biogenic material. Cohesive sediments are generally clay (e.g. kaolinite) with grain sizes <2µm. Data on grain sizes collected by Bone et al. (2007) indicated that the sediment consisted mainly of quartz and carbonate species with only a small fraction of clay minerals which contribute to cohesive sediment. Also, Bone et al. (2007) found that the quartz fraction of sediments was higher in the inshore region and the carbonate fraction being dominant in the offshore regions. The majority of the sea bed sediments have a high percentage of medium sand fraction (250-2000µm) and fine sand fraction (250-0.063µm) and only a small percentage of fine material <63µm (Bone et al., 2007). The fraction of the fine material (<0.063mm) in the sea bed samples were generally < 5%, particularly during the summer with maxima not exceeding 25% of any sample.

The sediment transport module uses the van Rijn (1984) method to predict re-suspension of non-cohesive sediments from the sea bed, in particular, the vertical profile of suspended sediment concentration due to the combined action of waves (from the wave module) and currents (from the hydrodynamic module) and provides a source term for the sediment input from the sea bed and the advection of the sediment is handled by the hydrodynamic model. Sediment input from rivers and storm drains were also were defined as sources and were advected throughout the model domain using equation 3.6. Flocculation effects from these discharges were not considered as no data were available to determine the clay fraction of the sediments or the inorganic and dissolved components of the sediments.

The main aim of this task (Subtask 2 – see above) is the 'Application of a numerical model to Adelaide's metropolitan coastal strip to predict dispersion patterns of freshwater, nutrient, and suspended particulate matter'. Therefore, the sediment transport module specifically excludes bedload transport of sediment as well as sediment transport within the surf zone. This also excludes the effects of feedback processes between changes in water depth (resulting from sediment transport) and the hydrodynamic processes.

The sediment re-suspension module used the Grant and Madsen (1979) wave–current interaction theory to define the bottom stress due to the combined action of waves and currents and the van Rijn (1984) formulation to predict the vertical profile of suspended sediment concentration as a source for sediment re-suspension from the sea bed. The module required the sediment grain size distribution maps as independent inputs. The model obtained the currents from the hydrodynamic module and outputted the suspended sediment concentration as a source function back to the hydrodynamic model, which through the advection-diffusion m determined the sediment transport throughout the model domain.

Hydrodynamic module

For this study, ELCOM (Estuary and Lake COmputer Model), developed at the Centre for Water Research, The University of Western Australia, was used to predict circulation and mixing within the ACWS region. ELCOM is a finite-difference model, which allows the specification of rectangular grids. The model requires, in addition to bathymetry, the point source discharges (rivers, wastewater, and storm outlets), boundary conditions (tides), and meteorological forcing (wind speed and direction, and heat fluxes). The model outputs included currents, water levels, and the distribution of temperature, salinity, and suspended sediment concentration across the model domain.

Model outputs

For each model scenario, different outputs were required and included residual circulation, flushing times, particle tracks, and dilution isopleths, in particular salinity, suspended sediment concentrations and nutrient (nitrogen and phosphorous) concentrations.

2. Wave model description and formulation

2.1 Introduction

Local near bed hydrodynamic conditions are critically important in the growth, maintenance, and recovery of macrophyte communities, which are in turn the result of water motion caused by waves and currents. This re-establishment of seagrass communities is important, as the reestablishment of macrophytes will cause the services they provide to the local ecosystem to resume; the major services are improvement of the water quality and the stabilisation of sediments (reducing sediment resuspension, erosion, and turbidity).

Knowledge, through measurement or prediction, of the characteristic properties of the wave field (i.e. wave height, wave period, and wave direction) and the wave field's spatial distribution over a region at different times allows the calculation of the near bed conditions in terms of wave-induced flow and bed shear stress.

The ocean wave field is a complex combination of many wave components, all possessing different periods and directions. The instantaneous wave motion experienced at any point can be considered the sum of all these component waves.

To characterise a wave field, three primary wave parameters are generally applied:

- Significant wave height (average of the highest one-third of waves)
- Peak spectral period (period of the component wave with the highest energy)
- Peak spectral direction (direction of component wave with the highest energy)

The wave field's distribution in space and time and hence the three defining parameters are determined by the offshore wave field, its transformation as it propagates into the area of interest, and the influence of locally generated wind waves. As waves travel into water that is of a similar depth to their wavelength, they refract (wave directions tend to turn perpendicular to bottom contours) and shoal (wave heights change as the speed at which wave energy travels changes). Wave energy is also dissipated because of bottom friction in shallow water, the reason wave-induced shear stress at the seabed occurs. Local wind wave generation also contributes significantly to the local wave climate.

The near bed orbital velocity, the oscillatory flow caused by a wave's motion, depends upon the wave height, period, and direction. The orbital flow speed varies, relative to the wave height, with both the wave period and water depth. The shear stress the bed experiences is determined by the wave orbital velocity and the hydraulic roughness of the bed itself.

Because of the difficulties involved in measuring large-scale spatial wave statistics, the use of a numerical hindcast model is the most effective method to obtain an estimate of these parameters. This part of the study describes the distribution in time and space of wave energy in the Adelaide coastal waters region. Wave conditions in the study area were analysed using both direct measurements and hindcasts made with a sophisticated numerical model.

2.2 Application of a numerical wave model for the Adelaide coastal waters

The numerical wave model SWAN, an acronym for Simulating WAves Nearshore (version 40.41AB, *last updated 29/04/2005*), was determined to be the most suitable model to fulfil the project requirements. The model source code (and DOS executable) is the public model obtained from the SWAN website (http://fluidmechanics.tudelft.nl/swan/default.htm) and is described fully in the user manual (Booij et al., 2004).

SWAN is a third-generation numerical wave model, developed for obtaining realistic estimates of wave parameters in coastal areas, lakes, and estuaries. The wave propagation processes it accounts for include propagation through geographical space; refraction due to spatial variations in bathymetry and current; shoaling due to spatial variations in bathymetry and current; transmission through, blockage by or reflection by obstacles; and diffraction based upon the mild slope equation.

The wave generation and dissipation processes accounted for included generation by wind (linear and exponential); dissipation by white capping, depth-induced breaking, or bottom friction; and wave–wave interactions (quadruplets and triads) (Booij et al., 2004).

The wave spectrum evolution used in SWAN is described by the spectral wave action balance equation (or the energy balance equation in the absence of currents) with sources and sinks, which, for Cartesian coordinates, is defined as:

$$\frac{\partial}{\partial t}N + \frac{\partial}{\partial x}C_x N + \frac{\partial}{\partial y}C_y N + \frac{\partial}{\partial \sigma}C_\sigma N + \frac{\partial}{\partial \theta}C_\theta N = \frac{S}{\sigma} \qquad (2.1)$$

where σ is the relative frequency (the wave frequency measured from a frame of reference moving with a current, if a current exists); *N* is wave action density, equal to energy density divided by relative frequency ($N = E/\sigma$); θ is wave direction; *Cg* is the wave propagation speed (in *x*, *y*, σ or θ space); and *S* is the total of source/sink terms expressed as wave energy density (Booij et al., 2004).

The first term in equation 2.1 represents the local rate of change in *N* with time. The second and third terms represent propagation in *x* and *y* space with C_x and C_y, the propagation velocities in the *x* and *y* directions. The fourth term represents shifting of the relative frequency due to variations in water depth and currents. The fifth term represents depth-induced refraction (Booij et al., 2004).

The energy source term, *S*, accounts for the generation, dissipation, and non-linear interactions between waves.

$$S = S_{in} + S_{ds} + S_{nl} \qquad (2.2)$$

Energy input results from wind (S_{in}). The mechanisms for dissipation (S_{ds}) comprise whitecapping, bottom friction, and depth-induced breaking. Non-linear interactions (S_{nl}) redistribute energy over the wave spectrum.

The SWAN output has been validated in several studies both in the field and in laboratory tests and has been found to give a good wave field approximation (Booij et al., 1999).

2.3 Model set-up

The simulations for the current study were carried out using the default model parameters. The effects of bottom friction, depth-induced breaking, and diffraction, all non-default options, were also included.

In all simulations (both coarse and nested) the directional spectrum was divided into 36 directional bins of 10° width over the entire 360° range. The frequency spectrum was discretised into 31 bins between 0.0313 and 1.00 Hz.

The GEN3 KOMEN AGROW (third order generation) setting used accounts by default for the following processes:

- Linear wind growth
- Exponential wind growth
- Whitecapping
- Quadruplet wave interaction

Default processes also included in the computations included:

- Bottom friction
- Depth-induced breaking
- Diffraction

For a detailed description of the above processes, the model formulation and their numerical implementations, please consult the SWAN user manual (Holthuijsen et al., 2003).

More specific details of the non-default options used in the simulations including depth-induced breaking, dissipation due to bottom friction, and diffraction are outlined below. Depth-induced breaking was accounted for in the bore-based model of Battjes and Janssen (1978) and included in calculations using a constant breaking parameter of 0.73. Dissipation of waves by bottom friction was included in the simulations using the JONSWAP formula with the recommended friction factor of 0.067 m^2s^{-3}. This is the value Bouws and Komen (1983) used for fully developed wave conditions in shallow water, as opposed to the JONSWAP value of C_{JON} = 0.038 m^2s^{-3} for swell conditions. The effects of diffraction were included using the default diffraction settings, since they are important for the offshore propagation of wave energy through the two narrow openings of Investigator Strait and Backstairs Passage into the Gulf of St Vincent.

2.4 Model input data

2.4.1 Bathymetry

Bathymetry with a resolution of 1000 m by 1000 m, discretised on a square 123 by 191 grid, for the Gulf of St Vincent region was used for the coarse model simulation. High resolution, 100 m by 100 m bathymetry, discretised on a square 892 by 360 grid, which covered the ACWS modelling domain, was used for the nested model simulation.

The data custodian, Dragan Ivic, Primary Industries and Resources of South Australia (PIRSA), provided the bathymetric data, which consisted of approximately 926,000 data points measured across the Gulf of St Vincent relative to mean sea level. The Royal Australian Navy (RAN) Hydrographic Service is credited as the data source for part of this data set.

2.4.2 Winds

Because of data limitations, a uniform wind field over the entire modelling domain was assumed for modelling purposes. This is somewhat unrealistic and introduced a source of error, as there would be significant variation in the wind field over the modelling domain due to orographic effects; however, it was the best that could be done with the available data.

Wind data, obtained from the Bureau of Meteorology, were recorded at the Adelaide Airport weather observation station, located at 34.96°S, 138.53°E [Easting, Northing: UTM Zone 54, 274474mE, 6128606mN], at an elevation of 16 m above sea level.
The wind speeds were adjusted to an elevation of 10 m above sea level (U_{10}) using the 1/7th power law (as according to CERC (2002)). The wind data were missing 3% of data points, which were 'interpolated' for use in the wave model using nearest neighbour interpolation.

Analysis of the 2003 wind data from Adelaide Airport illustrated the differing winds during the two seasons—summer and winter (note that for hydrodynamic and wave model the winds recorded in 2004 were used). During winter, the winds were predominantly from the north, whereas during summer, the winds had a southerly bias, with the south-west and south-east directions dominating.

2.4.3 Water level

The model domain's tidal regime (Gulf of St Vincent) is generally semi-diurnal, with diurnal tides occurring over some periods.

Because of data limitations, a uniform water level over the entire modelling domain was assumed for modelling purposes. Measured water level data from Port Stanvac was used to define the water level changes throughout the model domain.

2.4.4 Offshore wave conditions

Wave climate data, consisting of significant wave height, peak wave period, and peak wave direction at three-hourly intervals for 2004, were obtained from the NOAA Wave Watch 3 (WW3) global wave hindcast model. The data used as the coarse simulation boundary condition were taken from the WW3 model grid point nearest to Investigator Strait, the coarse modelling domain's main open boundary. This point was located at 36°S, 136.25°E [612662mE, 6015329mN, UTM Zone 53], and approximately 90 km from the coarse model domain's south-west corner. In the absence of a wave rider buoy deployed in the offshore region, these were the best available data for providing appropriate model boundary conditions.

The WW3 wave data files were obtained by ftp in GRIB format from NOAA (ftp://polar.ncep.noaa.gov/pub/history/waves), with information about the available data published on their website (http://polar.ncep.noaa.gov/waves/products.html). The required data were extracted from the GRIB files using a MATLAB® routine (extractWW3.m).

Analysis of the 2004 WW3 wave data showed a mean significant wave height of 3.0 m, with a maximum of 8.5 m. The significant wave height rarely dropped below 1 m (0.4%), with a minimum of 0.8 m. Waves from the SW quadrant dominated the directional distribution (94.2%), with a mean direction of 226° and 65% of measurements lying in the directional band 215° to 235°. It should also be noted that a peak wave period of 12–13 seconds was most frequent. This illustrates the dominance of swell generated by Southern Ocean low pressure systems in the offshore wave climate of the region.

2.5 Model methodology

For both the stationary and non-stationary simulations a nested modelling methodology was adopted, which involved first running a coarse simulation to generate boundary conditions for the subsequent nested simulation (Figure 2.2).

A non-stationary simulation was carried out from 1st January to 31st December 2003 using a temporal resolution of three hours. This simulation was divided into 24 parts and run using the HOTSTART initial conditions option in which initial conditions for each simulation are generated by the preceding simulation.

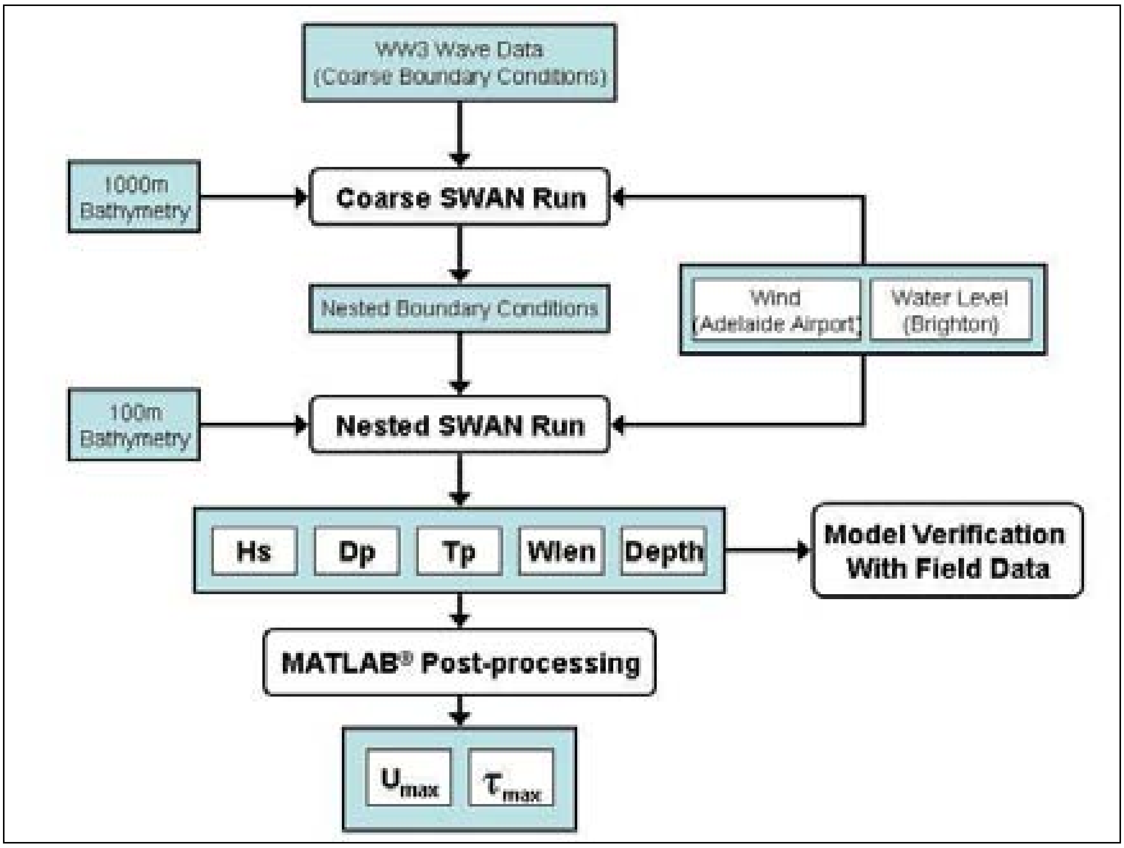

Figure 2.2: Flow diagram for the application of the SWAN model to Adelaide Coastal Waters

2.6 Model validation

A SWAN validation run was carried out from 3rd September to 15th October 2004 for comparison with the measured wave data. An identical model set-up and input data sources to the 2004 non-stationary run were used, with a point output of significant wave height, peak period, and peak direction generated by SWAN at the location of the wave measurements.

2.6.1 Measured wave data (Brighton Beach)

An InterOcean S4 was deployed, on a bottom-mounted frame at 10 m depth, off Brighton Beach (269540mE, 6124964mN, UTM Zone 54) from 3rd September to 15th October 2004.

Horizontal water velocity and pressure were sampled at 2 Hz. Data segments of 18 min were recorded every two hours.

Spectral analysis was performed on the raw data to obtain values of significant wave height, peak wave period, and peak wave direction, giving 567 data points at 2-hourly time intervals. This was then re-sampled to three-hourly intervals using MATLAB for direct comparison with the numerical model output data.

The measured wave data had a mean significant wave height of 0.49 m, with a maximum of 1.70 m and a minimum of 0.09 m. The peak wave period ranged between 4.47 sec and 12.02 sec, with a mean of 8.51 sec. Wave direction was confined to a tight directional band between 226.0° and 259.0°, with a mean direction of 245.2°. Because of the measurements' nearness to the shore, the shoreline orientation and the local bathymetry would strongly influence the wave direction via the effects of refraction acting to align the wave direction perpendicular to the bottom contours.

Generally, a good agreement was obtained between the SWAN-simulated significant wave heights and those measured at Brighton Beach, with the numerical model results showing a slight overestimation (Figure 2.3).

The agreement obtained was deemed to be sufficient given the assumptions made in the modelling procedure, particularly the use of spatially uniform wind and water level fields over the entire modelling domain.

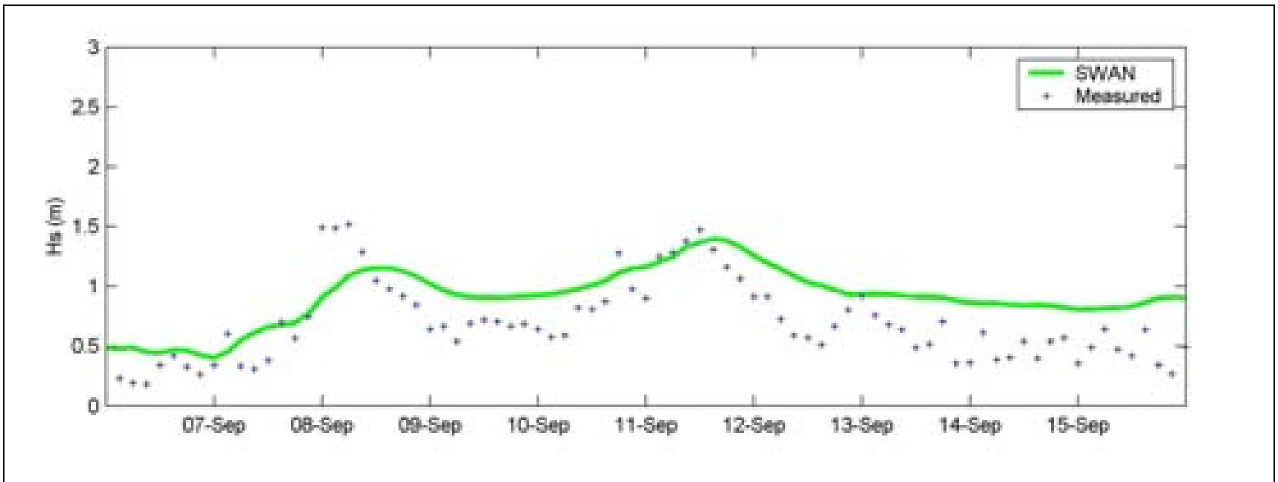

Figure 2.3: Time series of predicted and measured wave heights at Brighton

2.7 Wave orbital velocities and bottom shear stress

The peak orbital velocity (U_{max}), which is the maximum velocity of the water at the seabed, and peak shear stress due to the wave motion (τ_{max}) are the two most important hydrodynamic variables in terms of conditions for biota at the seabed. SWAN outputted the maximum near bed bottom velocity (U_{BOT}), which was then used to calculate peak shear stress at three-hourly intervals for 2004.

Since SWAN is a spectral wave model, simulating the effect of many waves of differing periods, it does not give a single output of maximum bottom orbital velocity; instead, it calculates the RMS of the maximum near bottom orbital velocity. This value was taken to be the maximum bottom velocity (U_{max}) for the purposes of this study.

2.8 Exceedance of critical shear stress

The three-hourly data of maximum bottom shear stress calculated from the SWAN output were used to calculate an exceedance (percentage of time that the threshold shear stress was exceeded) under the action of waves and currents.

The threshold shear stress of sediment movement was calculated, based upon the median grain size (D_{50}), using the Shields criterion; the procedure is outlined below.

The sediment–fluid parameter is calculated using

$$S_* = \frac{D_{50}}{v}\sqrt{(s-1)g.D_{50}} \qquad (2.3)$$

where D_{50} is the mean sediment particle diameter, v is the fluid viscosity, s is the sediment density relative to the fluid ($s = \rho_s/\rho$), and g is acceleration due to gravity.

The critical Shields parameter (ψ_{cr}) can be obtained from the modified Shields diagram (Figure 2.4) using the sediment–fluid parameter value (S_*) or as implemented in this study, the the critical Shields parameter, (ψ_{cr}), was nestimated numerically using the following fifth order polynomial:

$$\begin{aligned}\log_{10}(\psi_{cr}) = 0.002235x^5 - 0.06043x^4 + 0.020307x^3 \\ + 0.054252x^2 - 0.636397x - 1.03167\end{aligned} \qquad (2.4)$$

where $x = \log_{10}(S_*)$.

Once the critical Shields parameter is known the critical friction velocity (u_{*cr}) can be calculated using:

$$u_{*cr} = \sqrt{(s-1)g.D.\psi_{cr}} \qquad (2.5)$$

Since sediment sampling data were inadequate to construct a spatial distribution of median sediment grain sizes, critical shear stress exceedance was calculated for three sediment sizes (the size fraction cut-offs used in the sediment sampling: 2 mm, 0.25 mm, and 0.065 mm).

Percentage exceedance was defined as the percentage of time the estimated maximum bottom shear stress exceeded the critical value at each model grid location.

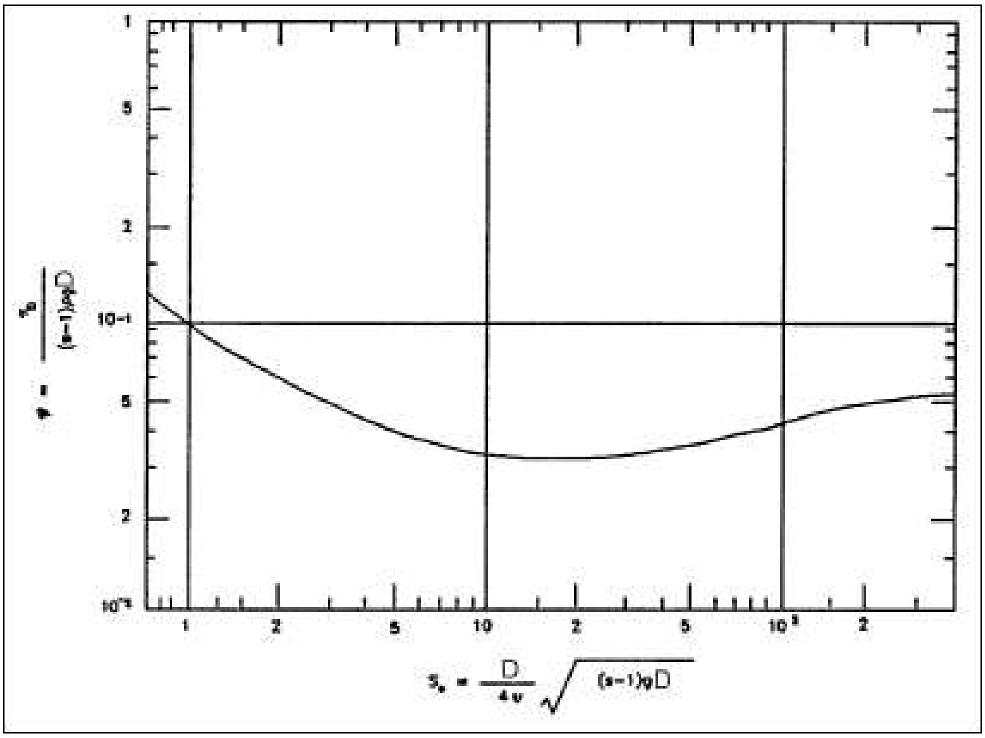

Figure 2.4: Modified Sheilds Diagram (after Madsen and Grant, 1976).

Percentage exceedance values were calculated under two different cases: (1) waves only; and (2) wave and currents in combination.

2.8.1 Waves only

The three-hourly output of significant wave height, wave period and water depth from the SWAN output used to calculate the maximum bottom shear stress using equation were used to calculate an exceedance (percentage of time that the threshold shear stress was exceeded) under the action of waves and currents.

The peak shear stress, τ_{max}, is the greatest shear stress the seabed experiences during one wave period. This is calculated directly from U_{max} using the following equation:

$$\tau_{\max} = \frac{1}{2}\rho f_w U_{\max}^2 \tag{2.6}$$

where ρ is the density of water and f_w is the wave friction factor. The wave friction factor depends on both the wave parameters and the bottom roughness, *R*, as (approximation of Grant and Madsen, 1986):

$$f_w = \exp\left[-7.02 + 5.5\left(A_0 / R\right)^{-0.12}\right] \tag{2.7}$$

$$A_0 = \frac{T_p}{2\pi} U_{\max} \tag{2.8}$$

For the bottom shear stress calculations, a spatially uniform bed roughness (*R*) of 0.001 was used. It should be noted that this is not realistic for all types of bottom substrate that are present in many locations.

Once the maximum bottom shear stress, over the whole year was calculated, the percentage exceedance values for were calculated for three grain sizes: 2 mm, 0.25 mm, and 0.065 mm.

2.8.2 Waves and Currents in combination

The shear stress under the combined action of waves and currents was calculated using the concept of Grant and Madsen (1979). The maximum bottom stress, $\tau_{b,\max}$, for a wave–current combination is defined as:

$$\tau_{b,\max} = \frac{1}{2} f_{cw} \rho \left[U_m^2 + u_c^2 + 2U_m u_c \cos\phi_c \right] \tag{3.12}$$

in which ρ is the water density, f_{cw} is an effective friction factor, U_m is the maximum near bottom wave orbital velocity determined from the SWAN output see section 2.8.1), u_c is the mean bottom current (predicted from the hydrodynamic module, ELCOM, see section 3), and ϕ_c is the angle between wave propagation and current direction.

The percentage exceedance values were calculated for both summer and winter conditions corresponding to the 45 day runs of the hydrodynamic model (section 3.3).

3. Hydrodynamic model description and formulation

ELCOM (Estuary and Lake COmputer Model) is a three-dimensional hydrodynamic model for estuaries, lakes, and reservoirs used to predict the variation of horizontal currents, water temperature, and salinity in space and time. ELCOM solves the unsteady Reynolds-averaged Navier-Stokes equations using a semi-implicit method similar to the momentum solution with the addition of quadratic Euler-Lagrange discretization, scalar (e.g. temperature) transport using a conservative flux-limited approach, and elimination of vertical diffusion terms in the governing equations. ELCOM does not assume a relationship between the vertical Reynolds stress terms and the resolved shear, but instead applies a mixing model to compute directly the vertical turbulent transport. Molecular diffusion in the vertical direction is neglected, as turbulent transport and numerical diffusion are generally dominant. The free-surface evolution is governed by vertical integration of the continuity equation for incompressible flow in the water column applied to the kinematic boundary condition.

ELCOM computes, at each model time step, in a staged approach consisting of:

- introduction of surface heating/cooling in the surface layer
- mixing of scalar concentrations and momentum using a mixed-layer model
- introduction of wind energy as a momentum source in the wind-mixed layer
- solution of the free-surface evolution and velocity field
- effects of the earth's rotation (the Coriolis Force)
- horizontal diffusion of momentum
- advection of scalars
- horizontal diffusion of scalars.

The fundamental numerical scheme is adapted from the TRIM approach of Casulli and Cheng (1992), with modifications for accuracy, scalar conservation, numerical diffusion, and implementation of a mixed-layer turbulence closure. The solution grid uses rectangular Cartesian cells with varying Δx and Δy (horizontal) and vertical Δz spacing. The grid stencil is the Arakawa C-grid: velocities are defined on cell faces, with the free-surface height and scalar concentrations on cell centres. The free-surface height in each column of grid cells moves vertically through grid layers as required by the free-surface evolution equation. Replacement of the standard vertical turbulent diffusion equation with a mixed-layer model eliminates the tridiagonal matrix inversion for each horizontal velocity component and transported scalar required for each grid water column in the original TRIM scheme. This provides computational efficiency and allows sharper gradients to be maintained with coarse grid resolution.

Examples of ELCOM applications include the modelling of a Microcystis bloom event in the Swan River Estuary, Western Australia (Robson and Hamilton, 2004); modelling of exchange flow between a tidal strait and coastal lake (Laval et al., 2003); circulation and exchange processes in Venice Lagoon (Yeates et al., 2004); the effects of Po River discharge, internal nutrient cycling, and hydrodynamics on the biogeochemistry of the Northern Adriatic Sea (Spillman et al., 2006); and internal wave processes in stratified lakes (Hodges et al., 2000).

3.1 Governing equations

The governing equations and fundamental models used for three-dimensional transport and surface thermodynamics in ELCOM are summarised in this section. The transport equations are the unsteady Reynolds-averaged Navier-Stokes (RANS) and scalar transport equations using the Boussinesq approximation and neglecting the non-hydrostatic pressure terms. The free-surface evolution is governed by an evolution equation developed by a vertical integration of the continuity equation applied to the Reynolds-averaged kinematic boundary condition. A detailed model description is available from: http://www.cwr.uwa.edu.au/~ttfadmin/model/elcom/index.html

The Reynolds-averaged, three-dimensional equations of motion may be written as (Blumberg and Mellor, 1987):

the continuity equation:

$$\frac{\partial u}{\partial x}+\frac{\partial v}{\partial y}+\frac{\partial w}{\partial z}=0 \qquad (3.1)$$

in the *x* direction (east-west component):

$$\frac{\partial u}{\partial t}+u\frac{\partial u}{\partial x}+v\frac{\partial u}{\partial y}+w\frac{\partial u}{\partial z}=-\frac{1}{\rho_o}\frac{\partial P}{\partial x}+fv+\frac{\partial}{\partial z}\left(A_z\frac{\partial u}{\partial z}\right)+F_x \qquad (3.2)$$

in the *y* direction (north-south component):

$$\frac{\partial v}{\partial t}+u\frac{\partial v}{\partial x}+v\frac{\partial v}{\partial y}+w\frac{\partial v}{\partial z}=-\frac{1}{\rho_o}\frac{\partial P}{\partial y}+fv+\frac{\partial}{\partial z}\left(A_z\frac{\partial v}{\partial z}\right)+F_y \qquad (3.3)$$

Here, u, v, w are the components of velocity in the x, y, z directions, respectively; f is the Coriolis parameter; ρ_o, the density of homogeneous seawater is taken to be a constant; and A_Z is the vertical eddy viscosity for momentum. The diffusive terms F_X and F_Y are horizontal diffusive terms parameterized in terms of the horizontal momentum eddy viscosity A_h as

$$F_x=\frac{\partial}{\partial x}\left[2A_h\frac{\partial v}{\partial x}\right]+\frac{\partial}{\partial y}\left[A_h\left(\frac{\partial u}{\partial y}+\frac{\partial v}{\partial x}\right)\right] \qquad (3.4)$$

and

$$F_y=\frac{\partial}{\partial y}\left[2A_h\frac{\partial v}{\partial y}\right]+\frac{\partial}{\partial x}\left[A_h\left(\frac{\partial u}{\partial y}+\frac{\partial v}{\partial x}\right)\right] \qquad (3.5)$$

The transport of tracers (temperature, salinity, and suspended sediment) are governed by

$$\frac{\partial C}{\partial t}+u\frac{\partial C}{\partial x}+v\frac{\partial C}{\partial y}+w\frac{\partial C}{\partial z}=\frac{\partial}{\partial z}\left(K_z\frac{\partial C}{\partial z}\right)+F_C+S \qquad (3.6)$$

where C is the tracer concentration and K_Z is the vertical eddy viscosity coefficient for mass. In equation (3.6), F_C is the term for sub-grid scale processes, defined similarly to F_X and F_Y as

$$F_C = \frac{\partial}{\partial x}\left(K_h \frac{\partial C}{\partial x}\right) + \frac{\partial}{\partial y}\left(K_h \frac{\partial C}{\partial y}\right) \tag{3.7}$$

It is generally assumed that the horizontal eddy coefficient for heat, salt, and sediment are the same.

In equation 3.6, the term S is the source/sink term. This defines the inputs external from the model domain. For temperature, this includes heat input/loss from the sea surface; for salinity includes evaporation/precipitation at the sea surface and freshwater inputs from point sources (from rivers, wastewater and stormwater) and for suspended sediments includes sediment re-suspension from the seabed and inputs from point sources (from rivers, wastewater and stormwater).

3.2 Hydrodynamic model—discretisation

The domain of the ACWS hydrodynamic grid is shown in Figure 3.1. The model grid corner coordinates are:

North-west corner: 243 000 East; 616 6000 North
South-east corner: 279 000 East; 607 7000 North

A rectangular grid with variable grid sizes in both north-south and east-west directions were adopted to apply ELCOM (Figure 3.1). In the north-south direction, the grid size was set to 200 m for the extent of the ACWS region, with an increase in grid size at the northern (to 1 km) and southern (to 2.2 km) boundaries. In the east-west direction, the regions closest to the coast were set to 50 m, which increased to 100 m to the west and then increased from 100 m to 3.7 km towards the western boundary (Figure 3.2).

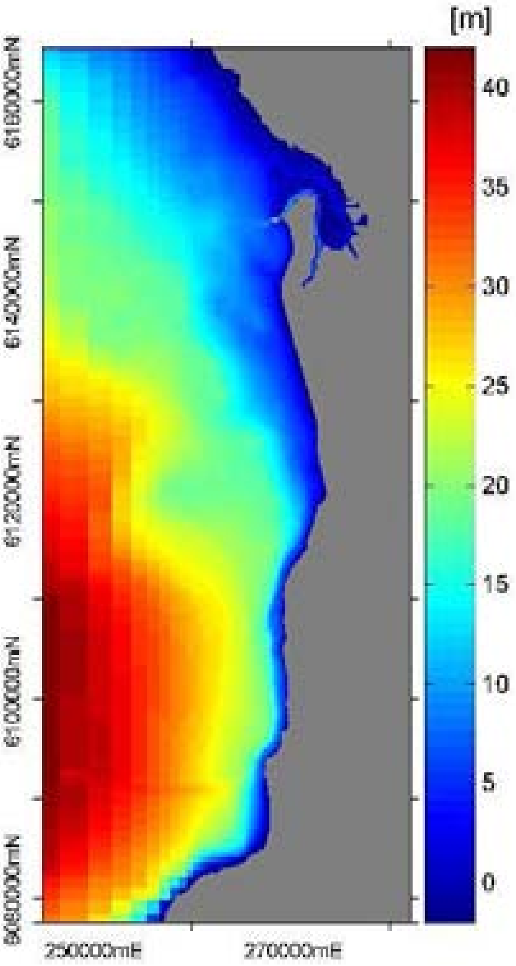

Figure 3.1: The bathymetry of the model domain.

A total 15 vertical layers were prescribed; details of each layer are given in Table 3.1. The top five layers were set to 1 m thickness, increasing to 8.76 m in the deeper parts of the model grid. The mean level was set to the second layer. ELCOM has the attribute that if the water level is below the prescribed layer depth, then the layer will cease to 'exist' until the water level increases to that particular depth. Thus during low water springs the surface two layers would not exist.

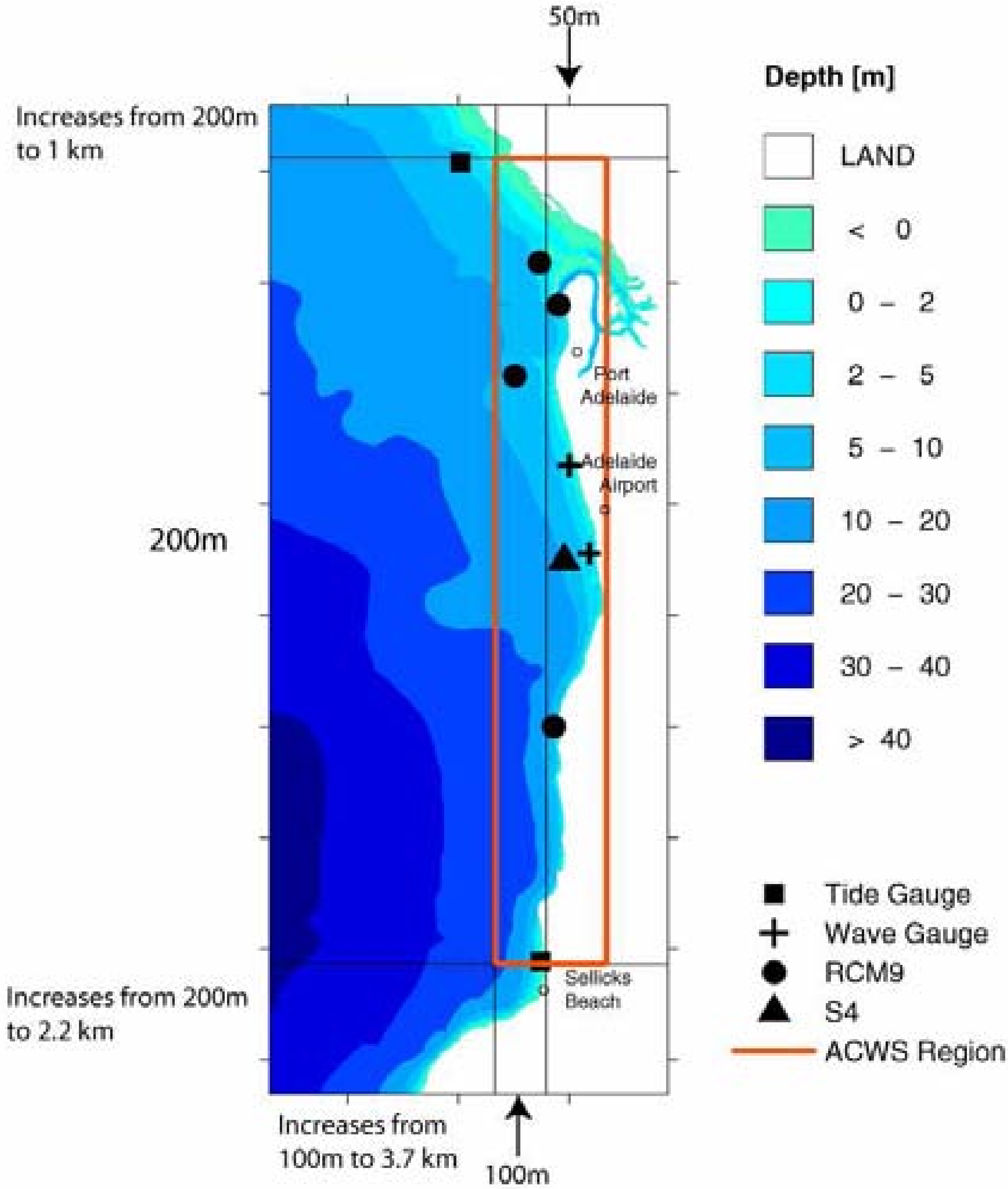

Figure 3.2: The horizontal discretisation of the ACWS model domain and the locations of field measurements for model validation

Table 3.1. Distribution of model layers in the ACWS

Layer no.	Thickness (m)	Depth of the lowest-part layer (l m)
1	1	1
2	1	0
3	1	–1
4	1	–2
5	1	–3.1
6	1.25	–4.35
7	1.5	–5.85
8	1.8	–7.65
9	2.35	–10
10	3	–13
11	3.75	–16.75
12	4.7	–21.45
13	5.75	–27.2
14	7.2	–34.4
15	8.76	–43.16

3.3 Hydrodynamic model forcing

To achieve the Adelaide Coastal Waters Study's overall objectives and to address the stakeholders' requirements, a series of model runs and scenarios was developed (Table 5.1). This included present (2004) conditions as well as past and future scenarios. A series of model scenarios was developed to investigate the present, past, and future dispersals of discharges to the coastal zone. To simulate these in the numerical model, a series of model forcing parameters was defined. Because of limitations in computer memory, run times, and model discretisation, each scenario was run for 45 days (three spring-neap cycles) during summer and winter. For summer, the period mid-January to end of February, which included the summer sea breeze pattern and low rainfall (Figure 3.3), was selected.

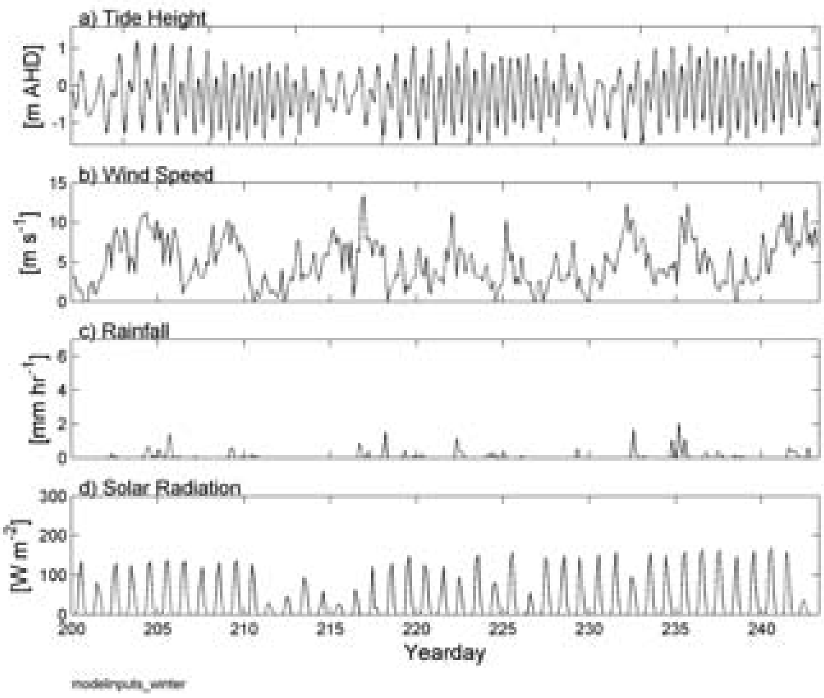

Figure 3.3: Model forcing winter (wet) scenario

For winter, the period mid-August to end of September included the typical winter winds and the period of high discharges to the coastal strip (Figure 3.4). To identify changes due only to variability in discharges, it was proposed the same bathymetry (applicable to present conditions) and meteorological conditions (winds and air–sea fluxes) be used for past, present, and future scenarios.

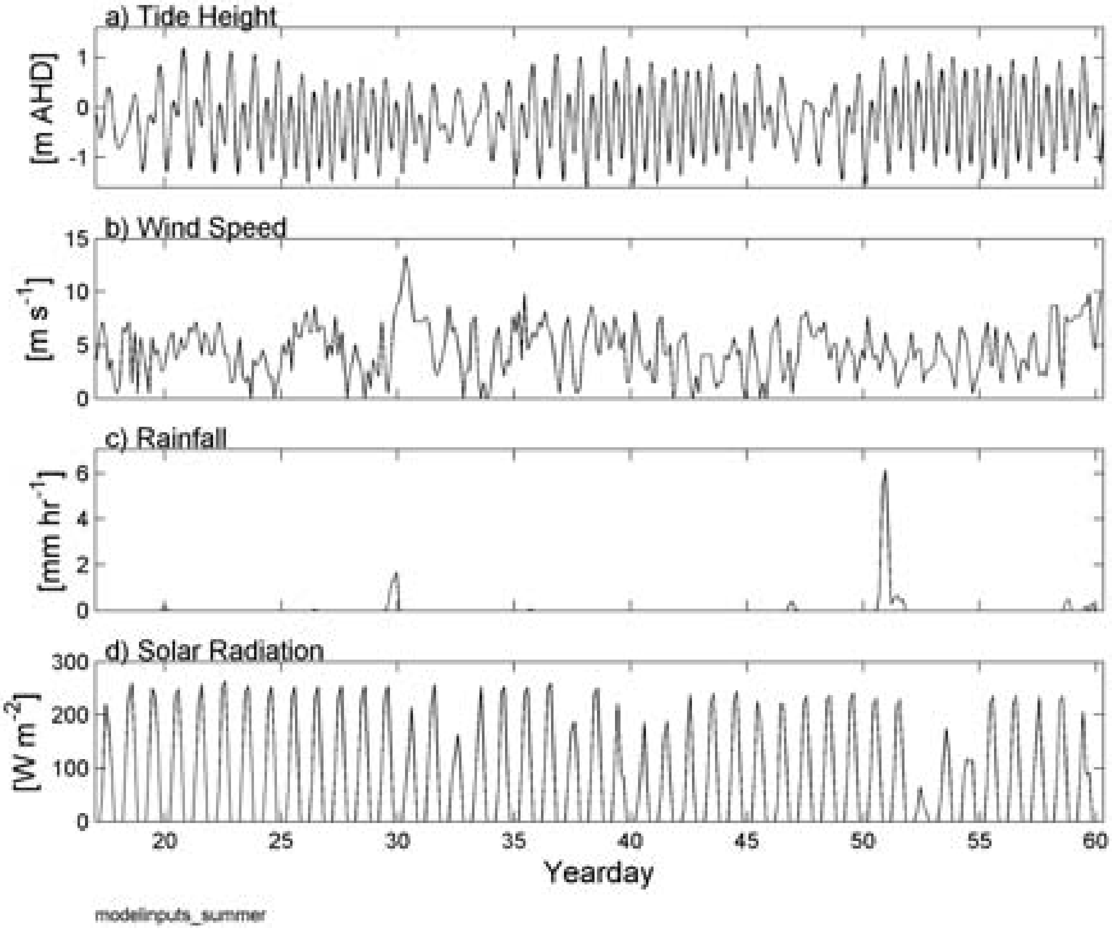

Figure 3.4: Model forcing summer (dry) scenario

The 'past' conditions were defined as the conditions that may have existed prior to the accelerated loss of large seagrass cover in the coastal waters, recorded as starting around 1970. Assuming there was a time lag for changes, the year 1965 was selected as a model scenario to simulate 'past' conditions. The 'future' conditions were defined as conditions that might exist at the end date in State's planning strategy; the year 2020 was selected.

3.3.1 Water levels

The forcing of water levels (tides) at the three open model boundaries (north, west, and south) was determined using a combination of field data and previous numerical modelling. Field data from PPM task 1 are available from two coastal tide stations: Sellicks Beach (Figure 3.5) and Port Gawler (Figure 3.6). These data were analysed, using a harmonic analysis method, to isolate the tidal components.

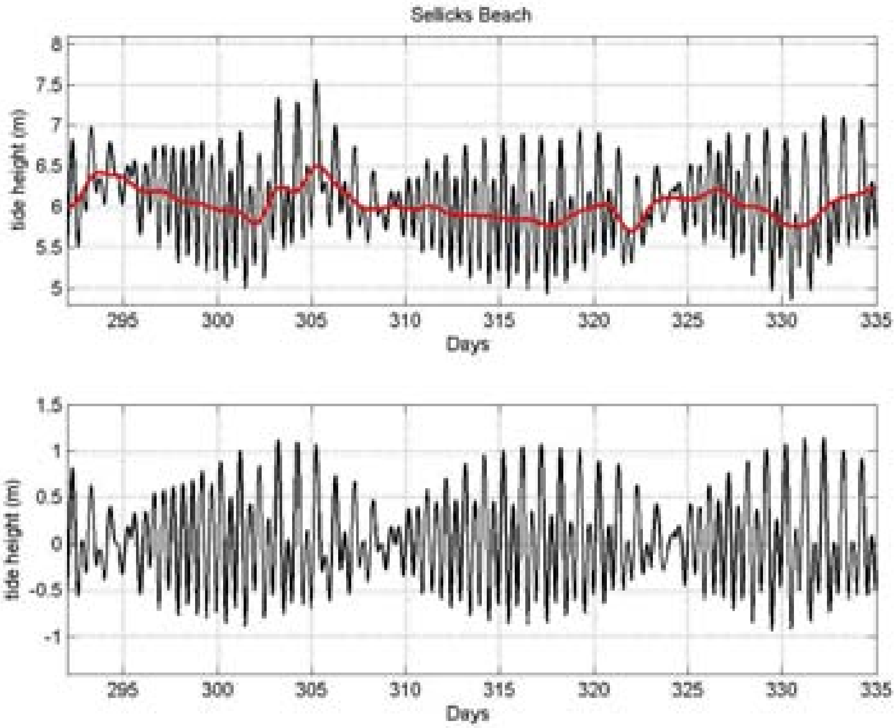

Figure 3.5: Water Level variability at Sellicks Beach. (a) the measured and low-pass filtered record; and (b) the tidal signal. Note that the low frequency oscillations of ~0.75m which are comparable with the mean tides.

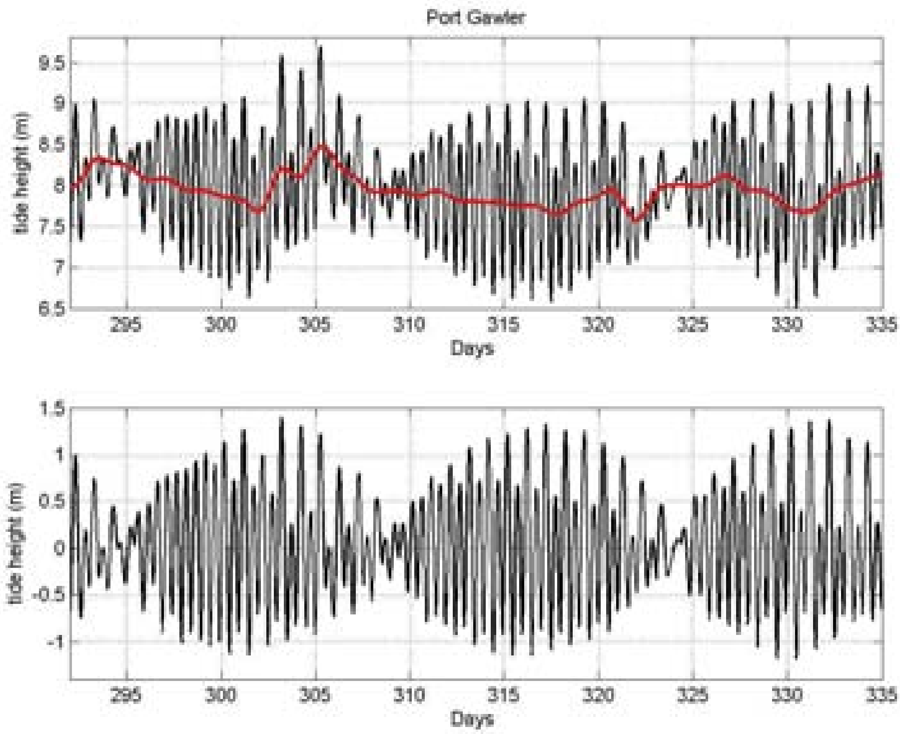

Figure 3.6: Water Level variability at Port Gawler. (a) the measured and low-pass filtered record; and (b) the tidal signal. Note that the low frequency oscillations of ~0.75m which are comparable with the mean tides.

The results indicated that, for both stations, the most dominant tidal constituents were M_2, S_2, K_1, and O_1. To interpolate the tidal constituents obtained from the field data (Table 3.2), previous studies and particularly the numerical modelling results of Grzechnik and Noye (1996) were examined. A summary of the Gulf of St Vincent tidal dynamics is presented below.

Matthew Flinders made the first tidal observations of the Gulf of St Vincent (Flinders, 1814). Tidal data collected from the Gulf have enabled the construction of co-tidal and co-amplitude charts for each tidal constituent within the Gulf (Figure 3.7). These charts indicate the tide's progression from the Southern Ocean into the Gulf of St Vincent via Investigator Strait and Backstairs Passage.

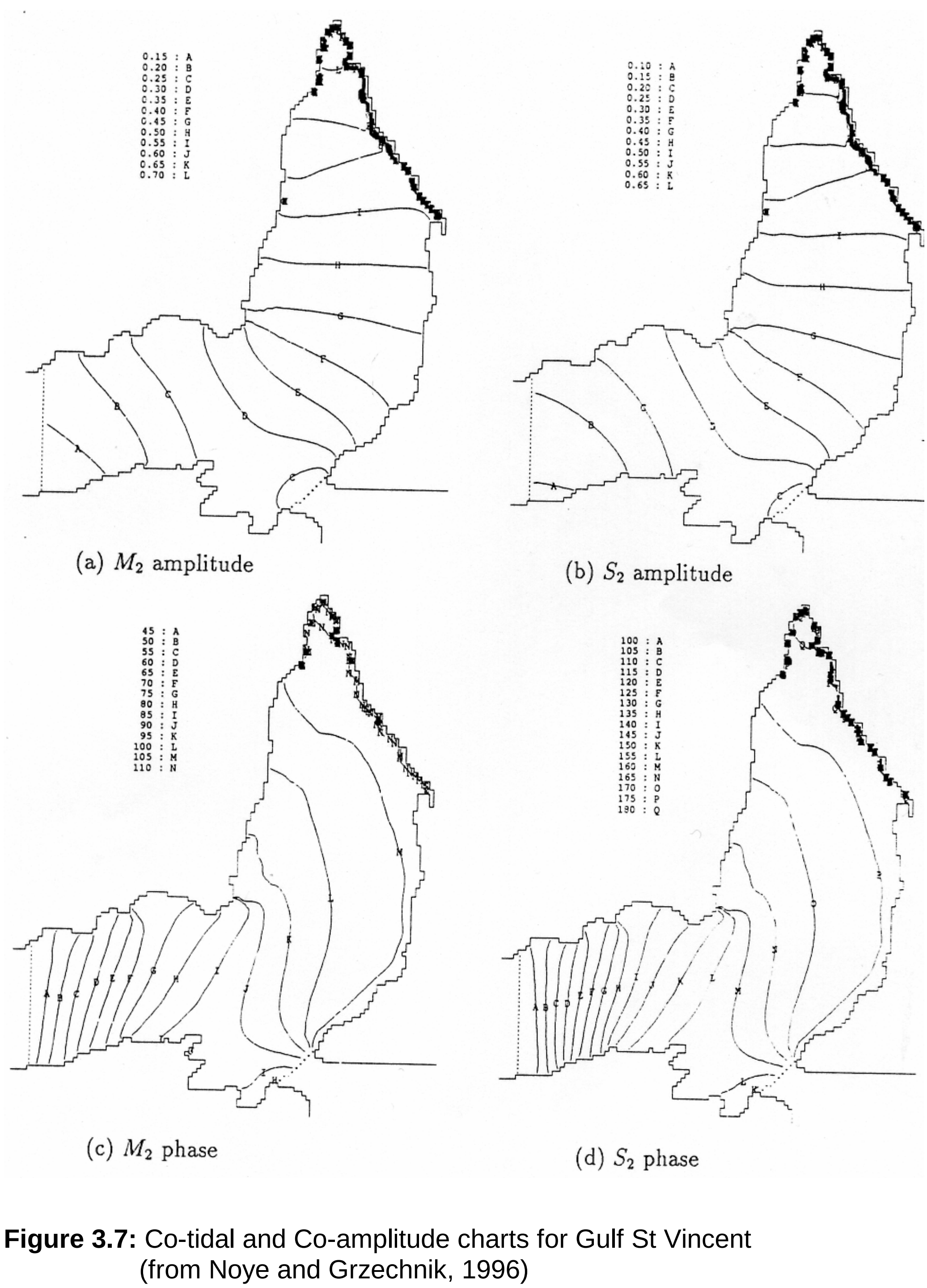

Figure 3.7: Co-tidal and Co-amplitude charts for Gulf St Vincent (from Noye and Grzechnik, 1996)

Examination of the tidal charts provided some interesting tidal phenomena within the study region that leads to the formation of 'dodge' tides within the Gulf. The relative amplitudes of the M_2 and S_2 constituents, which changed their respective strengths as they progressed up into the Gulf, resulted in a 'crossover' point where the two amplitudes coincided. The actual point where the amplitudes were equal appeared to be between Outer Harbour and Brighton (Grzechnik and Noye, 1996). Since the S_2 tide had a period of exactly 12 hours, and M_2 had a period of 12 hours and 25 minutes, every 14.77 days the two tides were either enhanced, resulting in a tidal range that was double the amplitude of each of the tidal constituents, resulting in spring tides, or cancelled each other out, resulting in the rise and fall of the tides ceasing, resulting in neap tides. Flinders named the absence of the tide during neap tides the dodge tide. Because of this feature, the Gulf waters are relatively stationary for a day or two each fortnight, and in some seasons may become stratified during neap tides if the weather is calm.

The results of Grzechnik and Noye (1996) indicated that the northern boundary's amplitude was higher by ~40%, which was due to changes in the semi-diurnal components (M_2 and S_2), whereas the diurnal components (K_1 and O_1) remained almost constant. They also indicated there were only negligible phase differences between north and south boundaries.

The field data also indicated the presence of low frequency oscillations, which lasted up to 10 days; these oscillations, which are due to the passage of weather systems, are termed coastal trapped waves. The signals were coherent between both stations. Because of the low frequency nature of these waves, they could significantly influence the net transport of material and were incorporated into the model.

Both the tidal and low frequency components were included in the model forcing. However, only limited data sets were available from the tide gauge stations at the boundary (Port Gawler and Sellicks Beach), which also did not correspond to the periods selected for model simulation. Hence the following procedure was adopted to prescribe the measured data (which included tidal and low frequency components). The National Tidal Centre at Port Stanvac, which is almost central to the model domain, records data continuously. Hence it was decided to use the data recorded at Port Stanvac to force the model, taking into account the amplitude and phase differences between the boundaries and Port Stanvac (Figure 3.8). These relationships for the amplitude and phase differences were obtained through analysis of the measured tidal data at Port Gawler and Sellicks Beach (applied at the northern boundary) and Port Stanvac (applied at the southern boundary). As previous studies (see above) showed that cross-shore changes in amplitude and phase were negligible, no cross-shore variation was prescribed.

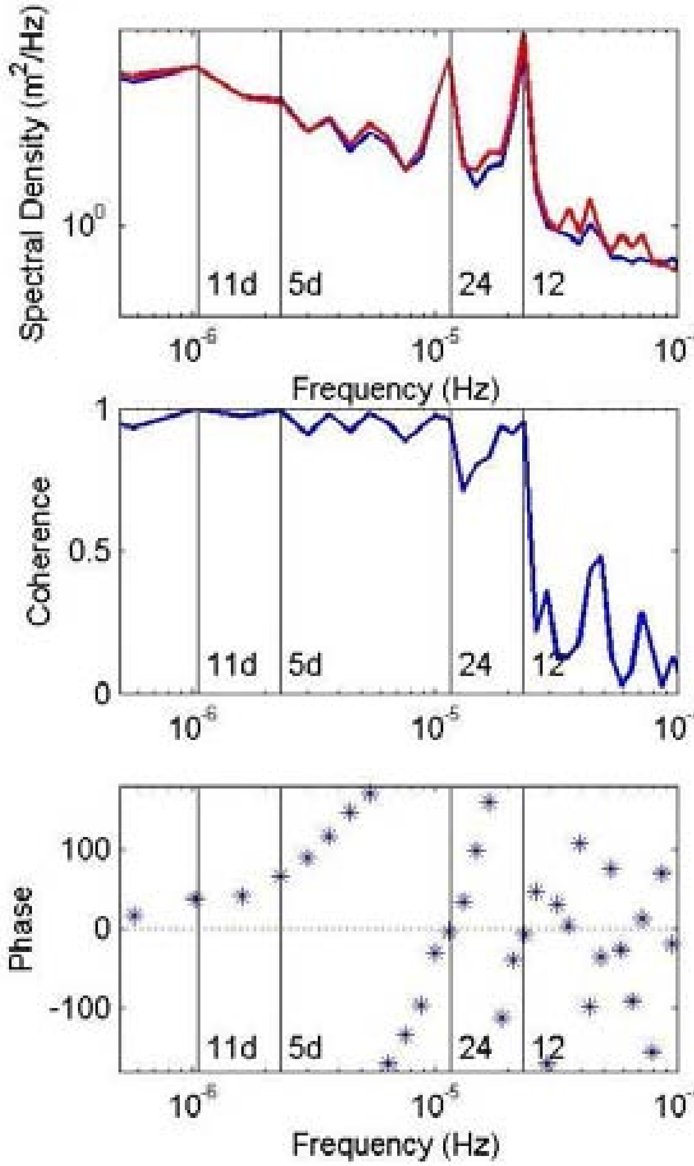

Figure 3.8: Cross-spectral analysis between the water levels at Sellicks Beach and Port Gawler. Note the high coherence of signals higher than 12 hour period.

Table 3.2. Results of the harmonic analysis of tidal elevations on the boundaries of the Adelaide coastal waters grid

		Sellicks Beach		**Port Gawler**	
Tidal constituent	Speed (^{o}/hour)	Amplitude (m)	Phase (^{o})	Amplitude (m)	Phase (^{o})
Z_O	–	6.016	–	7.932	–
M_m	0.5443747	0.087	180	0.093	192
M_{sf}	1.0158958	0.130	342	0.141	342
Q_1	13.3986609	0.067	45	0.064	54
O_1	13.9430356	0.212	239	0.219	250
M_1	14.4920521	0.010	289	0.013	292
K_1	15.0410686	0.267	56	0.267	69
J_1	15.5854433	0.017	250	0.022	271
OO_1	16.1391017	0.020	302	0.013	322
MU_2	27.9682084	0.054	298	0.073	327
N_2	28.4397295	0.037	226	0.048	252
M_2	28.9841042	0.334	328	0.450	355
L_2	29.5284789	0.029	196	0.044	216
S_2	30.0000000	0.415	158	0.574	186
$2SM_2$	31.0158958	0.044	182	0.054	207
MO_3	42.9271398	0.003	142	0.001	66
M_3	43.4761563	0.002	32	0.002	266
MK_3	44.0251729	0.004	250	0.008	240
MN_4	57.4238337	0.001	323	0.005	73
M_4	57.9682084	0.004	128	0.007	270
SN_4	58.4397295	0.001	158	0.004	318
MS_4	58.9841042	0.004	252	0.008	344

3.3.2 Wind field

The action of wind along the sea surface results in a stress that forces surface water in the wind direction; therefore it is an important forcing mechanism of the currents. Wind speed and direction data are available from Adelaide Airport for several years. Here, data for 2003 were obtained for analysis. The winds indicated a strong seasonality, with the winds changing by up to 180° between summer and winter (F igure 3.9). During winter, the wind direction ranged from north to north-east, with the strongest winds blowing from NNE. In summer, the winds were from the south-west to south-east quadrant, with the strongest winds from the south-west due to the action of the sea breeze.

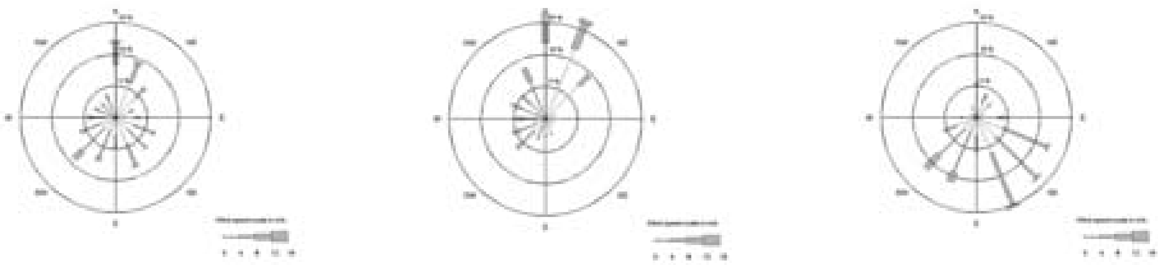

Annual Winter Summer

Figure 3.9: Distribution of wind speed and direction, annual, summer and winter at Adelaide Airport (2003 data)

The seasonal changes in the wind field described above were included in the model forcing for summer and winter based on data obtained from Adelaide airport in 2004 (Figure 3.10).

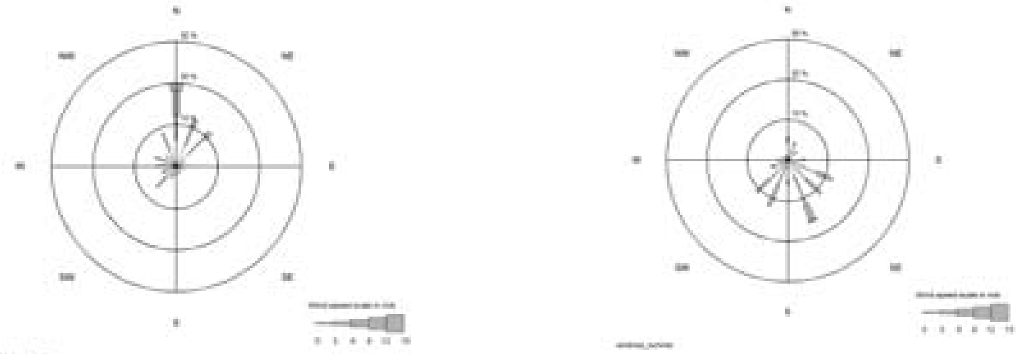

Winter Summer

Figure 3.10: Distribution of wind speed and direction for winter and summer used for model forcing (from 2004).

3.3.3 Air–sea exchange

The air–sea exchange of heat and water across the sea surface determines changes in temperature and salinity in the surface waters. In the hydrodynamic model, the air–sea exchanges were specified using meteorological data recorded at Point Stanvac.

The heat balance at the sea surface may be written as:

$$Q_{net} = Q_{SW} - Q_{LW} - Q_L - Q_S \qquad (3.8)$$

where

- Q_{SW} = incoming radiation from the sun (short wave radiation flux)
- Q_{LW} = long wave energy back-radiated by the ocean (long wave radiation flux)
- Q_L = heat loss by evaporation (latent heat flux)
- Q_S = heat loss by conduction (sensible heat flux)

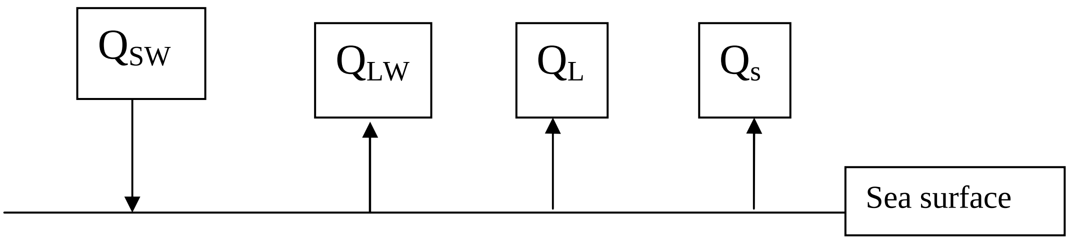

Short wave radiation flux

This is the amount of energy received at the sea surface because of the sun. Outside the atmosphere, the radiation received is 1360 Wm^{-2}. This is reduced at the sea surface because of the presence of clouds, etc. Q_{SW} varies during the day (sun elevation, day/night, clouds, etc.) and with season. This was estimated by using an idealised formula that provided the short wave radiation flux for the latitude of Adelaide as a function of local time (i.e. taking into account the local sun elevation) with a correction applied for cloud cover.

Long wave radiation flux

This is the amount of energy radiated back into the atmosphere because of the sea surface temperature (black body radiation). The amount of heat flux depends on the sea surface temperature:

$$Q_{LW} = \square\ T^4 \tag{3.9}$$

Q_{LW} changes whenever the sea surface temperature changes, which is estimated by ELCOM; hence the calculation of long wave radiation flux was undertaken within the model using the prescribed meteorological forcing and model-estimated sea surface temperature.

Latent heat flux

This is the amount of energy lost through evaporation and thus influences both surface temperature and salinity (through evaporation). This is the largest term of the heat loss terms. The latent heat flux depends on the humidity and wind speed:

$$Q_L = C_E\ (e_w – e_a)W \tag{3.10}$$

Here, e_a is the specific humidity of the air at 10 m, e_w is the specific humidity at the water surface, and W is the wind speed. The latent heat flux was estimated using the wet and dry bulb temperature measurements at Port Stanvac.

Sensible heat flux

This is the amount of energy lost through convection and conduction. This is the smallest term of the heat loss terms and depends on the air and sea temperature difference:

$$Q_L = C_H\ (T_w – T_a)W \tag{3.11}$$

Here, T_w is the sea surface temperature, T_a is air temperature, and W is the wind speed. Similar to the estimation of long wave radiation flux, the calculation of sensible heat flux was undertaken within the model using the prescribed meteorological forcing and model-estimated sea surface temperature.

As an example calculation of the air–sea heat fluxes, the meteorological data together with the sea surface temperatures measured at Port Stanvac were used to estimate the air–sea fluxes for 2004 and are shown in Figures 3.11 to 3.13. The raw data are shown in Figure 3.11; estimates of the air–sea flux at hourly intervals (Figure 3.12) and averaged into daily values (Figure 3.13) are also shown.

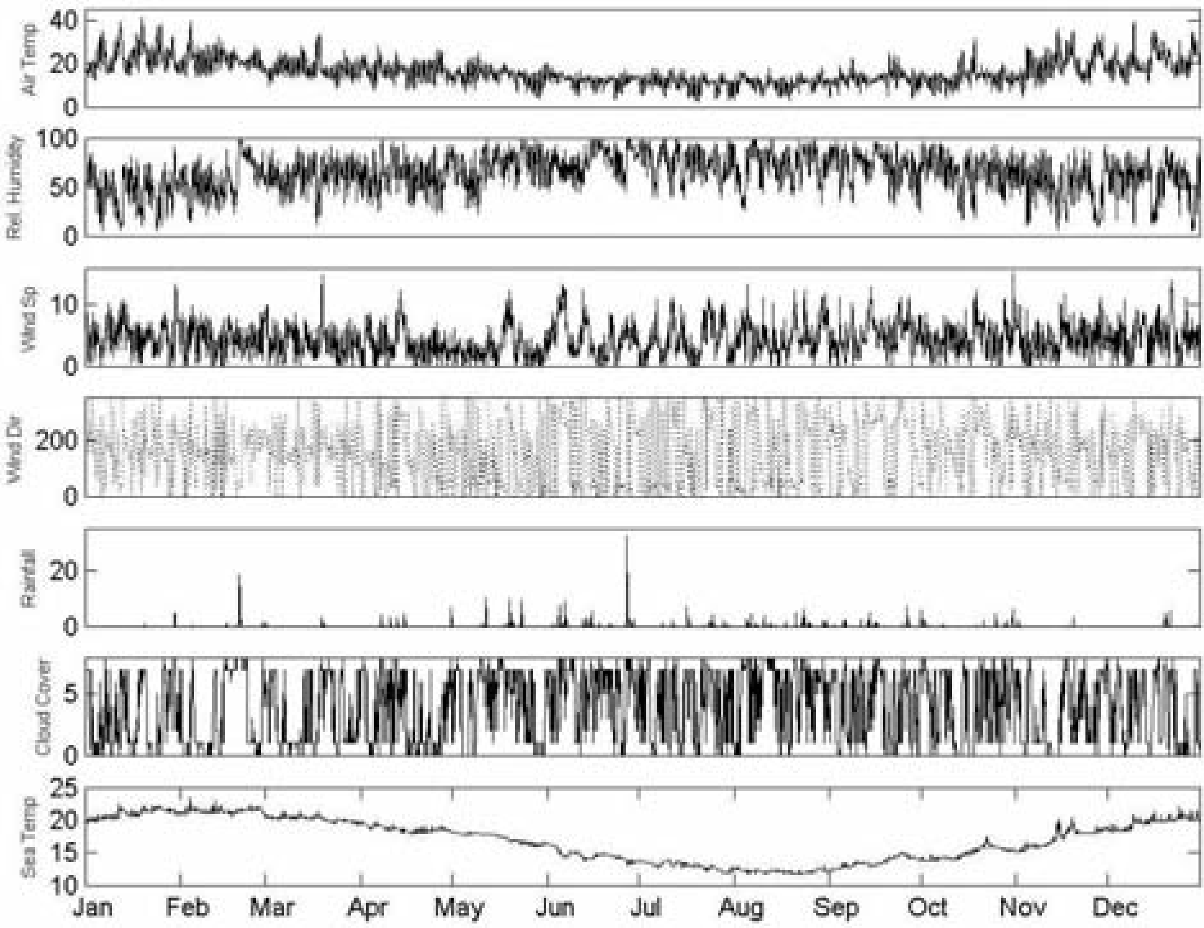

Figure 3.11: Time series of meteorological data and sea surface temperature measured at Port Stanvac in 2004.

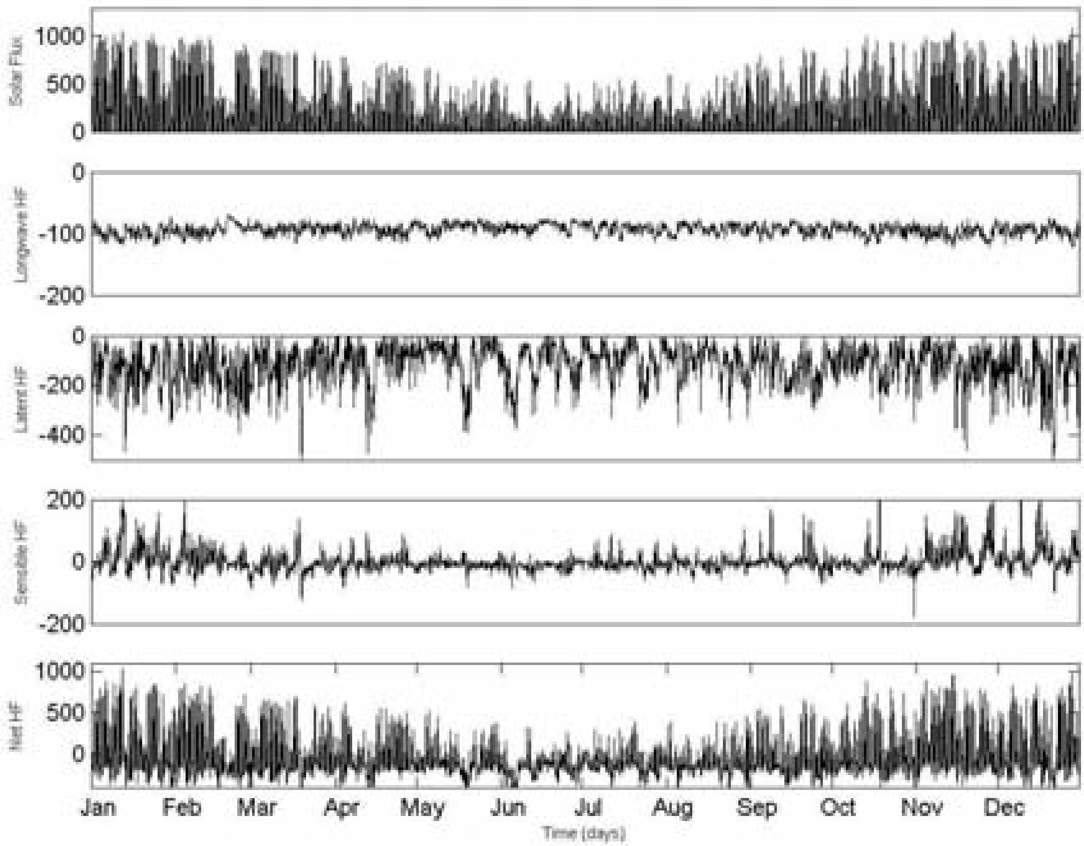

Figure 3.12: Time series, at hourly intervals, of air-sea fluxes estimated using meteorological data and sea surface temperature measured at Port Stanvac in 2004.

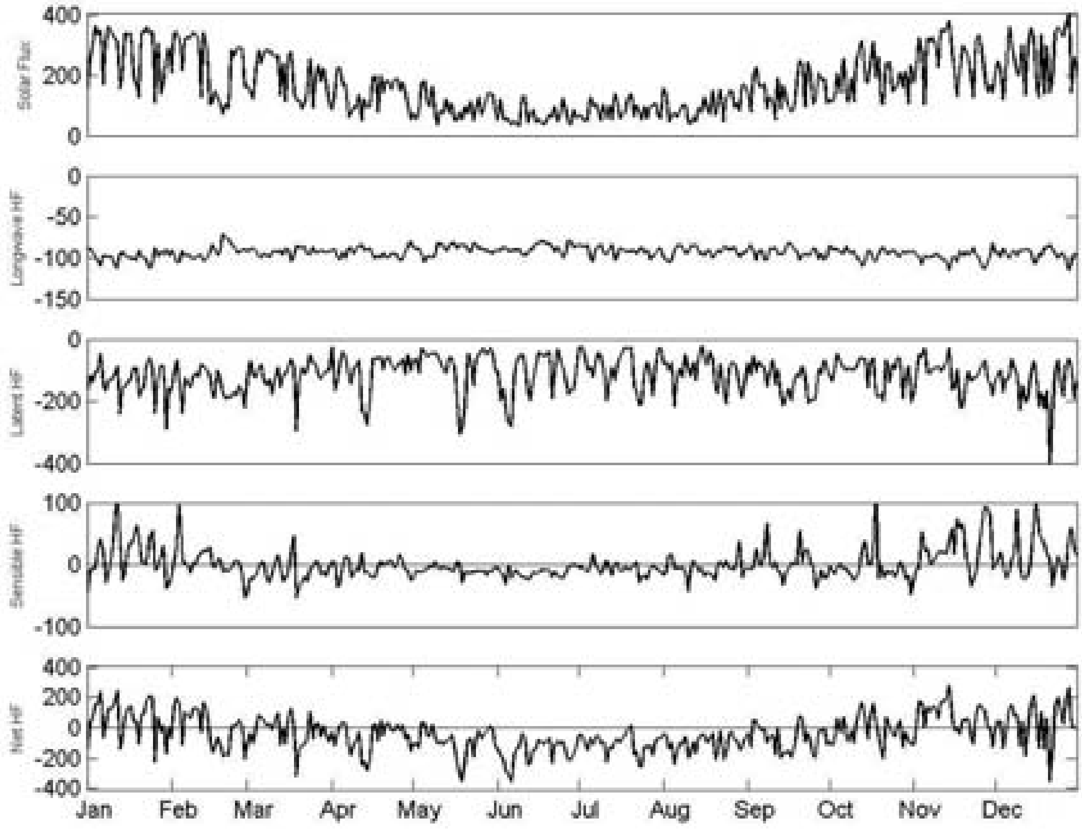

Figure 3.13: Time series of daily mean air-sea fluxes estimated using meteorological data and sea surface temperature measured at Port Stanvac in 2004.

3.3.4 Point source discharges

Specification of point source discharges into the coastal region of the Adelaide coastal waters is critical to the ACWS. To examine the effects arising from historical, present, and future discharges of freshwater, nutrient, and sediment transport patterns on changes in seagrass and suspended matter distribution, it is important to specify not only the current discharges (2004), but also the historic and future discharges. Outputs from the ACWS task IS 1 (Wilkinson 2003; Wilkinson et al., 2005) provided data, which were used for the specification of the point source discharges. Peter Christy of the EPA (SA) supplied the data for the Port River region. The point source discharges into the Adelaide coastal zone arise from three main sources: rivers, wastewater discharges, and stormwater discharges. The location of each of the inputs to the coastal region is shown in Figure 3.14.

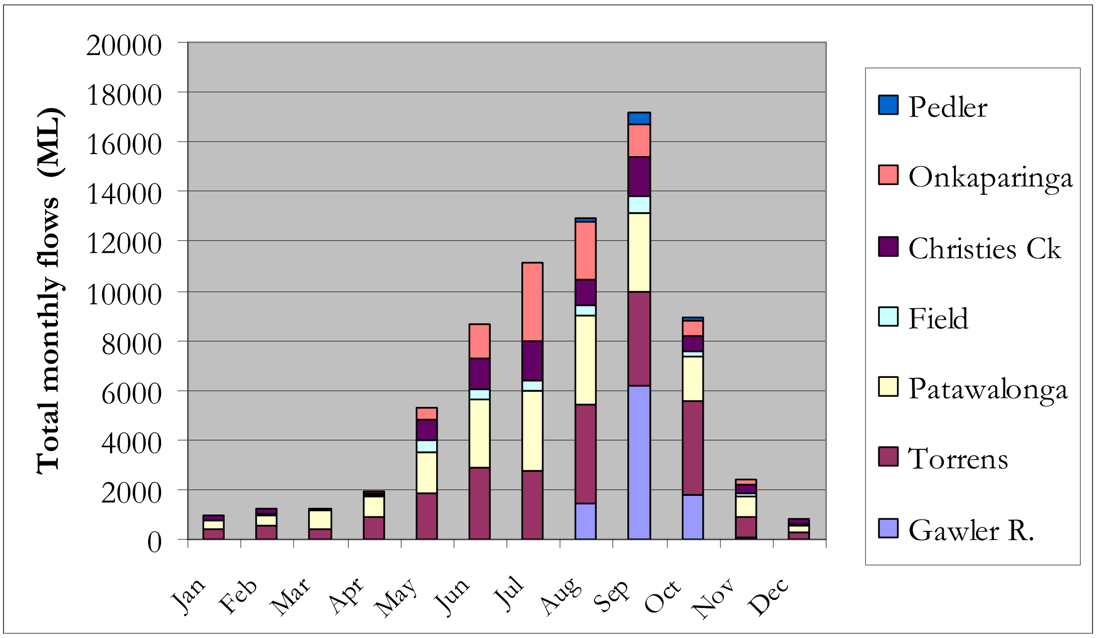

Figure 3.14: The seasonal pattern in river discharges to the Adelaide coastline, showing summed mean monthly discharge for selected major rivers and creeks.

Rivers

The main rivers include Gawler River, Port River, Torrens River, Patawalonga River, Field River, Christies Creek, Onkaparinga River, and Peddler Creek. The characteristics of each of these catchments are presented in Table 3.3. Wilkinson (2005) developed a rainfall-runoff model, which was used to specify the discharges from the rivers. The seasonal patterns in river discharges for selected major rivers and creeks are shown in Figure 3.14, and indicate the highest discharges occurred during September and the lowest discharges during February. The time series of freshwater discharge, suspended sediment concentration, and the sediment load, used for model runs are given in Figures 3.16 to 3.21. Here, the rainfall values (figures 3.3 and 3.4) were used through a rainfall-runoff model (Wilkinson, 2005) to specify the discharges from each river.

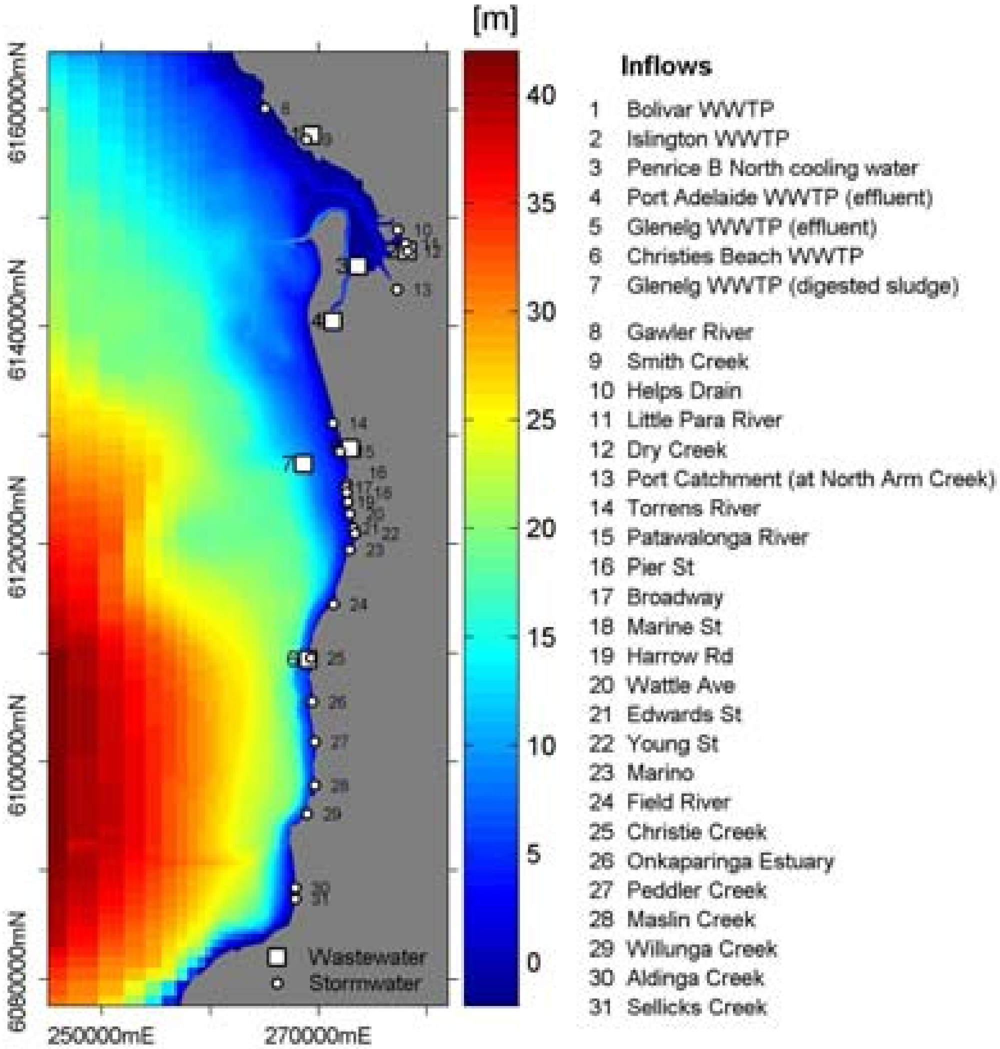

map_model_inflows

Figure 3.15: Locations of Point source discharges into the Adelaide Coastal Waters

Table 3.3. Mean annual discharge, catchment area, and runoff per unit area for selected major rivers and creeks in the ACWS area (Wilkinson, 2005)

	Effective catchment area (km^2)	Mean annual flow (GL)	Catchment yield (ML/km^2 = mm)
Gawler River[1]	883.0	10.3	11.7
Smith Creek[2]	205.6	5.2	25.3
Barker Inlet[2]	407.8	10.3	25.3
R. Torrens[3]	218.5	22.4	102.6
Patawalonga[3]	212.4	19.7	92.6
Holdfast drains[2]	8.8	2.1	239.1
Field River[1]	36.2	2.8	77.3
Christies Creek[1]	37.8	8.1	214.3
L. Onkaparinga[4]	138.7	9.5	68.5
O. Estuary[2]	28.2	5.6	197.5
Southern Creeks[5]	244.9	2.3	9.5

1. Annual mean of flows for April 2001 to April 2003. 2. Estimated from rainfall and volumetric runoff coefficients. 3. Average data for October 1994 to November 2003. 4. Modelled data for October 1994 to November 2003. 5. Flow in Pedler Creek at Stump Hill Road for April 2001 to April 2003 multiplied up to total southern creek catchment area. Note: Ten-year flows are consistent with the two-year flow period of 2001/3.

Wastewater discharges

There are three main wastewater discharges at Bolivar, Port Adelaide, Glenelg, and Christies Beach. Again, data collated from (Wilkinson et al., 2003) as monthly means were used to specify the discharges. The time series of freshwater discharge, suspended sediment concentration, and the sediment load are given in Figures 3.16 to 3.21.

Stormwater discharges

Holdfast drains is the main region for stormwater discharges, which includes seven main drains, as listed in Table 3.4. Similar to river inputs, the rainfall-runoff model developed by Task IS1 (Wilkinson, 2005) was used to specify the discharges from the drains. The time series of freshwater discharge, suspended sediment concentration, and the sediment load are given in Figures 3.16 to 3.21. Here, the rainfall values (figures 3.3 and 3.4) were used through a rainfall-runoff model (Wilkinson, 2005) to specify the discharges from the storm water drains.

Table 3.4. Catchment area and estimated mean annual flow for the Holdfast drains (Wilkinson, 2005)

Drain	Area (km^2)	Mean annual flow (ML)	Annual flow 1981–87
Pier St	1.237	269.7	
The Broadway	0.964	210.2	
Marine St	0.838	182.7	
Harrow Rd	2.254	491.4	
Wattle Ave	0.810	176.6	
Edwards St	2.177	474.6	300.0
Young St	1.169	424.8	587.5

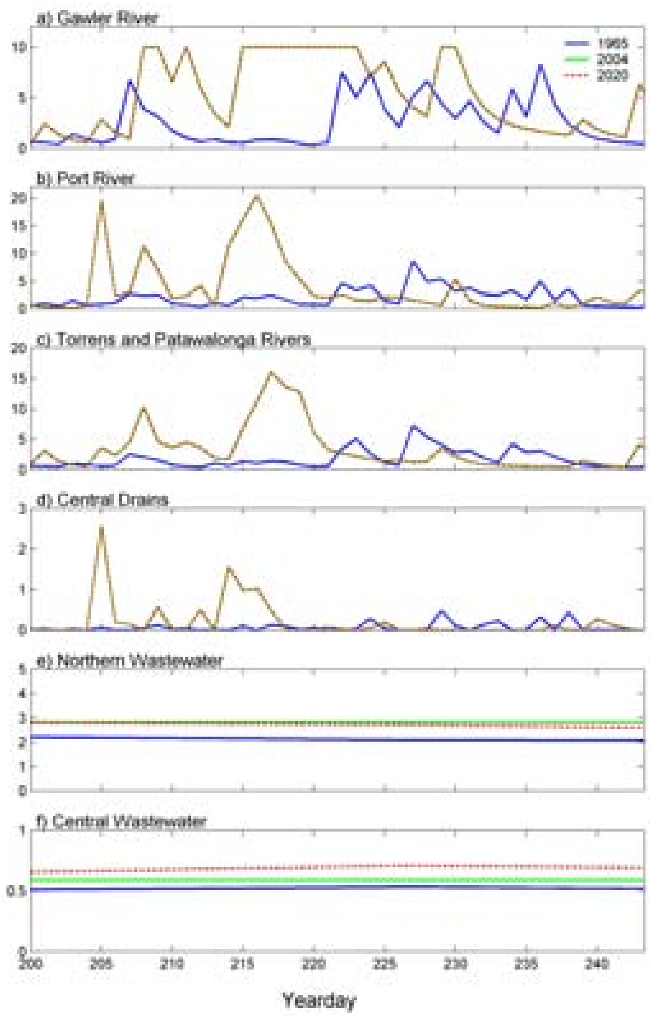

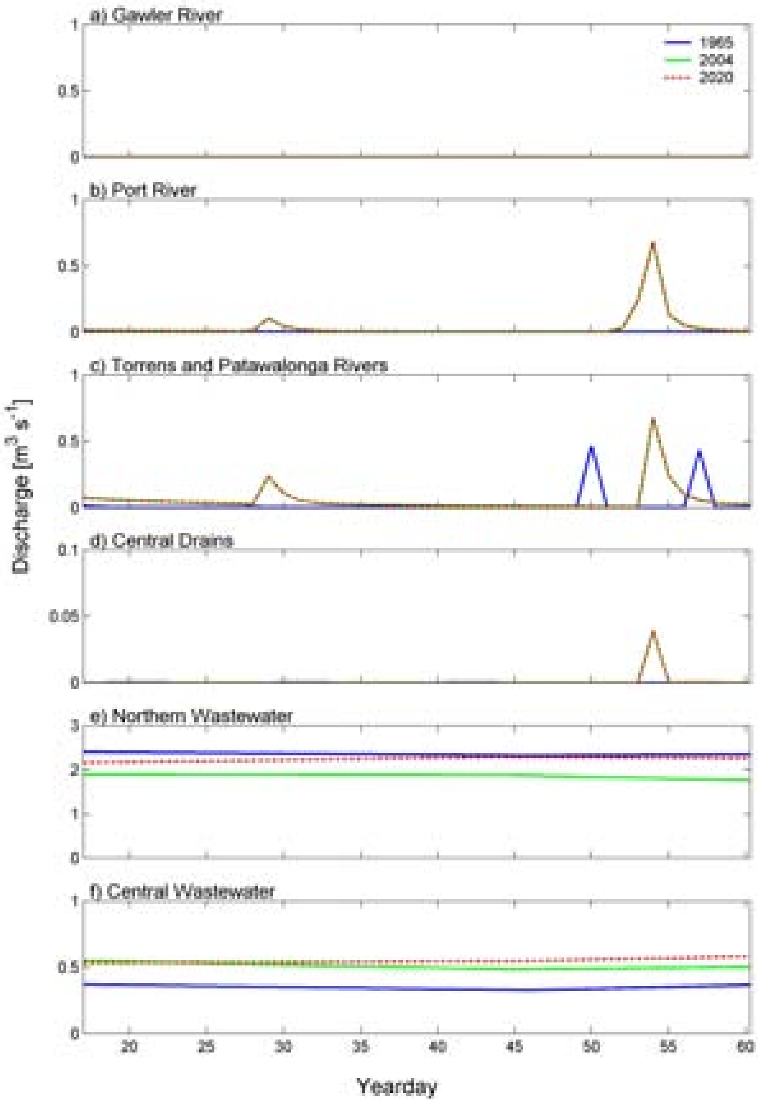

Figure 3.16: Time series of freshwater discharges from point sources for winter.

Figure 3.17: Time series of freshwater discharges from point sources for summer

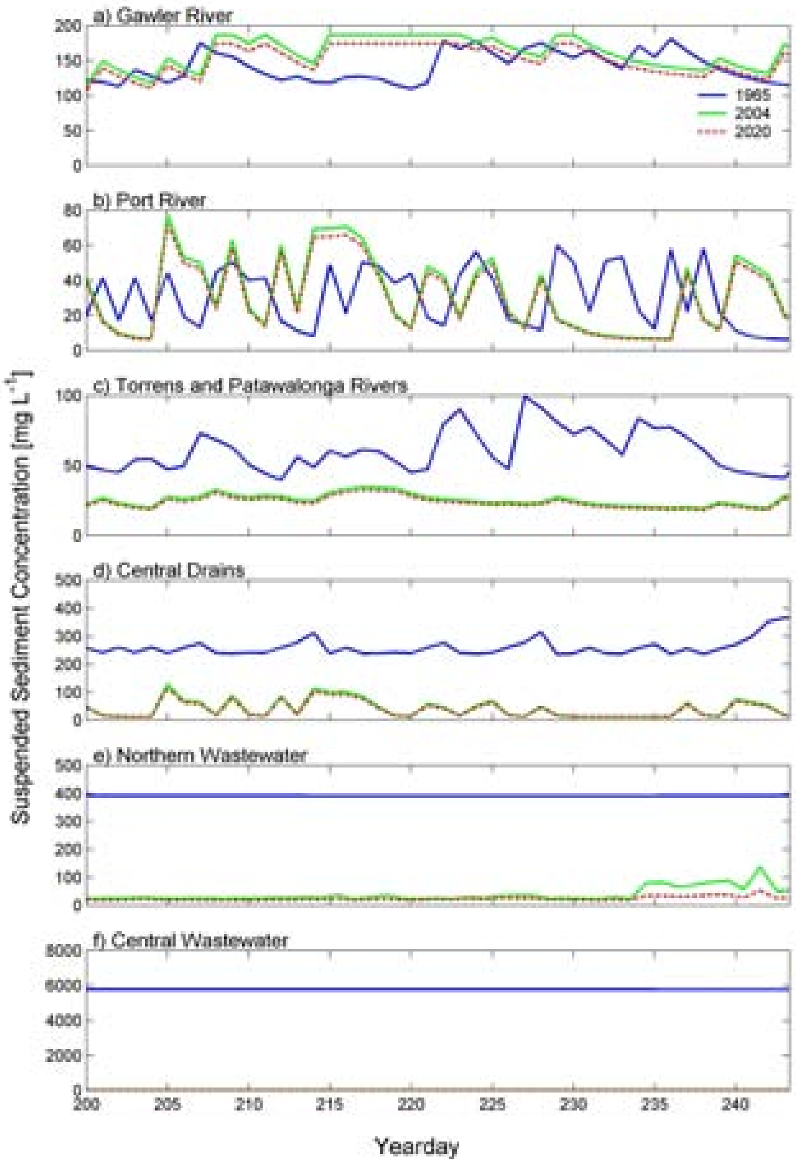

Figure 3.18: Time series of suspended sediment concentration from point sources for winter.

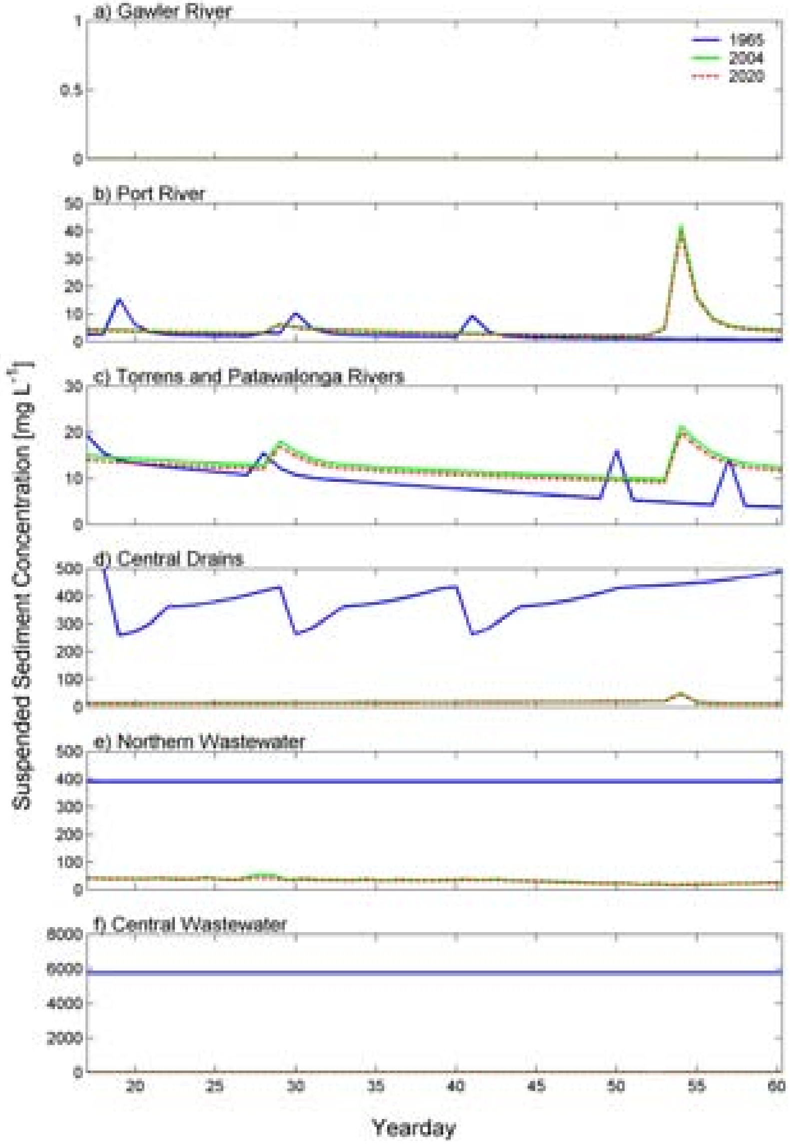

Figure 3.19: Time series of suspended sediment concentration from point sources for summer.

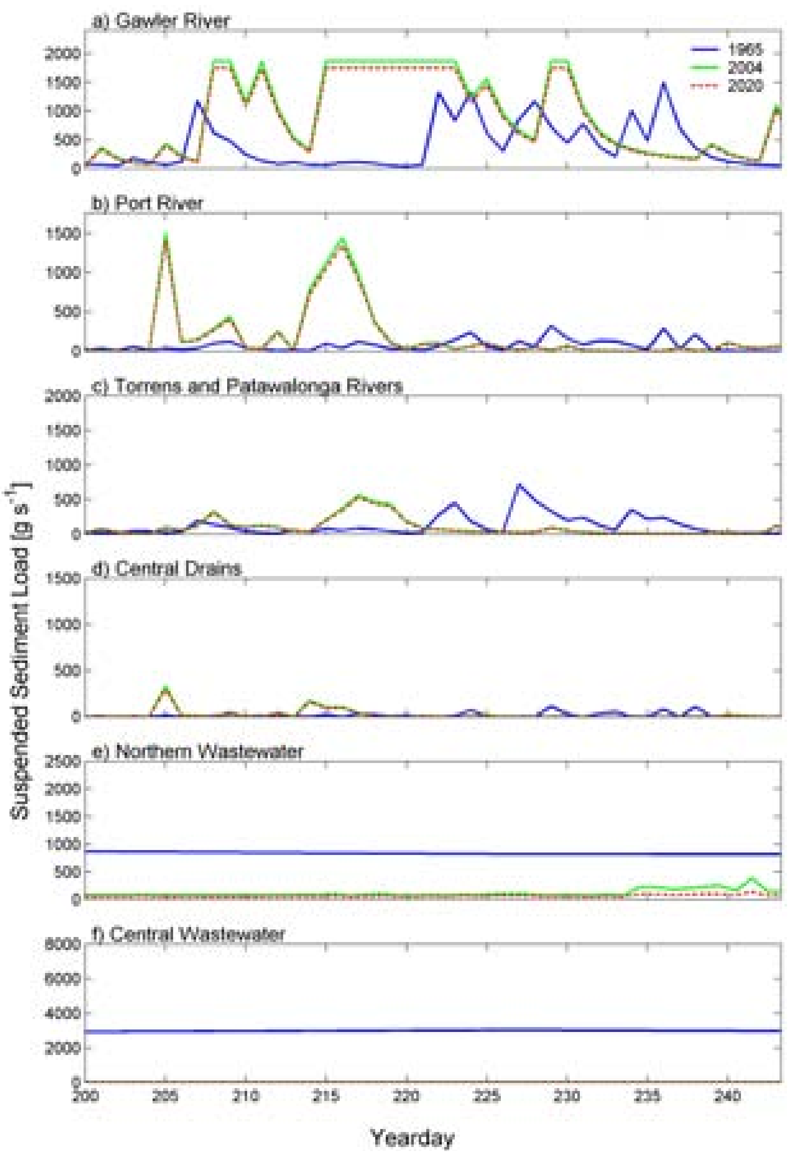

Figure 3.20: Time series of suspended sediment load from point sources for winter.

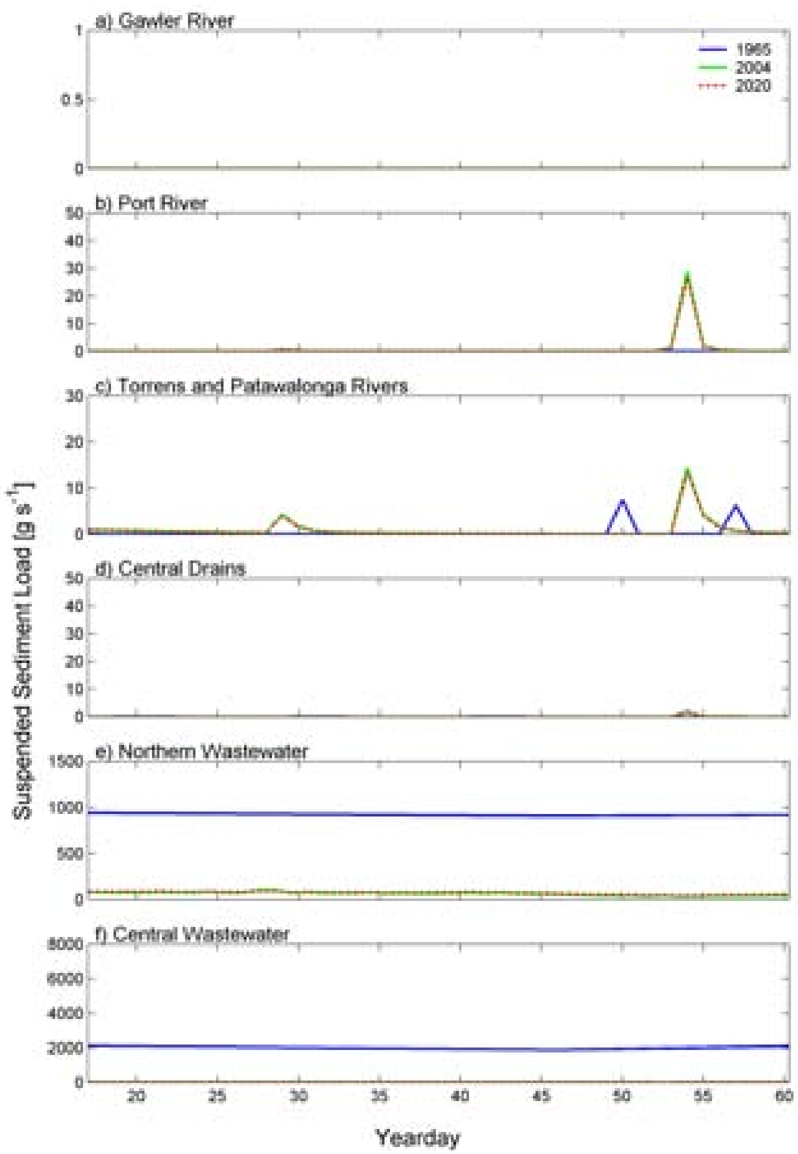

Figure 3.21: Time series of suspended sediment load from point sources for summer.

3.3.5 Sediment resuspension and transport

The sediment transport model was implemented on the same grid as the hydrodynamic model and calculated the total load under the influence of the local hydrodynamic conditions. These values formed the source term (equation 3.6) for sediment re-suspension from the sea bed. The formulae of van Rijn (1984) were chosen to predict the sediment resuspension and the vertical sediment profile through the water column. The bottom stress, one of the most important driving forces, is calculated by a bottom boundary layer model. The resulting stress is then used in the bottom boundary condition for the sediment transport model. The effect of wave–current interaction on the bottom shear stress is calculated based on the concept of Grant and Madsen (1979) in an iterative form. The maximum bottom stress, $\tau_{b,\max}$, for a wave–current combination is defined as:

$$\tau_{b,\max} = \frac{1}{2} f_{cw} \rho \left[U_m^2 + u_c^2 + 2U_m u_c \cos\phi_c \right] \qquad (3.12)$$

in which ρ is the water density, f_{cw} is an effective friction factor, U_m is the maximum near bottom wave orbital velocity determined from linear wave theory (from parameters provided from the wave module), u_c is the mean bottom current (predicted from the hydrodynamic module), and ϕ_c is the angle between wave propagation and current direction.

The non-cohesive suspended sediment concentration c_a at reference level $z = a$ above the bed is given by van Rijn (1989):

$$c_a = 0.015 \frac{D_{50}}{a} \frac{T}{D_*^{0.3}} \qquad (3.13)$$

Here, T is the bed shear stress parameter, $T = (\tau_b - \tau_{bc}) / \tau_{bc}$, where τ_b is the effective bed shear stress under the combined action of waves and currents, which can be calculated using the approach given in the previous section, and $\tau_{b,cr}$ is the Shields critical bed shear stress for sediment suspension. D_* is the non-dimensional sediment diameter:

$$D_* = D_{50} \left(\frac{(s-1)g}{\nu^2} \right)^{\frac{1}{3}} \qquad (3.14)$$

Usually, the horizontal diffusion effects in sediment mixing are small when compared with the vertical diffusion. Here, a constant horizontal diffusion coefficient has been assumed. Only the vertical diffusion coefficient for sediment particles is calculated. The sediment particle diffusion is different from fluid diffusion because of different effective particle mixing lengths, the diffusion rate, and the damping effect. However, for most practical situations where suspended sediment transport is the main mode of motion ($ws/u_* << 1$, where u_* is the bed shear velocity) and sediment concentration is relatively low, the sediment mixing coefficient can be estimated by the fluid diffusion.

Van Rijn (1986) proposed the following three-layer wave diffusion coefficient:

$$\varepsilon_w = \begin{cases} \varepsilon_{w,\text{bed}} = 6.5 \times 10^{-4} \alpha_b \delta D_*^2 u_{\text{orb}} & z \le \delta \\ \varepsilon_{w,\max} = 3.5 \times 10^{-2} \alpha_b \dfrac{hH_s}{T} & z \ge 0.5h \\ \varepsilon_{w,\text{bed}} + (\varepsilon_{w,\max} - \varepsilon_{w,\text{bed}}) \dfrac{z - \delta}{0.5h - \delta} & \delta < z < 0.5h, \end{cases} \qquad (2) \qquad (3.15)$$

in which ε_w is the wave-induced diffusion coefficient, $\varepsilon_{w,\text{bed}}$ is the wave-induced diffusion coefficient within the wave bottom boundary layer, $\varepsilon_{w,\max}$ is the maximum wave-induced diffusion coefficient, which applies to the upper half of the water column, δ is the thickness of the near bed mixing layer (or wave bottom boundary layer thickness), h is the water depth, H_s is the significant wave height, T is the peak wave period (T_p), u_{orb} is the near bottom orbital velocity and were were calculated from the wave module. α_b is the wave breaking coefficient, given by (van Rijn, 1990):

$$\alpha_b = 3\left[\frac{H_s}{h}\right] - 0.8 \qquad \text{for} \qquad \left[\frac{H_s}{h}\right] > 0.6$$

3.3.6 Wave-driven flows in the nearshore

When wind-generated waves arrive obliquely at a coastline and break at an angle to the beach, they generate a longshore current flowing parallel to the shoreline. This current is confined to the nearshore and rapidly decreases in velocity beyond the breaker zone. Many theories have been devised to account for the generation of these currents and to forecast their magnitudes, but only after Longuet-Higgins and Stewart's (1964) introduction of the radiation stress concept (defined as the excess momentum due to the action of waves) in the1960s was the distribution of the longshore current velocity across the surf zone successfully predicted. Here, it was assumed that changes in wave height as the waves approached the shoreline and the breaking process released momentum, part of which was used in driving a mean current parallel to the shoreline. As the predominant wave direction for the Adelaide coastal waters region is from the south-west (Jones and Pattiaratchi, 2005), this process will drive a current adjacent to the shoreline in a northward direction. As most of the point source discharges (rivers and storm water inputs) are direct inputs into the surf zone, it was deemed imperative that the wave-driven flow in the nearshore region be included in the hydrodynamic model. As the existing ELCOM code did not include this feature, it was specifically included in this application for the Adelaide coastal waters.

It was assumed the longshore current was steady and independent of the longshore direction, y (within a grid cell), and that the beach had a uniformly sloping bottom. The x-axis and y-axis were taken to be normal and parallel to the shoreline, respectively. For obliquely incident waves, the longshore current is driven solely by the cross-shore gradient in the alongshore component of the radiation stress, S_{xy}. This gradient results from the dissipation of radiation shear stresses across the surf zone and is opposed by bed and turbulent friction. A simplified expression of this relationship, neglecting turbulent friction (negligible compared with bed friction) is:

$$\frac{\partial S_{xy}}{\partial x} = -\rho g(h - \bar{\eta})\left[\frac{v^2}{C^2 h}\right] \qquad (3.16)$$

where $\bar{\eta}$ is the time-averaged wave set-up, v is the longshore current, and C = 60 is the Chezy coefficient with the wave set-up and radiation stress computed by SWAN.

Wave-driven currents were incorporated into the ELCOM simulation by coupling the hydrodynamic model ELCOM and the wave model SWAN. The method adopted was similar to that incorporated into similar models, which included wave-driven currents, such as DELFT3D (Dingemans et al., 1987) and ADCIRC (Cobb and Blain, 2003). Here, the wave model SWAN was initially run for the duration of the ELCOM simulation (i.e. 45 days) on the same model grid using offshore swell and local winds to predict the wave climate (see Section 2). One output from the SWAN model was the radiation stress, and the gradients in the radiation stress over the whole computational grid were calculated (Section 2). The radiation stress gradients then became a surface stress forcing for ELCOM. It should be noted that the radiation stress was determined on the finite difference grid using the peak frequency of the wave frequency spectrum, thus treating the SWAN wave data as monochromatic. As swell waves mainly drove the longshore currents and generally consisted of a single peak period, this assumption was not expected to introduce significant errors to the estimate of longshore currents. Example time series of predicted longshore currents off Brighton Beach and the nearshore wave heights for summer and winter are presented in Figures 3.22 and 3.23, respectively. Although the magnitudes of the currents are of the same order as predicted from equations in the literature (e.g. SPM, 1983), no field data were available to validate the model directly.

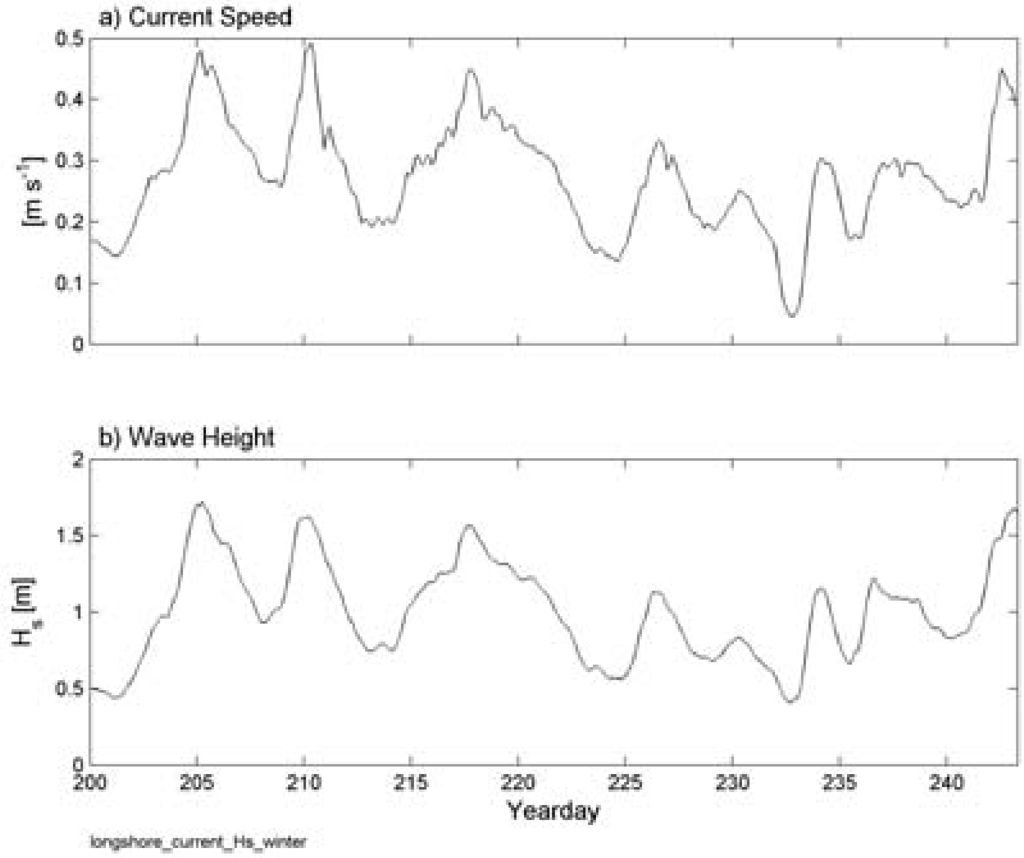

Figure 3.22: Time series of wave heights and predicted longshore currents off Brighton during winter.

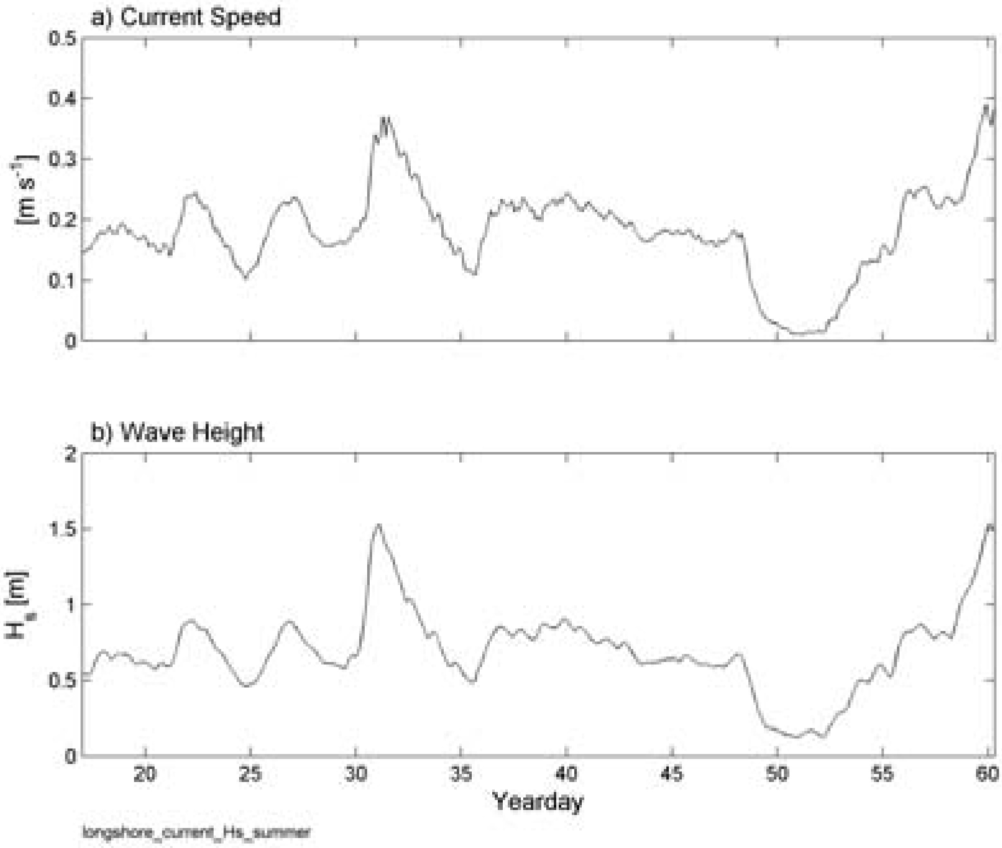

Figure 3.23: Time series of (a) predicted longshore currents and (b) wave heights and off Brighton during summer.

3.4 Hydrodynamic model validation

Field measurements of tidal elevations and currents were collected as part of task 1 (Kaempf, 2006) of the Adelaide Coastal Waters Study. The locations of the measurements are provided in Figure 3.24.

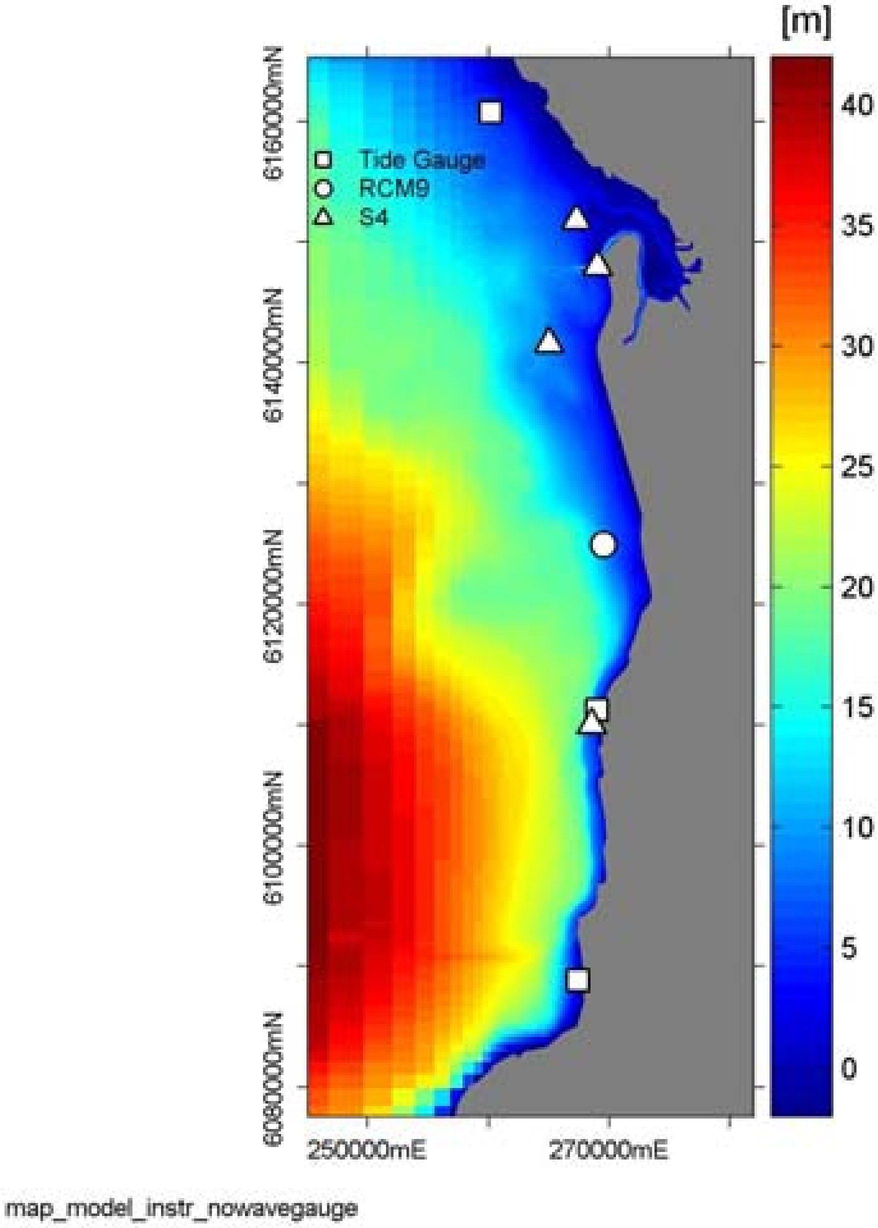

Figure 3.24: Location of time series measurements for validation of the hydrodynamic model. Tide gages were located at Port Stanvac, Sellecks Beach, Port Gawler, Semaphore, and Brighton.

3.4.1 Initial conditions

All the model runs were initiated as a ‘cold’ start such that all the velocities within the model were zero. The initial values of water temperature and salinity were set to be uniform throughout the model. The values of salinity and temperature for summer and winter, based on the field data collected through from Sub Task 1 of this project (Kaempf, 2006) are given in Table 3.5.

Table 3.5. Initial values of temperature and salinity for model scenario runs

Season	Temperature [°C]	Salinity
Summer	23.5	37.0
Winter	12.5	36.3

3.4.2 Water levels

The model domain consisted of many locations where tidal elevations were available for model validation (Figure 3.24). These included the permanent tide gauge at Port Stanvac, where the National Tidal Centre make continuous recordings and the gauges deployed as part of the ACWS with the aim of collecting data specifically for model validation. These latter gauges were located at Sellicks Beach, Port Gawler, Semaphore, and Brighton. The gauges at Sellicks Beach and Port Gawler were located close to the model boundary and were used to develop the boundary conditions for model forcing.

To validate the model predictions of tidal elevation with observations, the non-tidal components from both time series (i.e. measured and predicted) were initially filtered using a low-pass filter (half-power point = 36 hours), which removed all periods greater than the diurnal period. The resulting time series were then subjected to harmonic analysis to obtain individual tidal constituents.

Comparison between the observed and predicted time series for Port Stanvac indicated a high correlation (r^2 = 0.96), with similar results obtained for other locations (Figure 3.25). Port Stanvac also had a high correlation between observed and predicted tidal constituent amplitude and phase (Figure 3.26). Similarly, a good correlation existed between the observed and predicted tidal constituents at Sellicks Beach, Port Gawler, Semaphore, and Brighton (Figures 3.27 and 3.28). At Semaphore and Brighton, the model underestimated the M_2 and S_2 and overestimated the O_1 and K_1 tidal amplitudes.

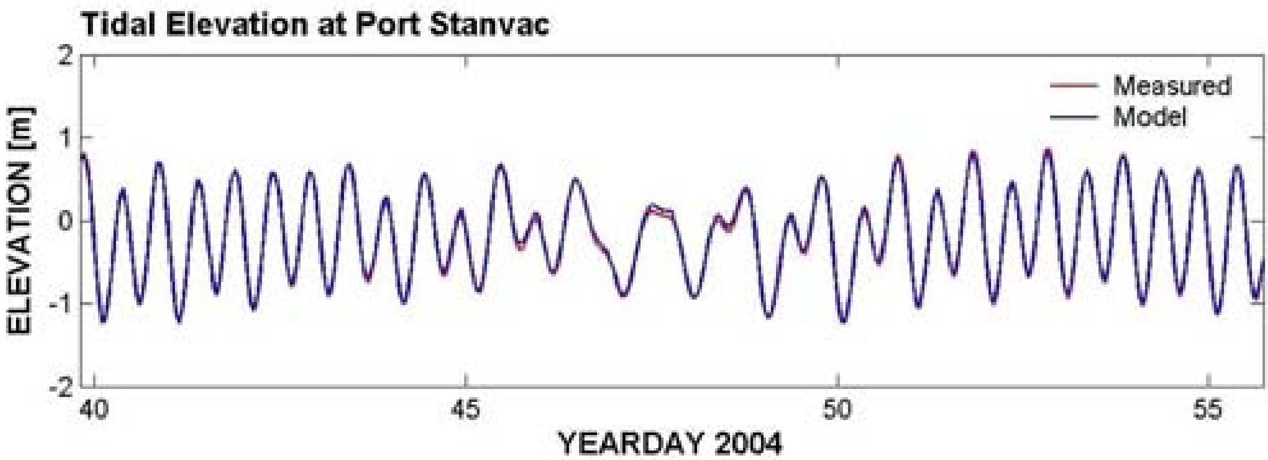

Figure 3.25: Time series of predicted and measured tidal elevation at Port Stanvac during the summer.

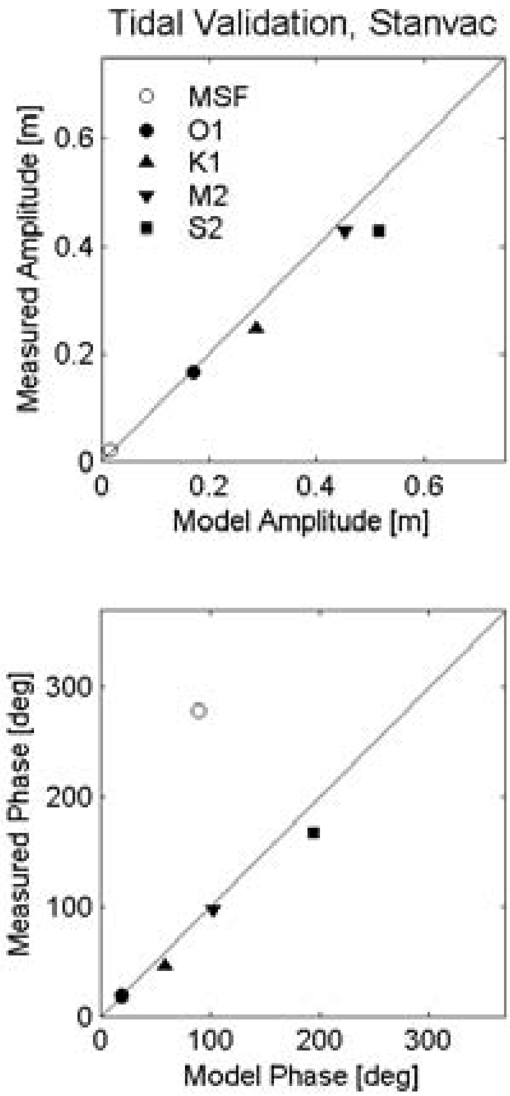

Figure 3.26: Comparison of measured and predicted tidal elevation characteristics (amplitude and phase of constituents) at Port Stanvac.

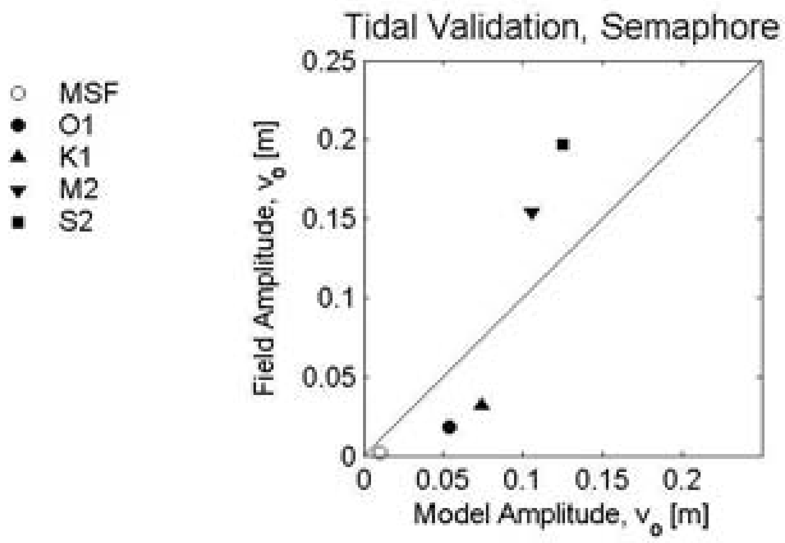

(a)

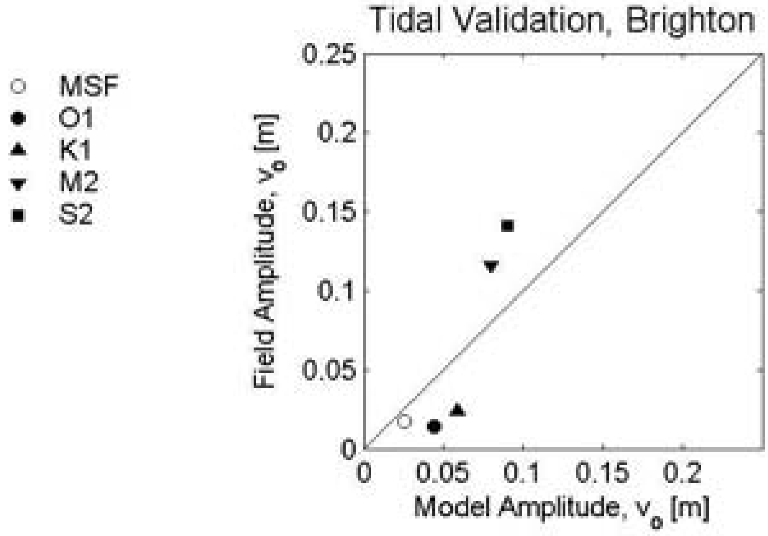

(b)

Figure 3.27: Comparison of measured and predicted tidal elevation characteristics (amplitude of constituents) at (a) Sellicks Beach and (b) Port Gawler.

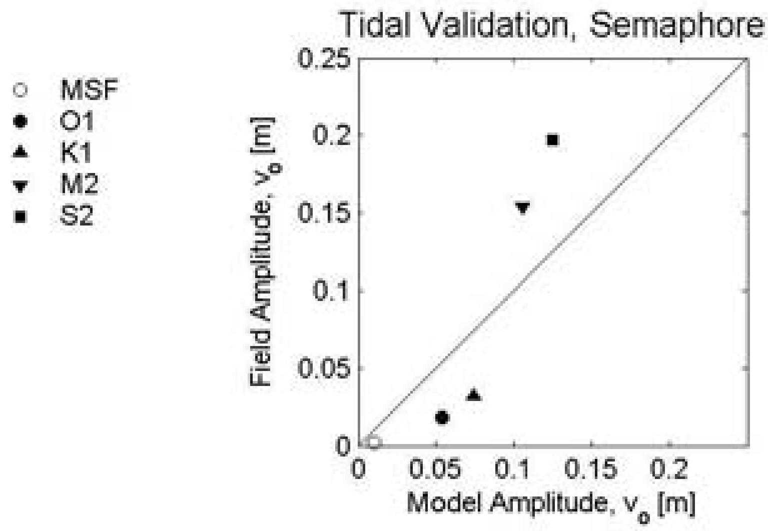

(a)

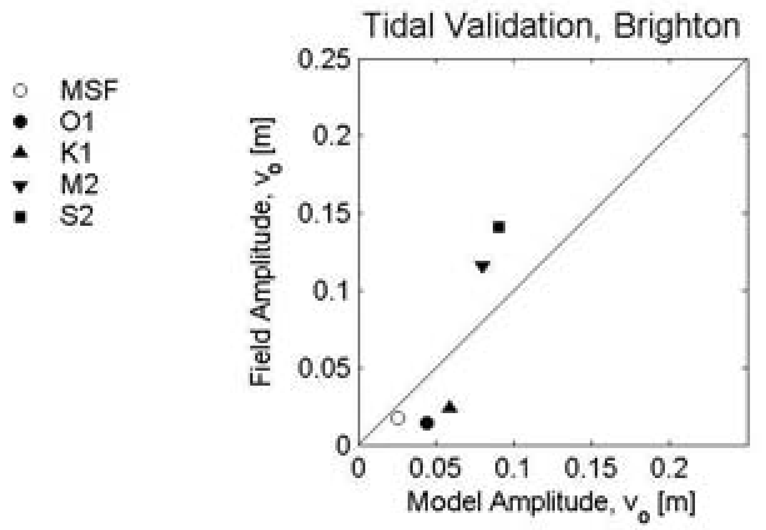

(b)

Figure 3.28: Comparison of measured and predicted tidal elevation characteristics (amplitude of constituents) at (a) Semaphore and (b) Brighton.

3.4.3 Currents

Similar to the tidal elevations, the model domain consisted of locations where currents were measured, as part of the ACWS, with the aim of collecting data specifically for model validation. These locations were Semaphore, Brighton, and Hallet Cove (Figure 3.24). The validation procedure for currents followed a similar approach to that for tidal elevations. Initially, the time series of current measurements were resolved into north-south (v) and east-west (u) components and then filtered to remove the non-tidal components from both time series (i.e. measured and predicted) using a low-pass filter (half-power point = 36 hours), which removed all periods greater than the diurnal period.

Comparison between the observed and predicted time series for the north-south (v) components at Semaphore, Brighton, and Hallet Cove (Figure 3.29) indicated a good overall correlation ($r^2 > 0.80$). However, the correlation between the measured and predicted currents was better during the spring tides when compared with the neap or dodge tides (Figure 3.29). There were also differences when compared with the location. The highest correlation was obtained at Brighton, the more ‘central’ location. At the northern station (Semaphore) the model slightly over-predicted the measured values; at the southern station (Hallet Cove) the model slightly under-predicted the measured values (Figure 3.29).

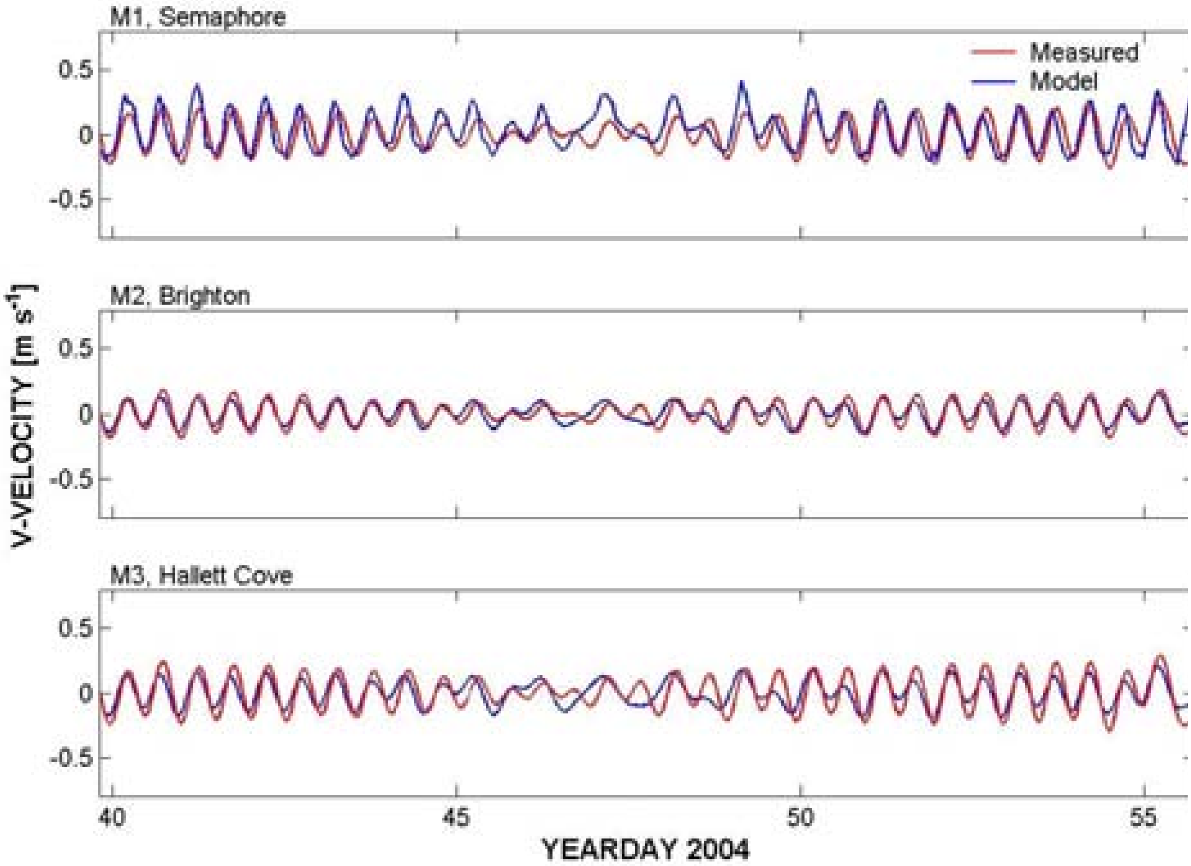

Figure 3.29: Time series of predicted and measured v-component (north-south) of tidal currents at Semaphore, Brighton and Hallett Cove during the summer

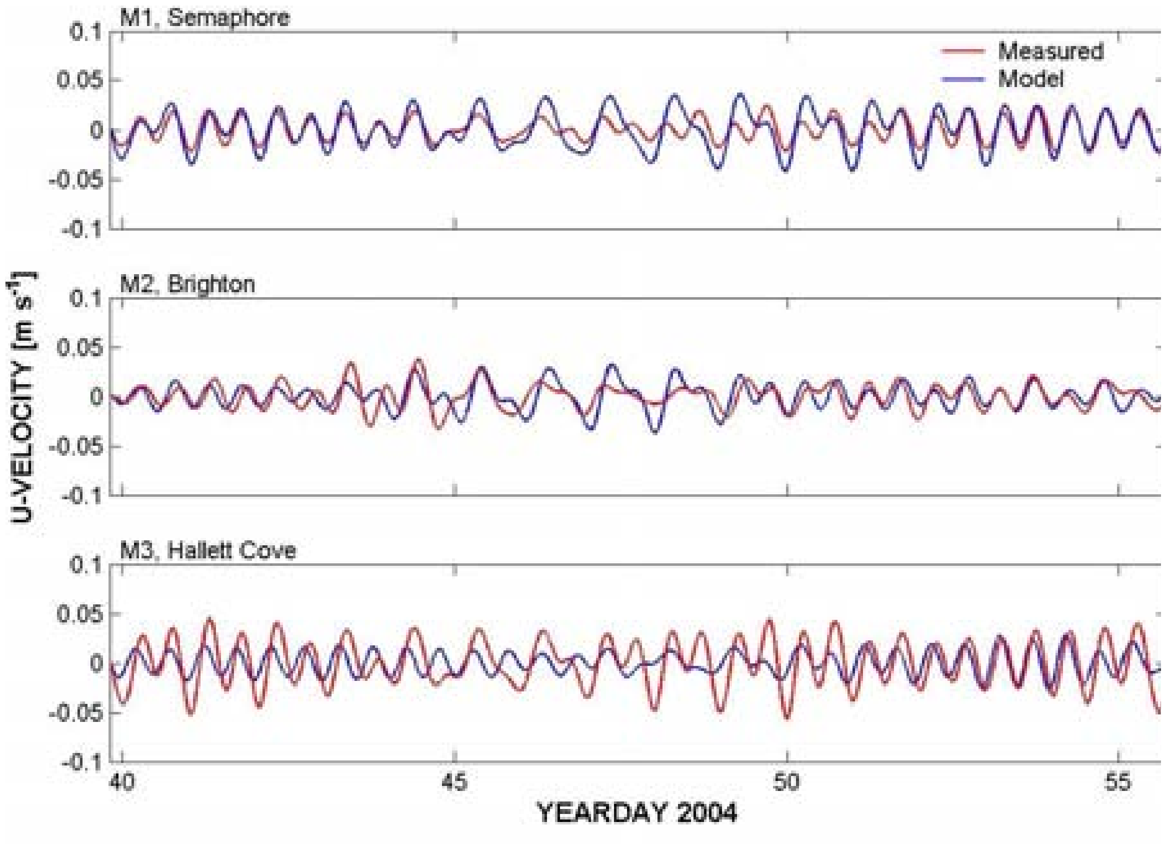

Figure 3.30: Time series of predicted and measured u-component (east-west) of tidal currents at Semaphore, Brighton and Hallett Cove during the summer

The measured and predicted east-west components were both small (< 0.05 ms^{-1}), and although the comparison between them is reasonable—due to the accuracy of the measurements ($\pm$0.03 ms^{-1}) being close to the measured values—no meaningful statistical measures were possible. However, a similar pattern to that observed for the north-south components was also observed, i.e. better correspondence at spring tides, over-prediction at the northern station, and under-prediction at the southern station.

3.4.4 Comparison with aerial imagery

The Adelaide Coastal Waters Study region includes the Port River Barker Inlet system, located towards the northern section of the model domain. The system includes two openings to the coastal waters: (1) the northern entrance, which connects Barker Inlet—a shallow region with large areas of inter-tidal flats; and, (2) Port River, with a relatively narrow entrance and consisting of a shipping channel dredged to a depth > 15 m. The entrance to Port River also has structures (breakwaters), which act to direct the flow along the dredged shipping channel. Aerial photos and remotely sensed data (Figure 3.31) showed that the water exiting Port River during the ebb tide formed an eddy (or gyre) at the entrance; here, the higher suspended sediments in the water exiting Port River acted as a passive tracer to indicate the circulation pattern. The eddy's presence also had an influence on the bottom habitat: bare sand and an absence of seagrass characterised the seabed in the region of the eddy (Figure 4.6), perhaps reflecting the effects of the sediment-laden plume on the bottom light climate. The development of this feature was examined in the model output, as it may form an important link in the transfer of material between the Barker Inlet/Port River system and the metropolitan coastal waters, and also as a qualitative measure of the model performance to reproduce observed features of the study region.

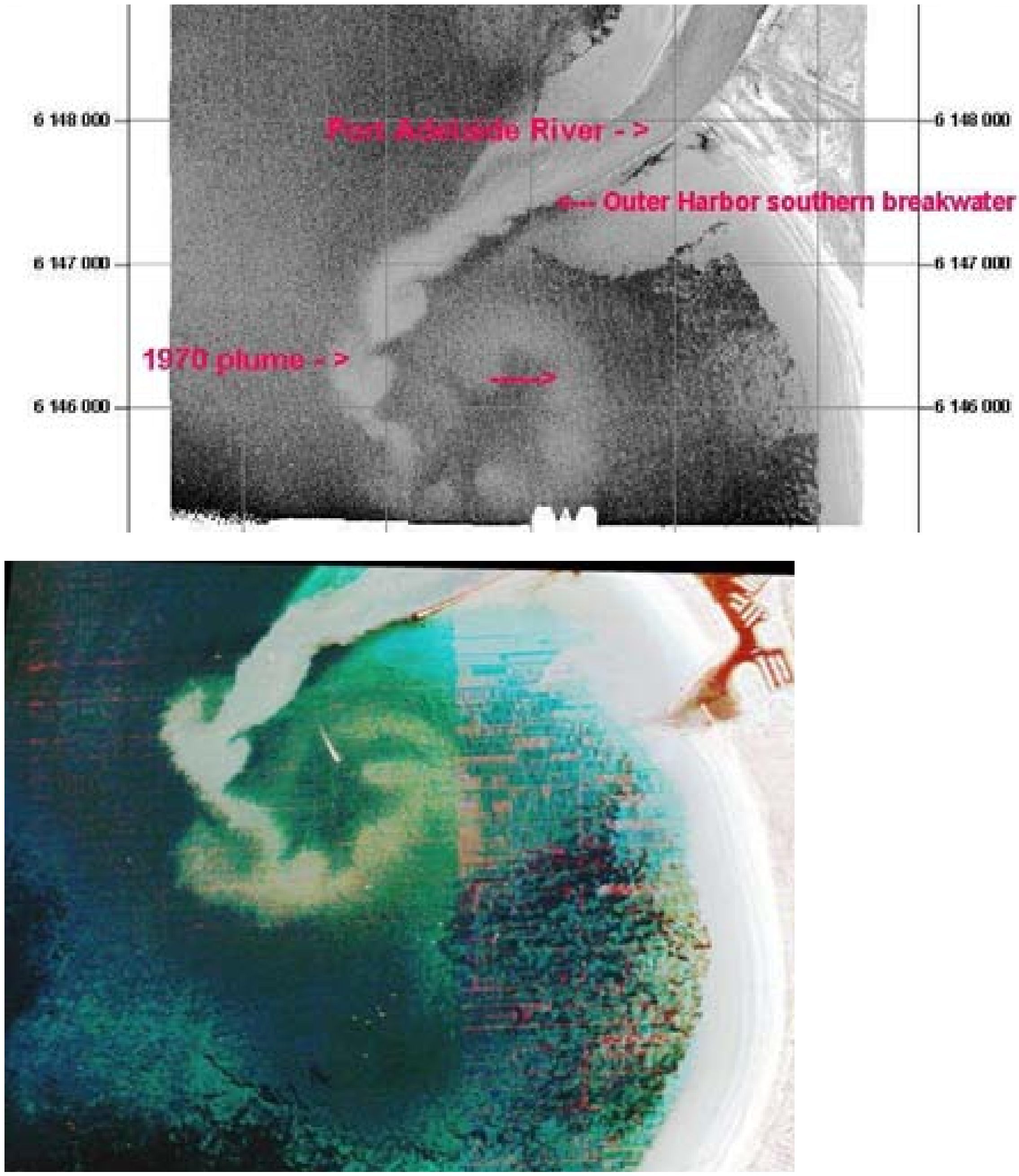

Figure 3.31: (a) An aerial photo taken in 1970; and (b) CASI data in 2004 showing the existence of an eddy at the entrance to Port River.

To illustrate the eddy's development at the Port River mouth, a time series of suspended sediment concentration at three-hourly intervals over a 24-hour period (two tidal cycles) is shown in Figure 3.32. The model was run under present-day (2004) winter conditions (Run 4, Table 5.1) and included forcing by tides, winds, and point source discharges. The model output sequence began during the tide's ebb stage (Figure 3.32a), where the higher suspended sediment concentration (SSC, derived from the point source discharges) exiting Port River and forming an anti-clockwise eddy was evident and comparable to the observations (Figure 3.31). The lower eddy also entrained lower SSC water, which the ebb currents transported southwards (Figure 3.31). Three hours later (Figure 3.32b), the ebb tide was still continuing and the eddy was still present, but the higher SSC from Port River now extended into the coastal waters. After another three hours (Figure 3.32c), the tide had changed, with the currents flowing north (flood tide); this had the effect of moving the plume and the associated eddy northwards. A further three hours later, the flood tide was still active, the plume was still deflected to the north of the mouth, and there was a flow of lower SSC into Port River (Figure 3.32d).

In the next stage, 12 hours into the sequence, the tide had started to ebb (Figure 3.32e), with plume transported southwards and present at the Port River mouth. As the tide continued to ebb (Figures 3.32f and g), the eddy began reforming; here, the ebb tidal currents deflected southwards the higher SSC water exiting Port River, which was entrained into the eddy. As the ebb continued, the water was advected farther southwards, the higher SSC was mixed with the coastal waters, and the eddy signature was absent (Figures 3.32h and i).

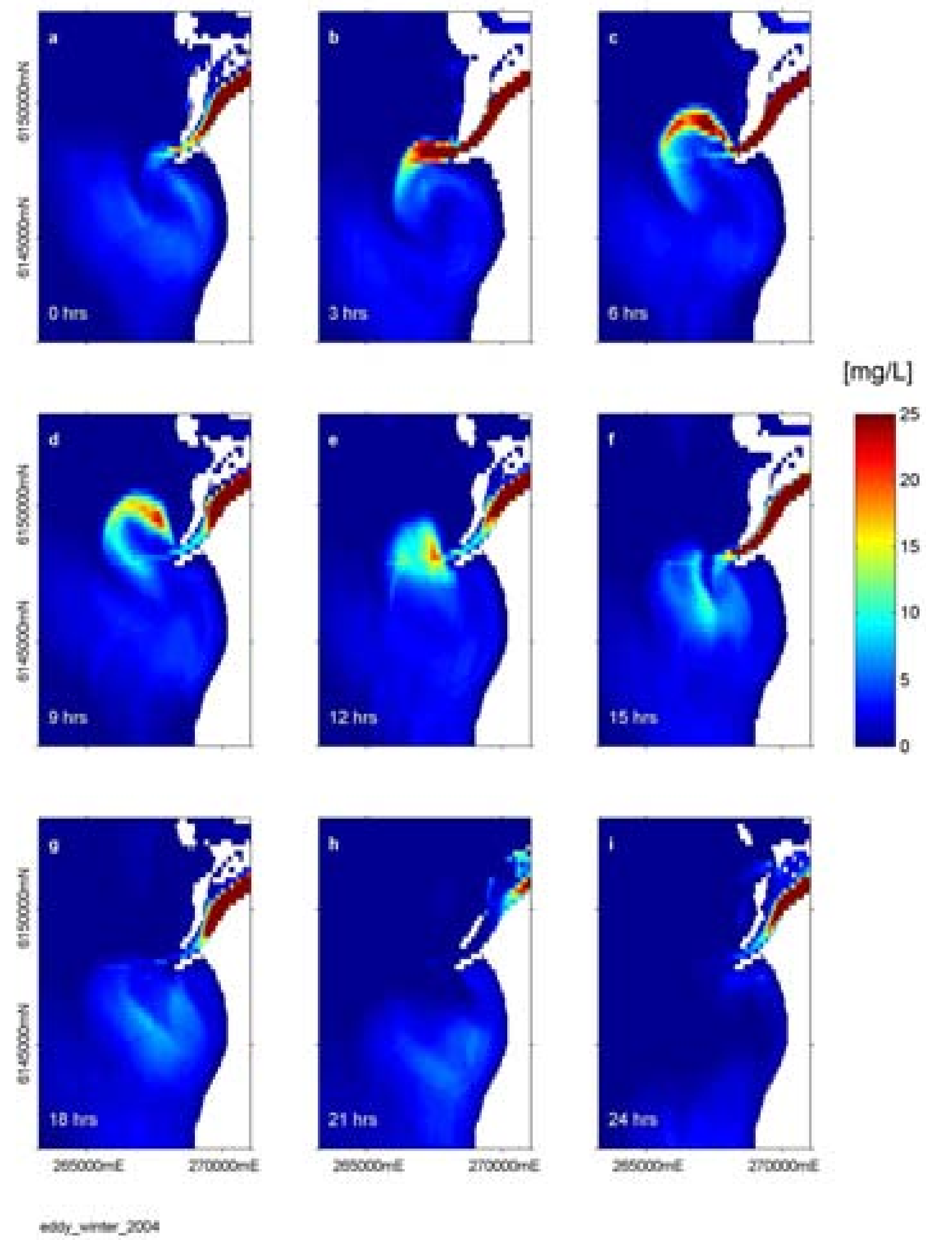

Figure 3.32: Time series (every 3 hours) of the suspended sediment concentration over a 24 hour period showing the development of the eddy at the mouth of Port River during the ebb tide.

The sequence of model outputs (Figure 3.32) showed the model was capable of reproducing the eddy observed at the Port River mouth during the ebb tide and also provided an insight into the eddy dynamics.

4. Surface wave modelling of the Adelaide coastal waters

4.1 Introduction

In this study, the modelling of surface waves was undertaken to: (1) input to the sediment transport module to calculate wave-induced sediment resuspension (Section 3.3.5); (2) input radiation stress values to the circulation model as a forcing mechanism for (nearshore) wave-induced longshore currents (Section 3.3.6); and, (3) estimate bottom shear stress and the percentage exceedance of critical shear stress within the model domain (Sections 2.7 and 2.8). The latter was undertaken to obtain a measure of the seabed mobility within the study region. In this section, the study region's wave climate is briefly presented as output from the model together with the results of the bottom shear stress and the percentage exceedance of critical shear stress studies. The wave-induced sediment resuspension and nearshore currents are included in the overall results of the circulation model and will not be presented separately.

The numerical wave model SWAN (Simulating WAves Nearshore) was applied and validated for the study region (Section 2). The model inputs were bathymetry, offshore swell conditions (wave period, height and direction), wind speed and direction from Adelaide Airport and water levels from Port Stanvac. Note that Brighton water levels were used for model validation (section 2.6) and were limited to the period of data collection. For the production runs (6 week runs for the hydrodynamic model and annual runs for the percentage exceedance) the water level data from Port Stanvac was used. The model outputs were significant wave height, wave period, wave direction, and near bed orbital velocity.

4.2 Mean and seasonal wave climate—Gulf of St Vincent

The mean annual significant wave heights and direction are shown in Figure 4.1. The main source of wave energy propagation into the Gulf is through the Investigator Strait. The wave energy propagates in an easterly direction into the Gulf, diminishing in height relative to the distance of propagation. The areas of greatest sheltering are located in the lee of Kangaroo Island and at the Gulf head, approximately 160 km north of the opening. Significant levels of wave energy are incident upon the western coast of the Gulf; however, the level of intensity decreases in the northerly direction, resulting in relatively limited conditions occurring offshore from Adelaide.

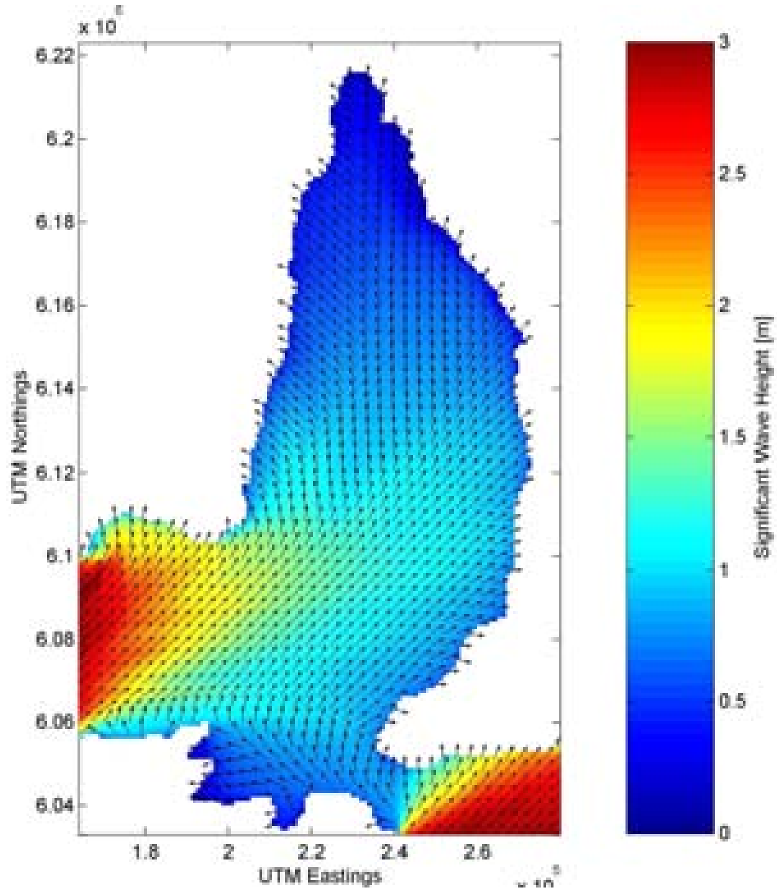

Figure 4.1: Annual mean significant wave height and direction for the Gulf of St Vincent.

The seasonal variation in the prevailing wave conditions is significant and is represented in Figure 4.2. During September (Figure 4.2a), the level of wave energy propagation into the Gulf is higher due to the higher energy wave conditions in the Southern Ocean that are experienced through the winter and early spring; the passage of high energy storm fronts through a subtropical ridge of high pressure located to the south of Australia produces these conditions. In contrast, the amount of swell energy present in the Gulf during March is relatively low, as during summer, the subtropical high-pressure ridge that contains the storms responsible for the high energy conditions during winter moves farther southwards.

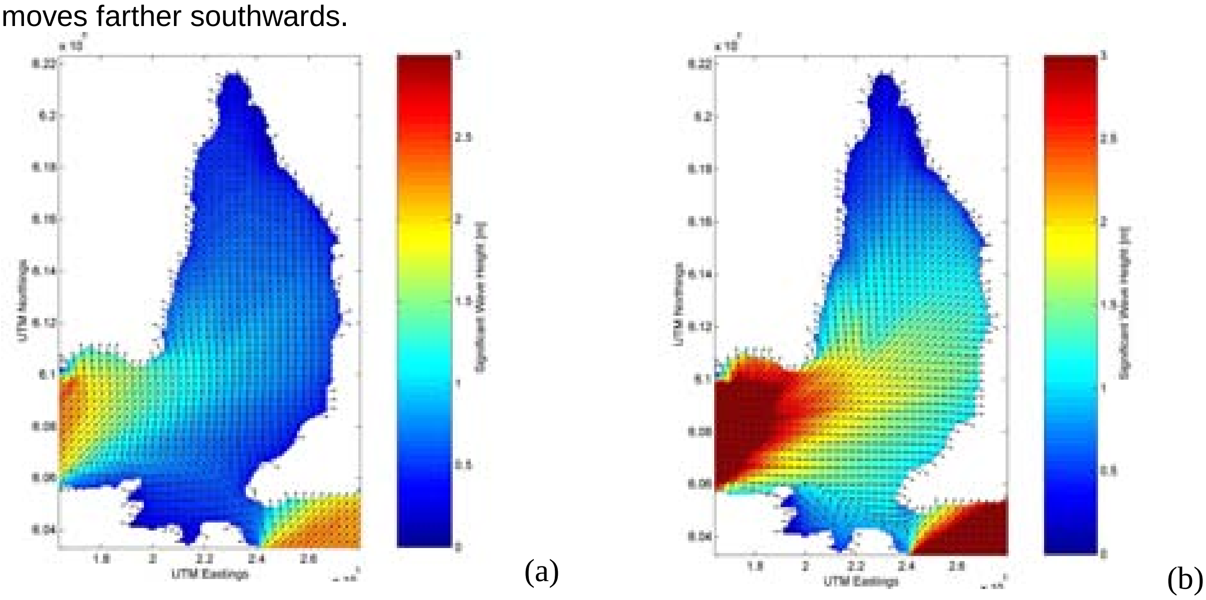

Figure 4.2 (a & b): Mean significant wave heights and direction for the Gulf of St Vincent for (a) March and (b) September 2004.

4.3 Mean and seasonal wave climate—ACWS domain

The mean annual significant wave heights and directions for the ACWS region indicated a reduction in the significant wave heights from south to north, while the directions also changed from a predominantly westerly direction in the south to south-westerly in the north (Figure 4.3). Along the region, the mean annual nearshore wave heights ranged from 1.2 to 1.5 m in the south to < 0.6 m in the north. Because of refraction effects offshore, there was also a concentration of wave energy in the nearshore region of Brighton (Figure 4.3).

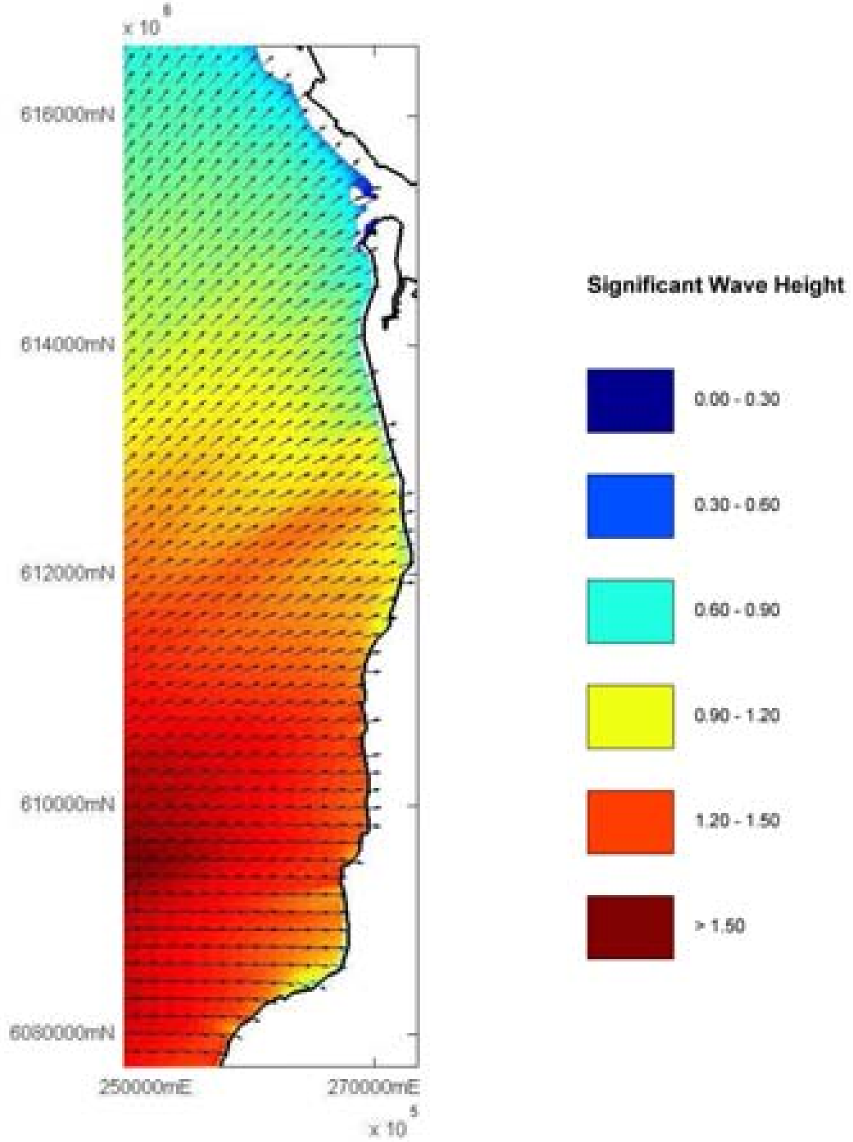

Figure 4.3: Annual mean significant wave height and direction for the Adelaide Coastal Waters region.

The seasonal change in wave climate indicated that during September the wave heights were larger when compared with those predicted for March; there was no change in the prevailing wave directions (Figure 4.4).

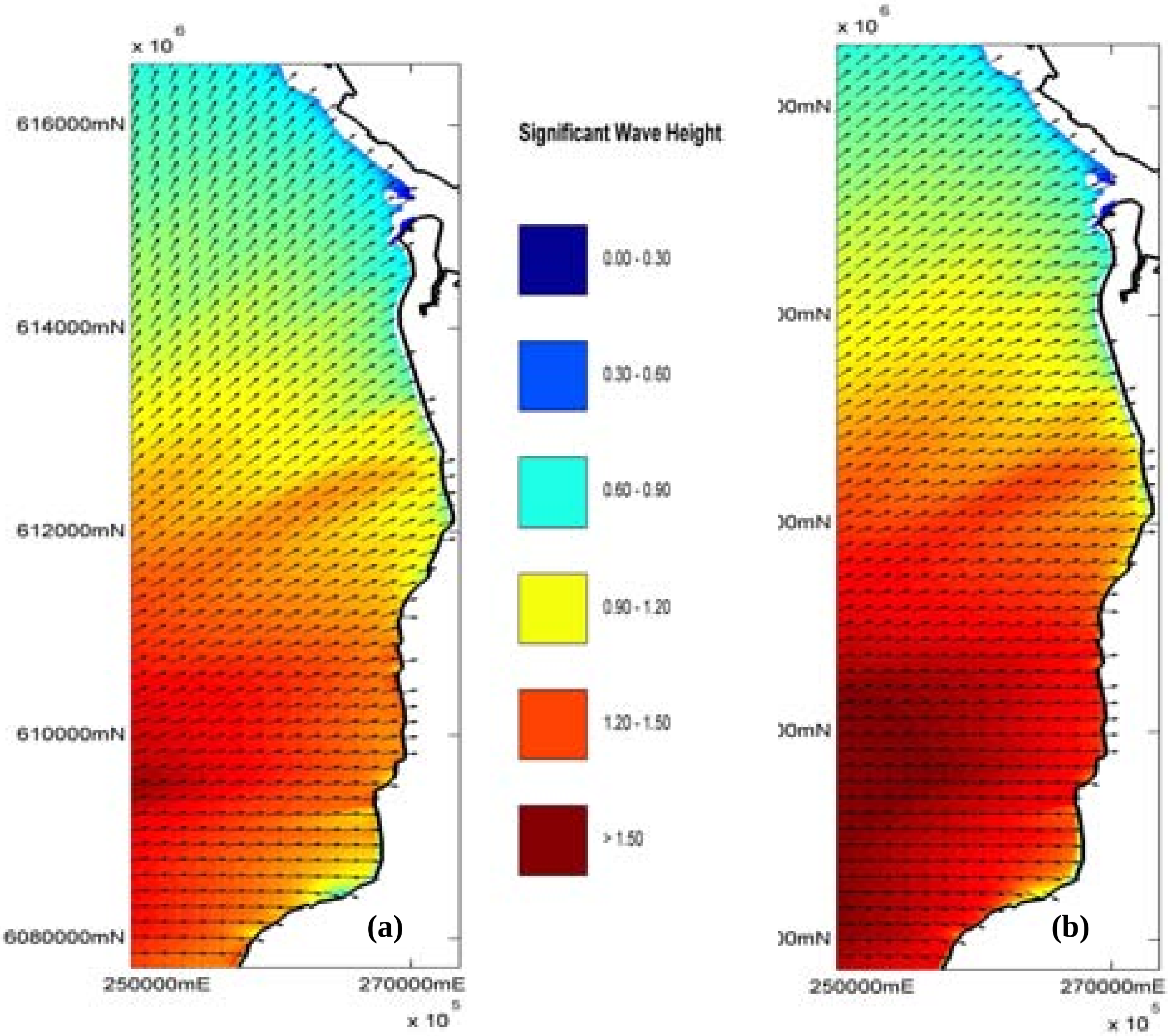

Figure 4.4: Mean significant wave heights and direction for the Adelaide Coastal Waters region during (a) March and (b) September 2004.

The time series of significant wave height at the 10 m bathymetry contour was extracted over one month to determine the alongshore variation in wave heights along the study region. The results indicated (Figure 4.5) that the wave heights along the southern part of the model domain were similar, but decreased north of Port Stanvac (location 3 in Figure 4.5 is offshore Port Stanvac). The wave heights offshore Semaphore were generally 80% of those along the southern locations; farther north they reduced to 60% of the southern values (Figure 4.5).

4.4 Bed shear stress and percentage exceedance of threshold

4.4.1 Waves Only

One of the main influences of the surface waves on the seabed is through the generation of near bed currents and the associated shear stress, which in turn is capable of mobilising sediment. Thus the seabed stability is directly related to these two parameters. The maximum near bed bottom velocity (U_{BOT}), predicted from the SWAN model over an annual cycle (see Section 2.7), overlaid on the bottom habitat, is shown in Figure 4.6. Here, the maximum near bed bottom velocities ranged from < 0.2 ms^{-1} in the offshore to a maximum of 0.8ms^{-1} close to the shore. There appeared to be a close relationship between the maximum near bed bottom velocity and the bottom habitat, with the boundary between seagrass and bare sand close to the 0.4 ms^{-1} contour. The maximum near bed bottom velocity is also related to the water depth; thus it is not possible to conclude that the wave-induced currents alone determine the bottom habitat.

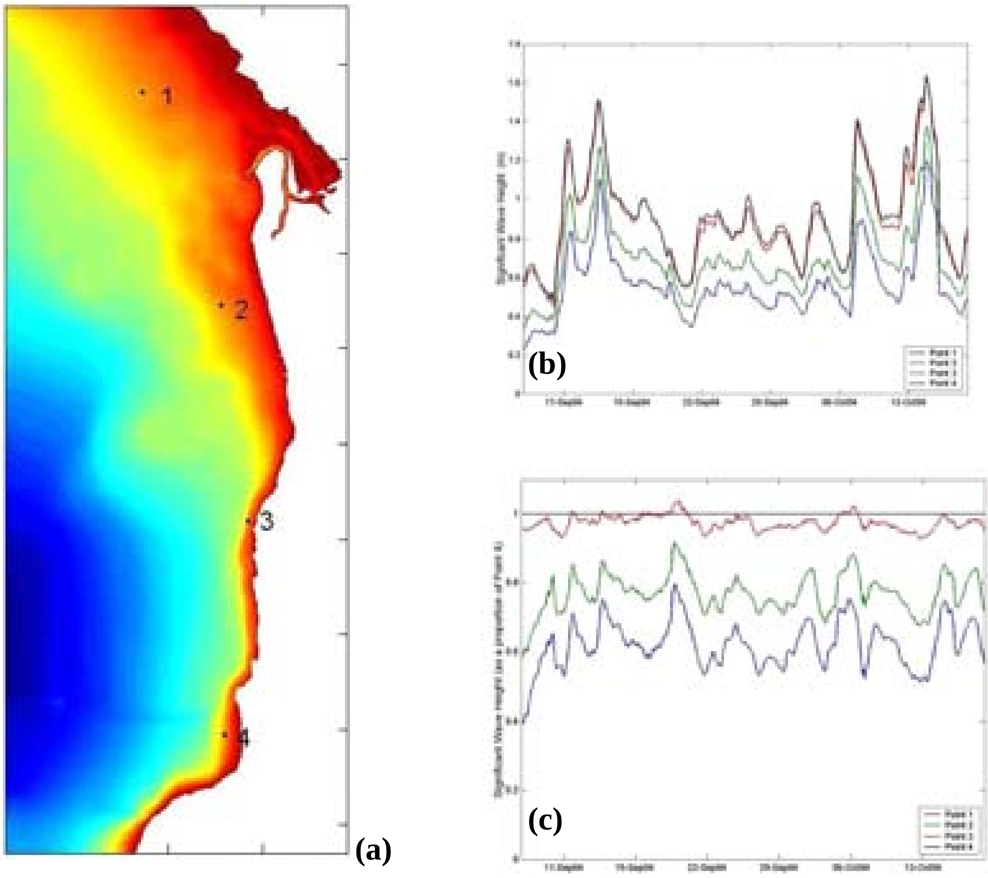

Figure 4.5: Alongshore variation in wave heights along the Adelaide Coastal Waters Region: (a) location of data extraction points; (b) time series of significant wave heights; and, (c) fraction of wave height related to offshore conditions.

The percentage exceedance of the critical shear stress is a measure of the amount of time sediment is being transported, and is related to the seabed stability. As the threshold of sand movement is dependent on the grain size—and there is a range of grain sizes within the study region (Bone et al., 2006)—percentage exceedance of the critical shear stress was estimated (see Section 2.8) for three different grain sizes: 2 mm, 0.25 mm, and 0.065 mm, which are the limits for coarse sand, medium sand, and fine sand, respectively. The results (Figures 4.7 and 4.8) indicated that, within the nearshore region, the coarser material was mobilised only 10% of the time, whereas the medium and finer-grained material was mobilised more than 90% of the time. Thus these results indicate the nearshore region of the study region is energetic, with the wave-induced currents capable of mobilising fine to medium sized sands almost continuously.

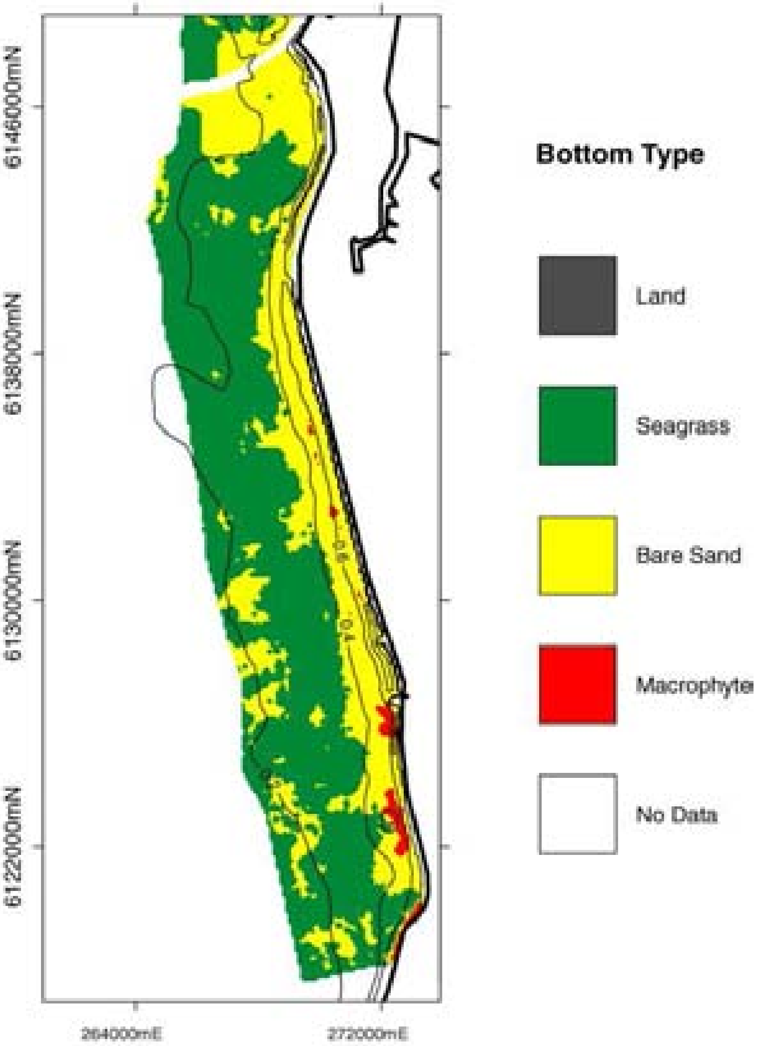

Figure 4.6: Maximum near-bed wave induced velocities (units= m/s) along the Adelaide Coastal Waters region overlaid on the habitat distribution.

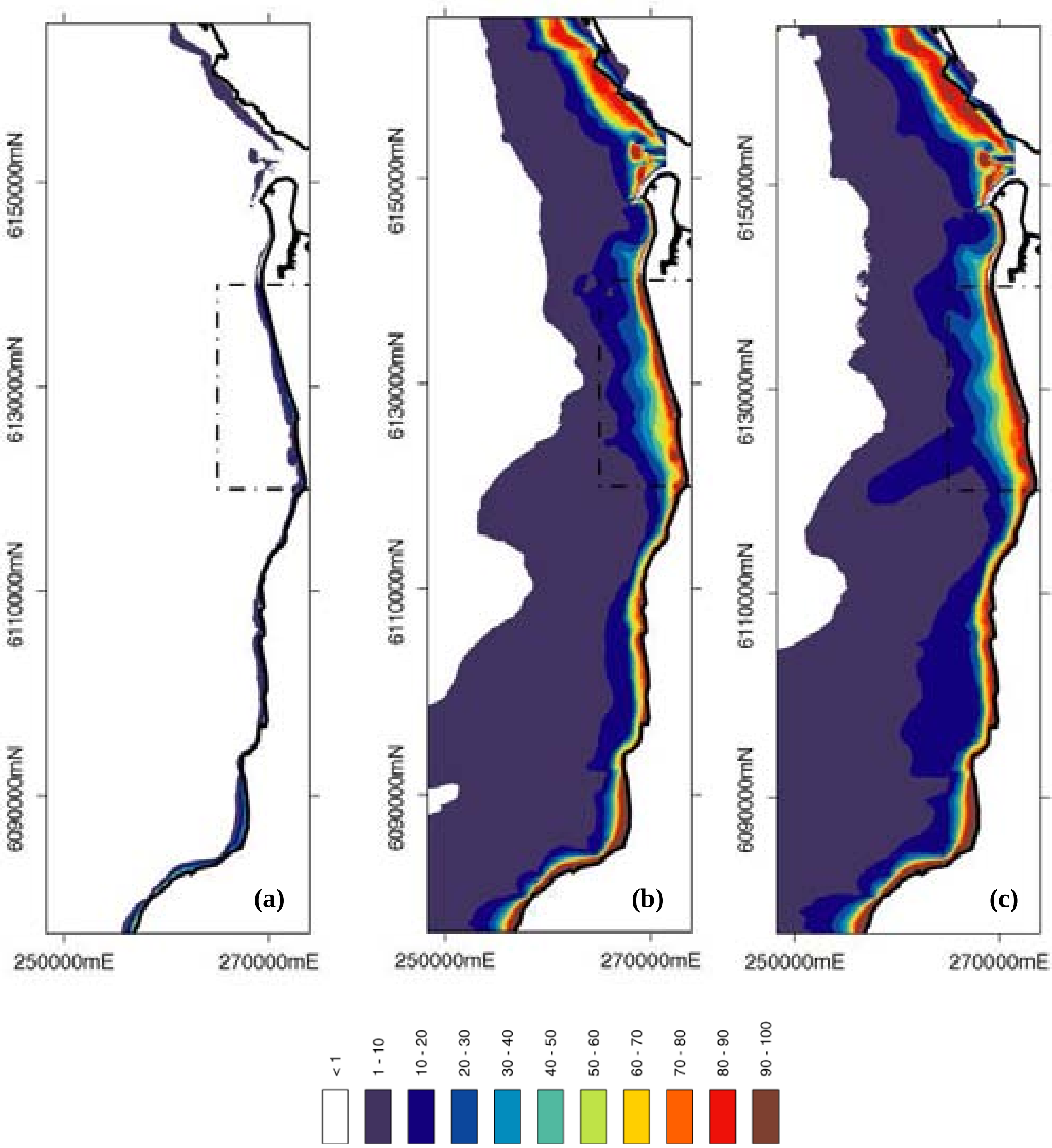

Figure 4.7: Percentage exceedance of the critical shear stress for sand transport under wave-induced currents for 2004. (a) mean grain size of 2mm; (b) mean grain size of 0.25 mm; and, (c) mean grain size of 0.063 mm.

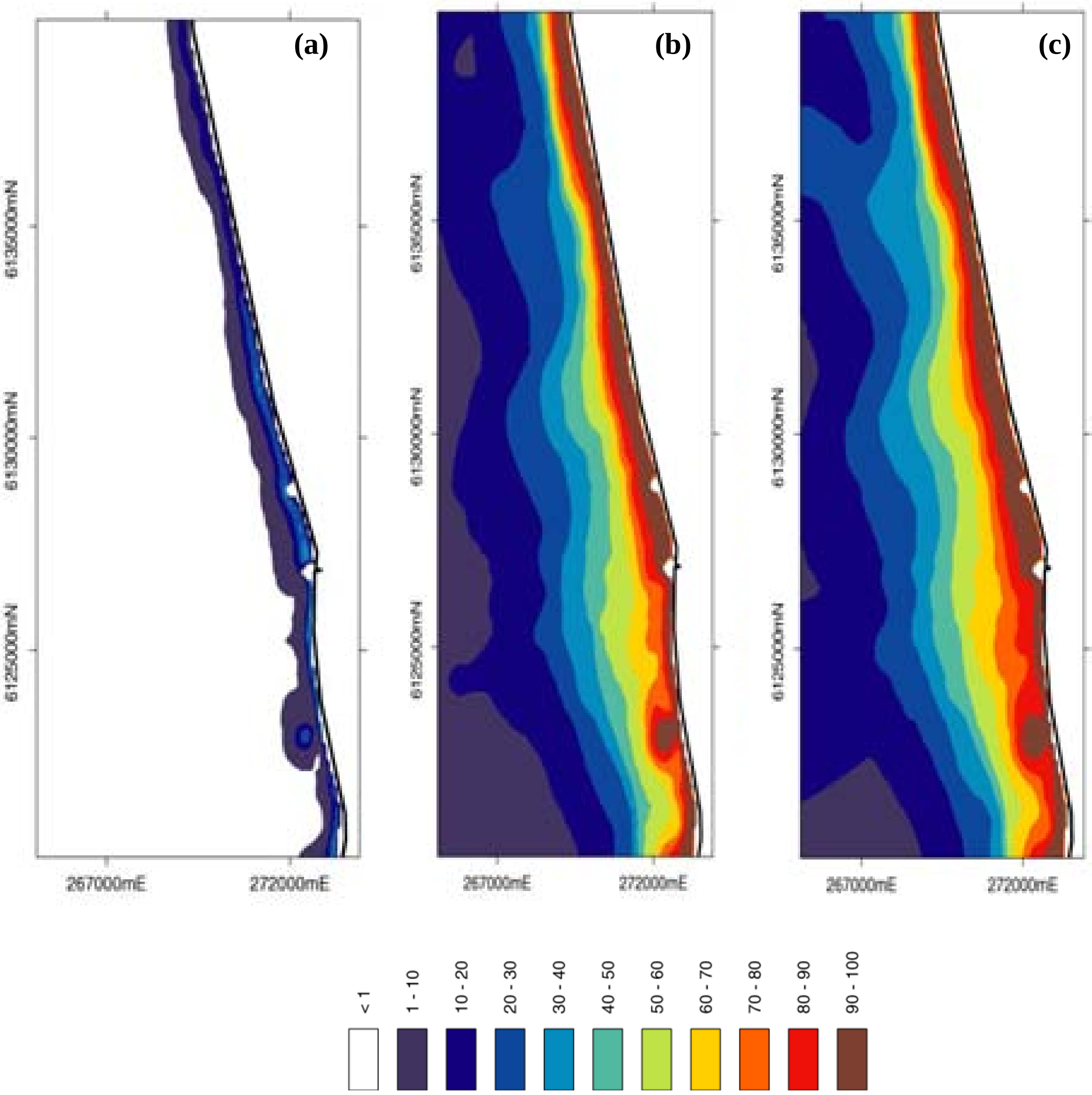

Figure 4.8: Percentage exceedance of the critical shear stress for sand transport under wave-induced currents for 2004 (Adelaide Coastal Waters region). (a) mean grain size of 2mm; (b) mean grain size of 0.25 mm; and, (c) mean grain size of 0.063 mm.

4.4.2 Waves and Currents in Combination

The effects of including the currents have the general effect of increasing the bottom shear stress (equation 3.12) across the study region. However, as the hydrodynamic module was run for two 45 day periods corresponding to summer and winter, the seasonal changes in wave climate (Figure 4.4) has a larger influence. Hence, during the winter, due to the higher wave heights, (Figure 4.4b) the contours of maximum bottom stress are located further inshore than during the summer (cf Figures 4.9a and 4.9b). Similarly, the percentage exceedance values were higher (Figure 4.10) when compared to the summer values (Figure 4.9). Both the waves only (Figure 4.8) and waves and currents in combination (Figures 4.10 and 4.11) had similar patterns reflecting that the wave action was the dominant component in determining the bottom shear stress within the ACWS region, in particular the regions where sand form the bottom habitat (Figure 4.9). It is also interesting to note that the 0.2 Nm^{-2} maximum bed shear stress value almost corresponds to the boundary between the seagrass and sand habitats. This is most likely due to the fact that the bottom stress is dominated by the wave-induced component which is controlled by water depth.

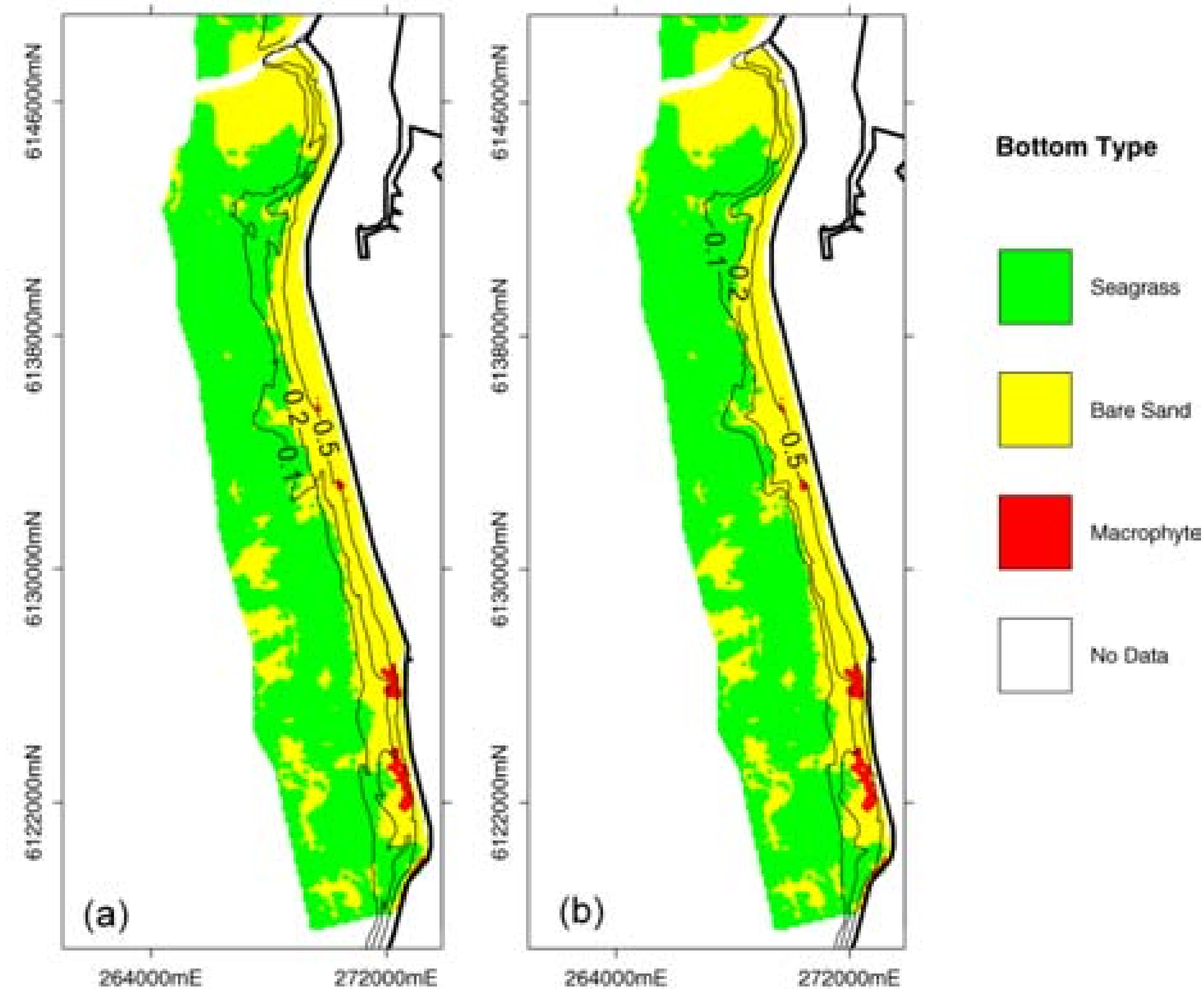

Figure 4.9: Distribution of maximum near-bed shear stress values under the combined action of waves and currents during (a) summer and (b) winter (units: Nm^{-2})

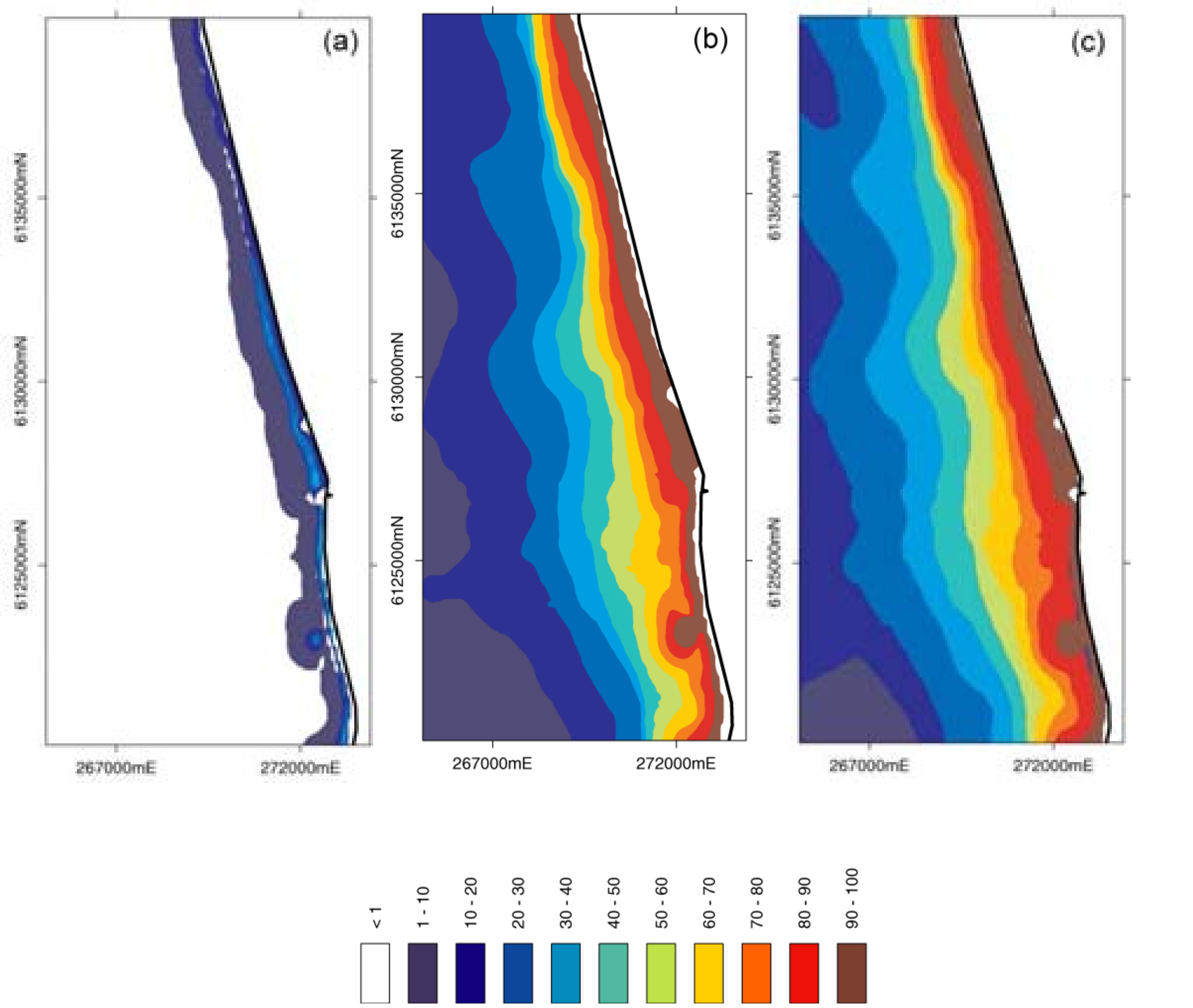

Figure 4.10: Percentage exceedance of the critical shear stress for sand transport under the combined action of waves and d currents for during summer (Adelaide Coastal Waters region). (a) mean grain size of 2mm; (b) mean grain size of 0.25 mm; and, (c) mean grain size of 0.063 mm.

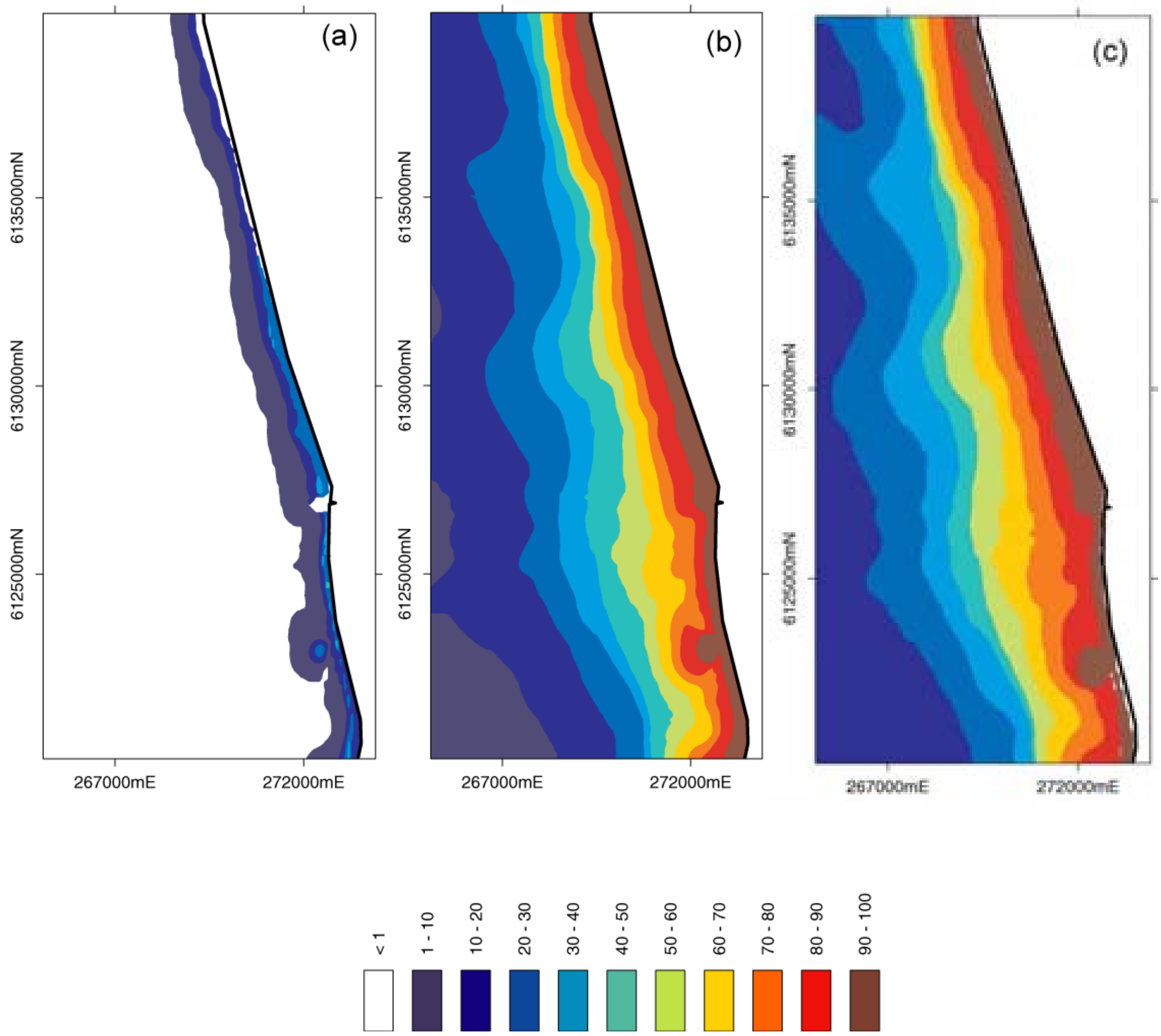

Figure 4.11: Percentage exceedance of the critical shear stress for sand transport under the combined action of waves and currents for during winter (Adelaide Coastal Waters region). (a) mean grain size of 2mm; (b) mean grain size of 0.25 mm; and, (c) mean grain size of 0.063 mm.

5. Hydrodynamic modelling of the Adelaide coastal waters

5.1 Circulation patterns

The currents along the Adelaide metropolitan coast generally flow parallel to the shoreline and are mainly driven through tidal action. Within the study region, the amplitudes of the major semi-diurnal (M_2, S_2) components are similar in magnitude, resulting in a unique situation (see Section 3.3.1). During spring tides, the tidal range is high, resulting in maximum tidal currents; during neap tides, the tidal variations are mainly due to the diurnal (O_1, K_1) constituents, resulting in a small tidal range and thus weaker currents. During the tide's flood stage the currents flow northwards, whereas during the tide's ebb stage the currents flow southwards. The maximum tidal currents along the metropolitan coastline are ~0.40 ms^{-1}, with the north-south component dominant (Figure 3.29). In comparison, the maximum east-west component of the tidal currents is < 0.05 ms^{-1} (Figure 3.30). These features result in minimal cross-shore advection (and mixing), and any discharges into the coastal region will be transported north-south with the prevailing currents.

The wind field in the study region indicated a strong seasonality, with the winds changing by up to 180° between summer and winter (Figure 3.9). Durin g winter, the wind direction ranged from north to north-east, with the strongest winds from NNE. In summer, the winds were from the south-west to south-east quadrant, with the strongest winds from the south-west due to the action of the sea breeze. The surface residual currents reflected these changes (Figure 5.1). During winter, the surface residual currents were directed towards the south, reflecting the southward (northerly) wind forcing; during summer, residual currents were directed northwards because of the northward (southerly) winds. However, the winter residual currents were weaker when compared with those of summer. In winter, the maximum southward residual currents were ~0.15 ms^{-1}, whereas during summer they ranged up to a maximum of ~0.25 ms^{-1} towards the north Figure 5.1).

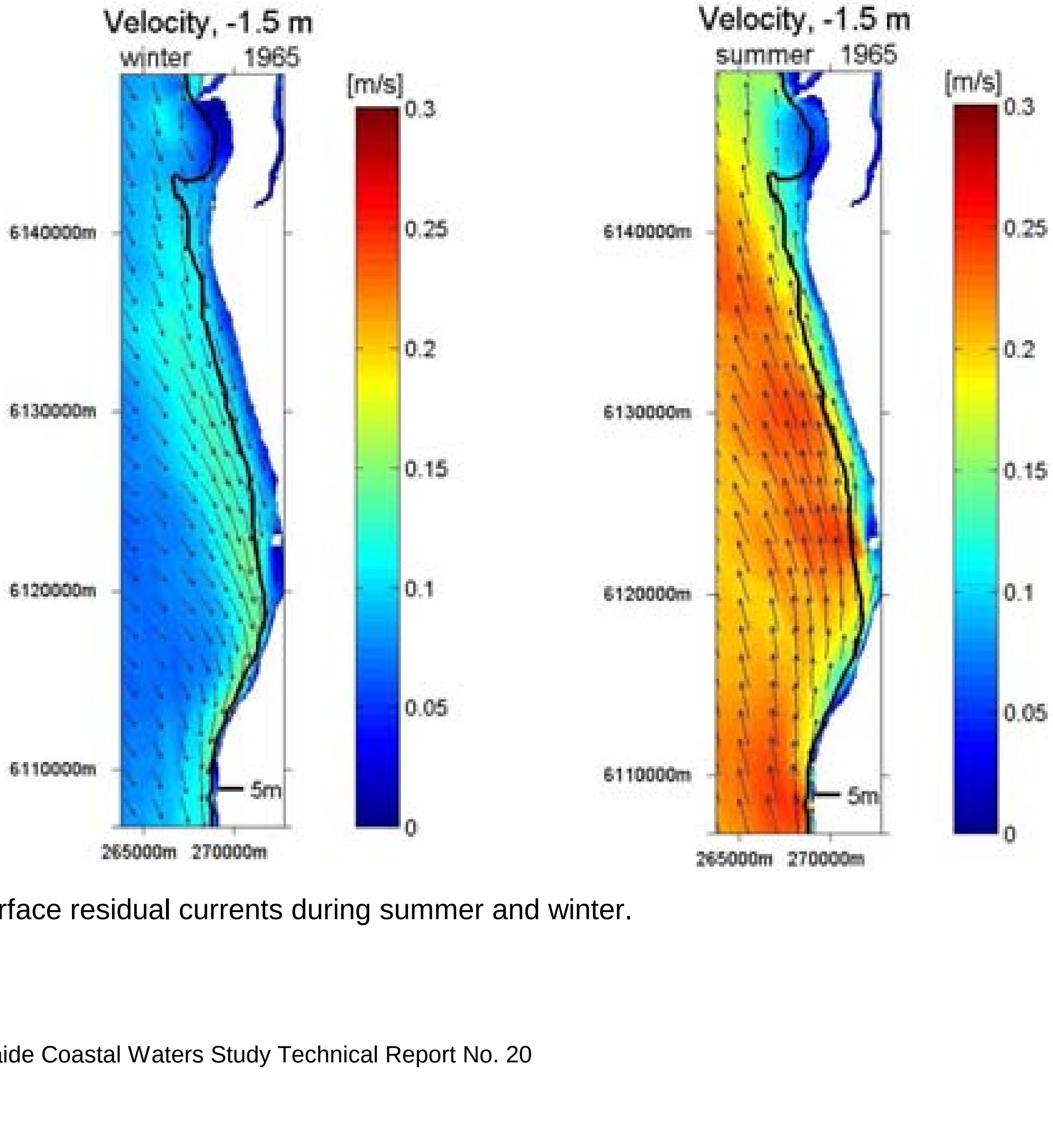

Figure 5.1: Surface residual currents during summer and winter.

Table 5.1. Summary of model runs undertaken

	AIM	Model forcing/inputs[1]	Model outputs
1	Examine present conditions (tides only)	• point source inputs	• Residual circulation • Flushing times • Particle tracks/connectivity • Mean distribution of properties (salinity, SSC, nutrients)
2	Examine present conditions	• point source inputs—divided into wastewater and stormwater flows • summer and winter conditions	• Mean distribution of properties (salinity, SSC, nutrients)
3	Examine present summer conditions (January/February)	• summer winds (2004) • summer air–sea fluxes (2004) • 2004 point source inputs	• Residual circulation • Flushing times • Particle tracks/connectivity • Mean distribution of properties (salinity, SSC, nutrients)
4	Examine present winter conditions (August/September)	• winter winds (2004) • winter air–sea fluxes (2004) • 2004 point source inputs	• Residual circulation • Particle tracks/connectivity • Mean distribution of properties (salinity, SSC, nutrients)
5	Examine past (1965) summer conditions (January/February)	• summer winds (2004) • summer air–sea fluxes (2004) • 1965 point source inputs	• Mean distribution of properties (salinity, SSC, nutrients)
6	Examine past (1965) winter conditions	• winter winds (2004) • winter air–sea fluxes (2004) • 1965 point source inputs	• Mean distribution of properties (salinity, SSC, nutrients)
7	Examine future summer conditions	• summer winds (2004) • summer air–sea fluxes (2004) • 2020 point source inputs	• Mean distribution of properties (salinity, SSC, nutrients)
8	Examine future winter conditions	• summer winds (2004) • summer air–sea fluxes (2004) • 2020 point source inputs	• Mean distribution of properties (salinity, SSC, nutrients)

[1]All model runs have tidal forcing over three spring-neap cycles or 44 days.

5.2 Flushing estimates

The flushing or residence time is a parameter often used as an indicator to determine the residence times of tracers, such as contaminants and nutrients within a volume of water. Higher flushing times (longer residence times) often indicate tracers are likely to be retained within a particular region; lower flushing times (short residence times) indicate tracers are readily transported out of the water body.

Flushing times are often difficult to obtain through field measurements. Therefore estimates are usually derived through the use of appropriate numerical models. However, the methodology to obtain such estimates, in a tidal-dominated water body such as the Adelaide coastal waters, is not straightforward and may be classified into three major approaches: (1) Control volume method: here, the volume flux of water into a control volume is calculated and the flushing time is defined when the total volume flux is equal to the volume of water within the control volume; (2) Tracer method: here, the transport and dispersion of a conservative tracer defined in a control volume is tracked through time. When the tracer mass has reduced to a value 1/e of the original mass, the control volume is assumed to be flushed (e-folding time); and, (3) Particle tracking method: here, neutrally buoyant particles are released at different locations within a control volume and allowed to be transported by the advection-diffusion field simulated by the numerical model.

Particles were released only in the surface layer and constrained to remain within this layer through the simulation period. By recording the paths taken by the particles, it is possible to arrive at a qualitative estimate of the spatial variability of flushing time within the control volume. All the above methods were tested during the present study, but it was found that for all the methods the flushing time was very sensitive to the definition of the control volume. However, the most reliable flushing time estimates were obtained through the particle tracking method. Initially, a control volume was established for the nearshore region with the offshore boundary located at approximately the 5 m contour (Figure 5.2). Particles were released at different locations and three forcing conditions—tides only, summer winds, and winter winds. The particles' excursions varied with location and forcing conditions and can be summarised as follows (Figure 5.2):

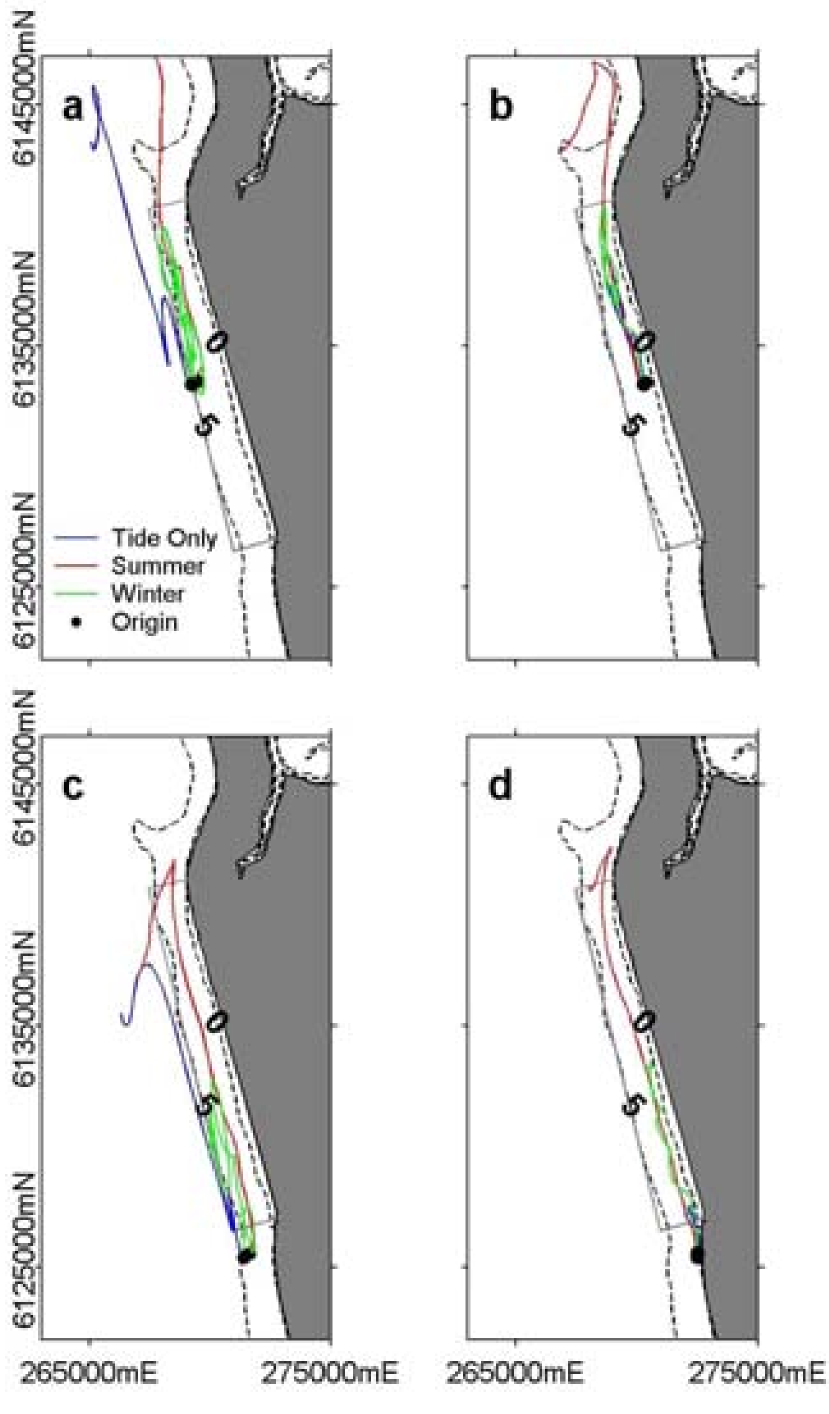

Figure 5.2: Predicted surface drifter tracks in the Adelaide Coastal Waters region showing the differences in the mean excursion paths for different seasons and locations

Tides only:

- Particles released near the shore were retained within the inshore region, with the residence time (in the box) between 4 and 10 days.
- Particles released offshore were transported slowly offshore with the mean residence time < 1 day.
- All particles were transported in a northerly direction.

Summer:

- All particles moved through the control volume, with the mean residence times between 1 and 1.5 days.
- All particles were transported in a northerly direction.

Winter:

- All particles moved through the control volume, with the mean residence times < 2.5 days.
- Almost all particles were retained within the 5 m contour.
- All particles were transported in a southerly direction, except for nearshore particles, which had a northerly drift due to the action of waves.

To examine the connectivity between the Bolivar wastewater treatment plant and the metropolitan coastal strip, a particle tracking exercise was undertaken to compare the transport of particles during summer and winter. The results indicated that during the summer, particles were transported northwards because of the dominance of southerly winds, and there was no pathway for the particles to be advected onto the metropolitan coastal strip (Figure 5.3). During winter, the northerly winds initially transported the particles onto Barker Inlet, where they remained for some time and then exited through the Port River mouth onto the metropolitan coastal strip (Figure 5.3).

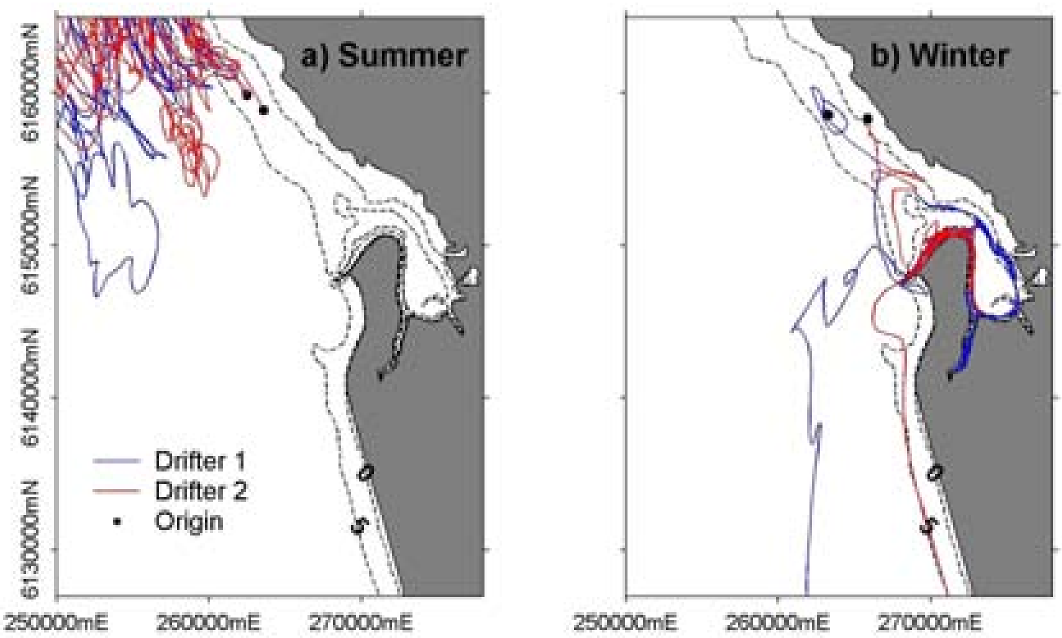

Figure 5.3: Predicted surface drifter tracks released at Bolivar outfall showing the differences in the excursion paths for summer and winter

5.3 Distribution of conservative properties: past, present and future

Several model runs were undertaken with a view of achieving the Adelaide Coastal Waters Study's overall objectives and to address the stakeholders' requirements (Table 5.1). These included present (2004) conditions as well as past and future scenarios (see Section 3.3). Each scenario was run for

45 days (three spring-neap cycles) during summer and winter. For summer, the period mid-January to end of February, which included the summer sea breeze pattern and low rainfall (Figure 3.3), was selected. For winter, the period mid-August to end of September included the typical winter winds and periods of high discharges to the coastal strip (Figure 3.4). To identify changes due only to variability in discharges, the same bathymetry (applicable to present conditions) and meteorological conditions (winds and air–sea fluxes) were used for all model scenarios.

The mean values of salinity, suspended sediment concentration, nutrients (nitrogen and phosphorous), and dilution (using salinity) over the model domain for each of the model scenarios are presented below. It should be noted that in the numerical model there was no uptake or production of nitrogen and phosphorous and is thus considered conservative.

5.3.1 Salinity

Freshwater inflows from the rivers, wastewater, and stormwater discharges, and to a lesser extent by evaporation during the summer, influence the salinity distribution. The distribution of mean salinity during the summer indicates the main changes in the northern region were mainly due to the Bolivar wastewater discharge (Figure 5.4). The differences in mean salinity between 1965 and 2004 (Figure 5.5) indicate that the mean salinity decreased along the entire coastal region, whereas the Barker Inlet/Port River system increased in salinity. The largest decrease in salinity was observed along the northern coastal region, which was influenced by the Bolivar wastewater discharge (Figure 5.5). The differences in mean salinity between 2004 and 2020 (Figure 5.5) indicate the mean salinity will remain unchanged along the coastal region while the Barker Inlet/Port River system will decrease in salinity.

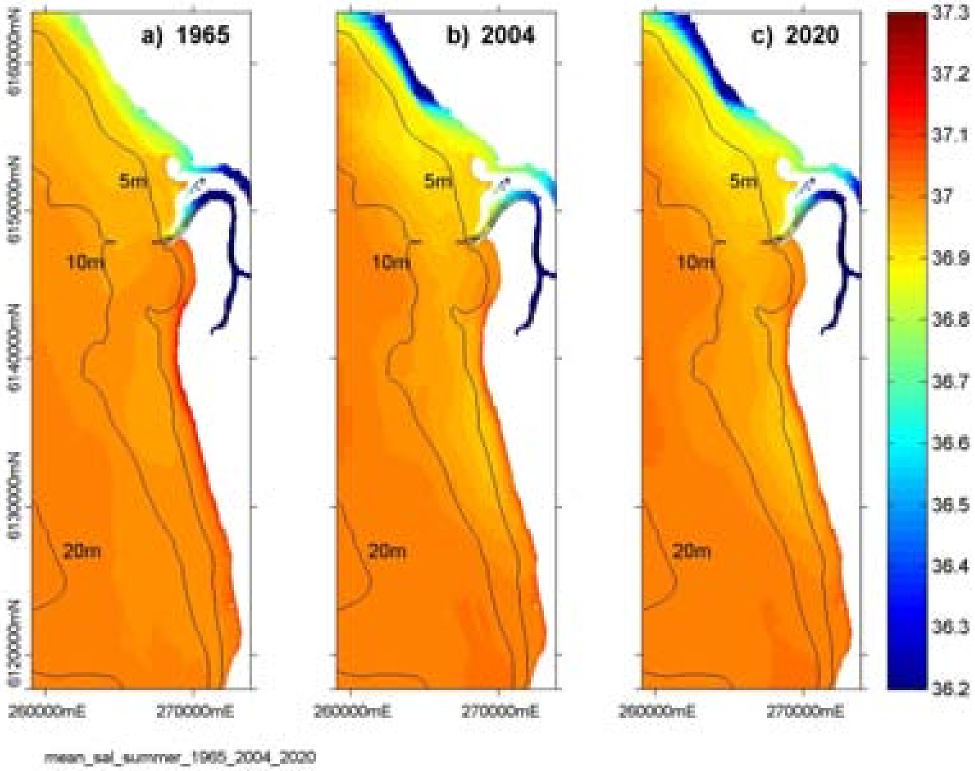

Figure 5.4: Predicted mean summer salinity distribution for (a) 1965; (b) 2004; and, (c) 2020.

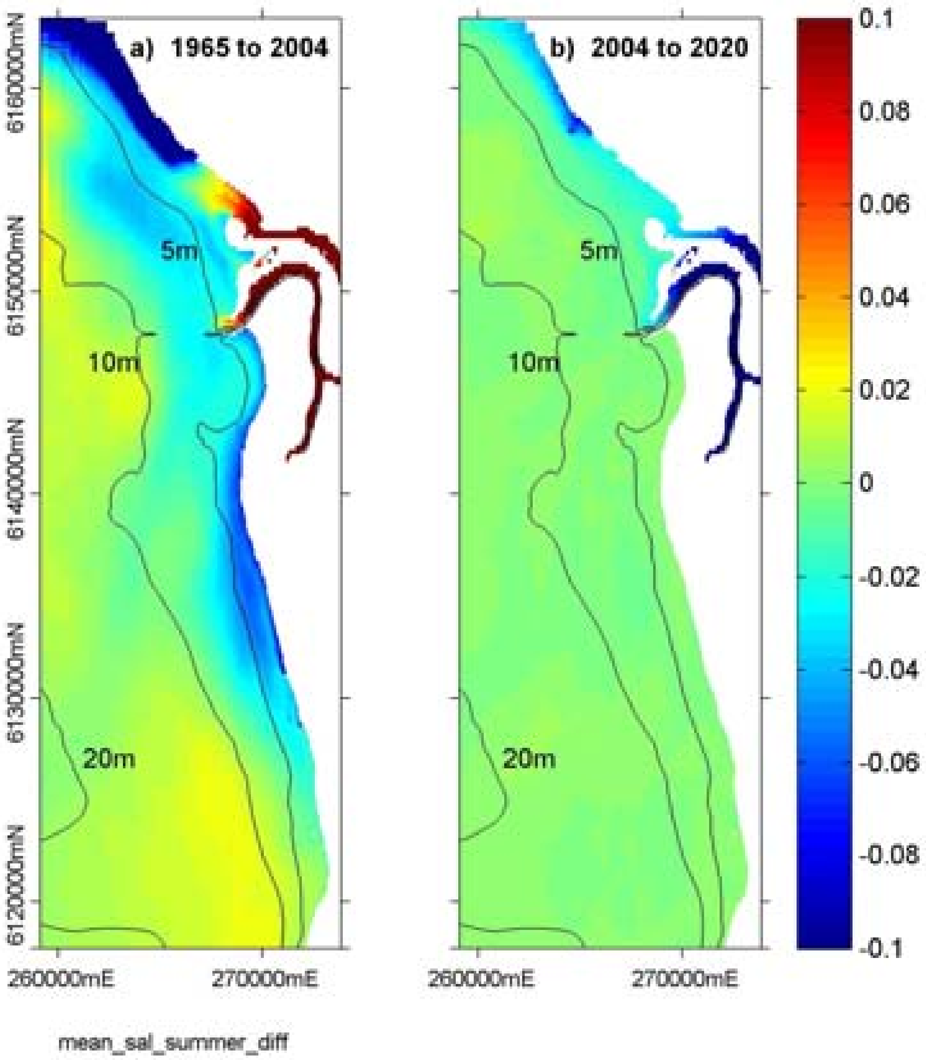

Figure 5.5: Predicted mean summer salinity distribution differences for (a) between 1965 and 2004; (b) between 2004 and 2020.

In winter, when there is higher freshwater inflow due to increased rainfall, the absence of mixing in the cross-shore directions was evident; with the lower salinity being retained in the near-coastal region inshore of the 5 m depth contour (Figure 5.6). These results reiterate the findings of the residual circulation and the particle tracks (Sections 5.1 and 5.2), which indicated the north-south advection of water. Thus any tracer that is discharged into the coastal region through point sources such as rivers, stormwater drains, and wastewater outfalls will be advected north and south and will remain within the nearshore region. The differences in mean salinity between 1965 and 2004 (Figure 5.7) show salinity decreased along the entire coastal region, particularly in water depths shallower than 5 m. This also included the Barker Inlet/Port River system. The differences in mean salinity between 2004 and 2020 (Figure 5.7) indicate the mean salinity will remain unchanged along the coastal region except for the Bolivar outfall region, where a slight increase in salinity is predicted due to a decrease in the Bolivar discharge.

5.3.2 Suspended sediment concentration (SSC)

The suspended sediment concentration (SSC) is influenced by the hydrodynamic conditions (tidal currents and wave climate) and the SSC concentration contained in the point source discharges. The plume of high SSC discharging from the Port River and transported northward under prevailing summer conditions dominated the predicted distribution of SSC during the summer (Figure 5.8).

The high sediment load was due to discharge from the Penrice plant. The decrease in sediment discharge from Port River (derived from Penrice) dominated the differences in SSC between 1965 and 2004 (Figure 5.9), which covered the entire northern region. The differences in SSC between 2004 and 2020 (Figure 5.9) indicate no changes except within the Port River system, which decreased in SSC.

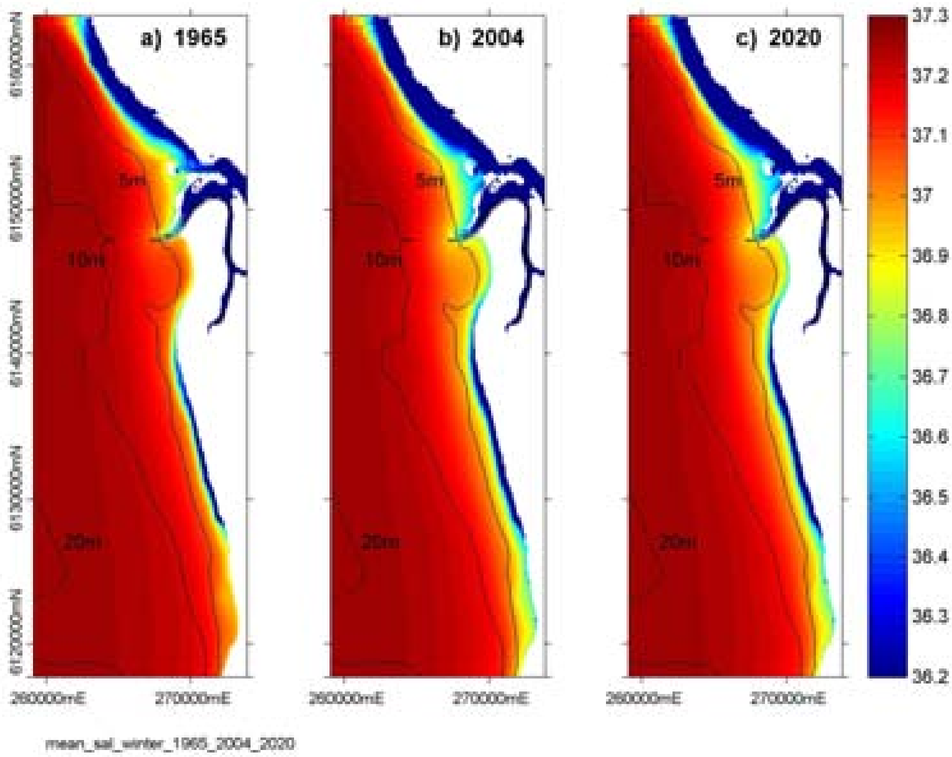

Figure 5.6: Predicted mean winter salinity distribution for (a) 1965; (b) 2004; and, (c) 2020.

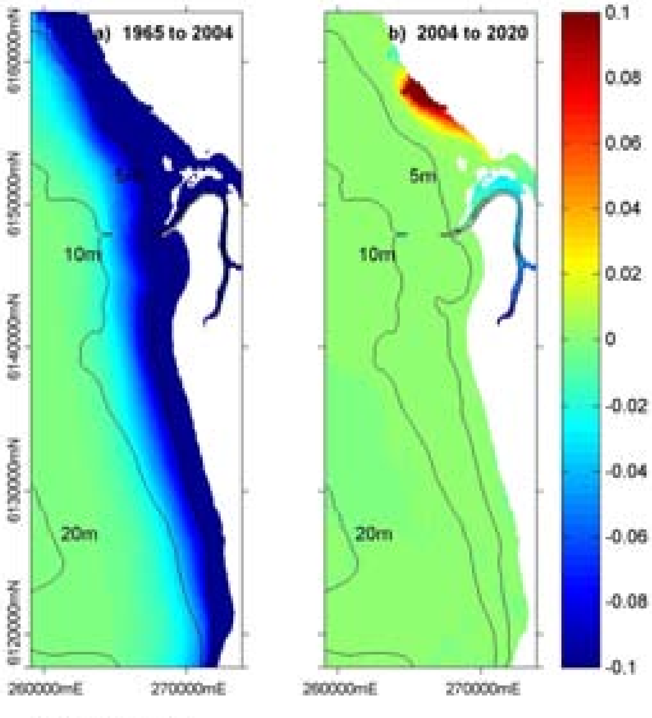

Figure 5.7: Predicted mean winter salinity distribution differences for (a) between 1965 and 2004; (b) between 2004 and 2020.

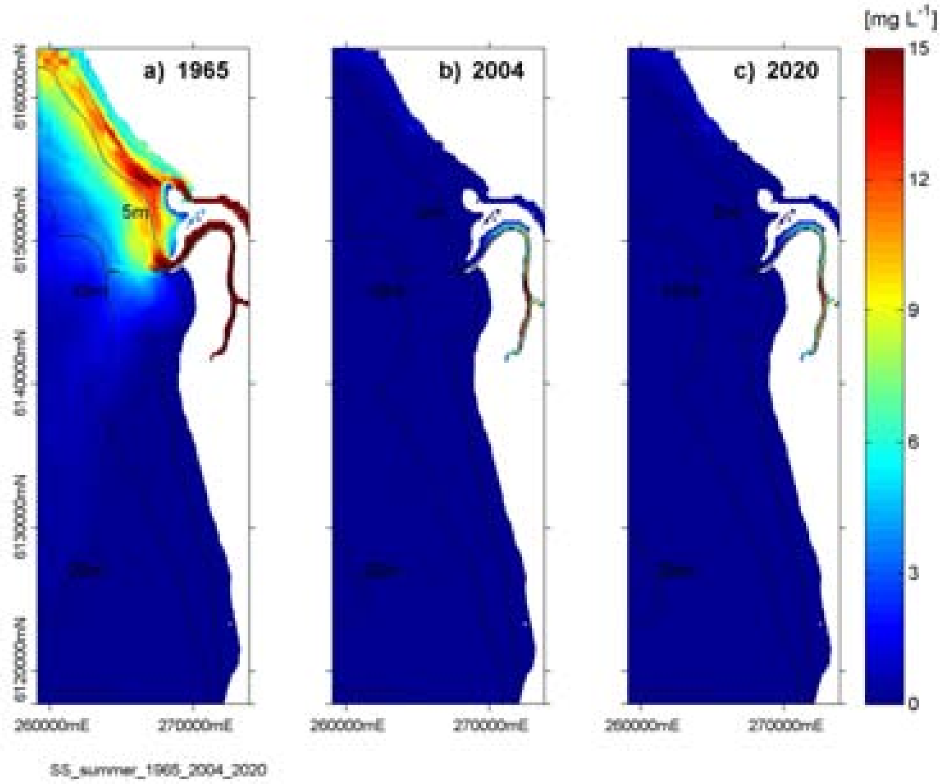

Figure 5.8: Predicted mean summer suspended sediment concentrations for (a) 1965; (b) 2004; and, (c) 2020.

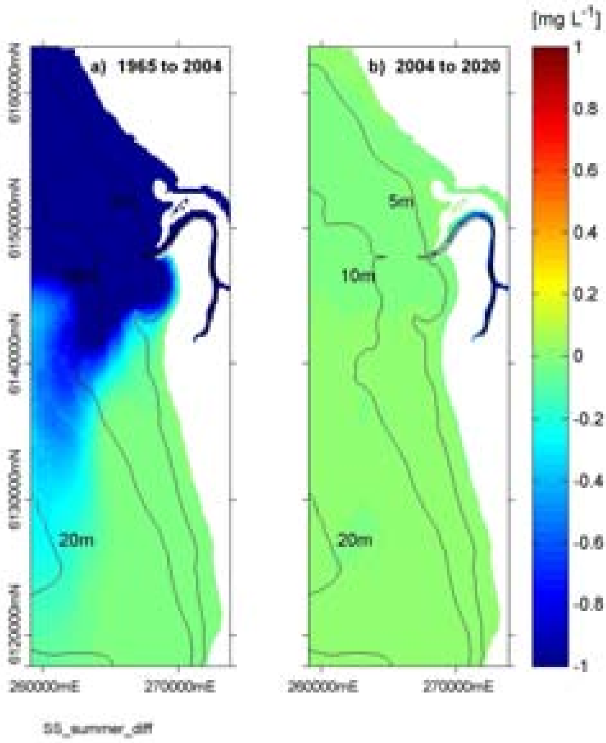

Figure 5.9: Predicted mean summer suspended sediment concentration distribution differences for (a) between 1965 and 2004; (b) between 2004 and 2020.

The predicted distribution of SSC during the winter also showed the plume of high SSC discharging from the Port River, but under winter conditions the higher concentrations remained close to the river mouth (Figure 5.10). The influence of the Bolivar discharge was also prominent. The decrease in sediment discharge from Port River dominated the differences in SSC between 1965 and 2004 (Figure 5.11), which covered the entire region south of the Port River mouth. In the northern region there was an increase in SSC due to the increased discharge from the Bolivar discharge. The differences in SSC between 2004 and 2020 (Figure 5.11) indicate no changes except within the Port River system, which decreased in SSC, and in the vicinity of Bolivar due to reduction in the discharge.

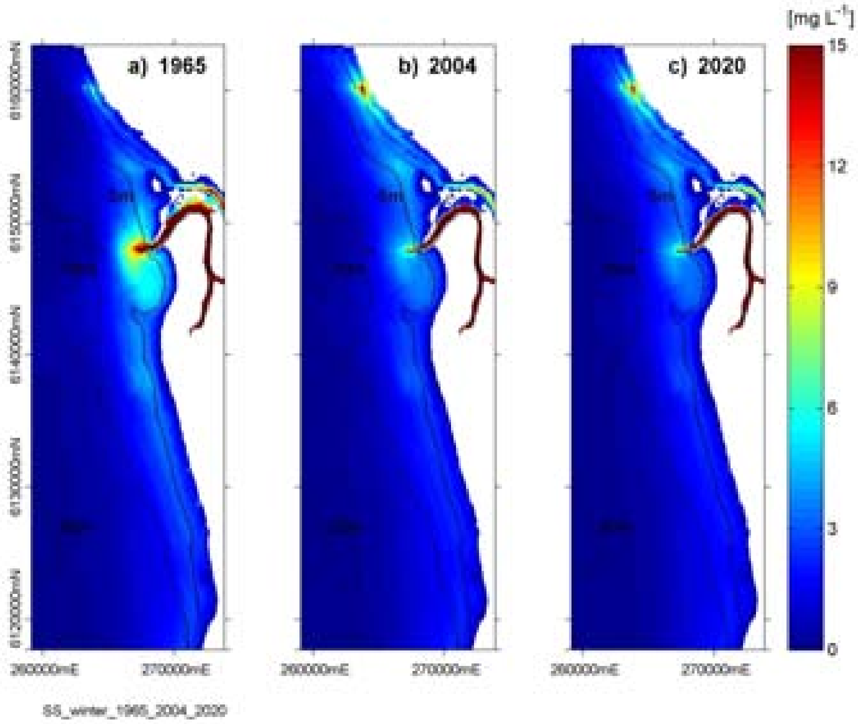

Figure 5.10: Predicted mean winter suspended sediment concentrations for (a) 1965; (b) 2004; and, (c) 2020.

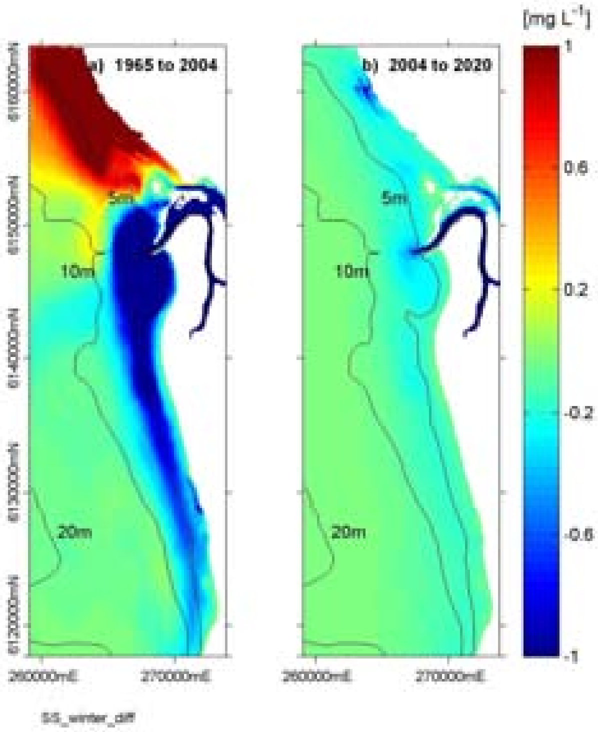

Figure 5.11: Predicted mean winter suspended sediment concentration distribution differences for (a) between 1965 and 2004; (b) between 2004 and 2020.

5.3.3 Nitrogen concentration

Nitrogen is considered to be a conservative tracer. Hence the distribution will follow similar trends to that of salinity except that the concentration of nitrogen input from the point source discharges was variable. The Port River plume dominated the predicted distribution of nitrogen during the summer and was transported northward under prevailing summer conditions (Figure 5.12). The high nitrogen load is derived from the Penrice discharge. The decrease in nitrogen discharge from Port River (derived from Penrice) dominated the differences in nitrogen between 1965 and 2004 (Figure 5.13), which covered the entire northern region. The differences in nitrogen between 2004 and 2020 (Figure 5.13) indicate no changes except in the northern section (north of Port River), where an increase in the nitrogen concentrations is predicted.

During the winter, the plume from the Port River is transported southward although not visible in the predicted concentrations (Figure 5.14), it is apparent in the predicted decrease in nitrogen concentration between 1965 and 2004 (Figure 5.15a). There is also a slight reduction in nitrogen concentration between 2004 and 2020 (Figure 5.15b).

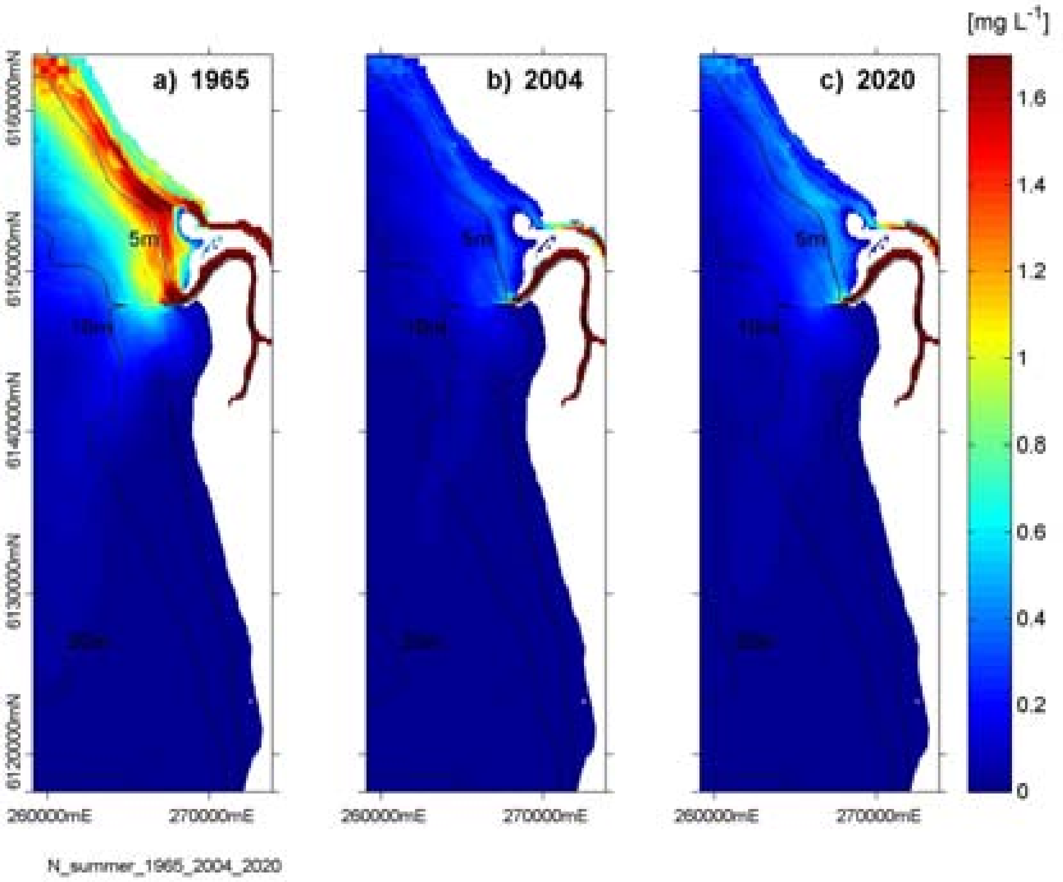

Figure 5.12: Predicted mean summer nitrogen concentrations for (a) 1965; (b) 2004; and, (c) 2020.

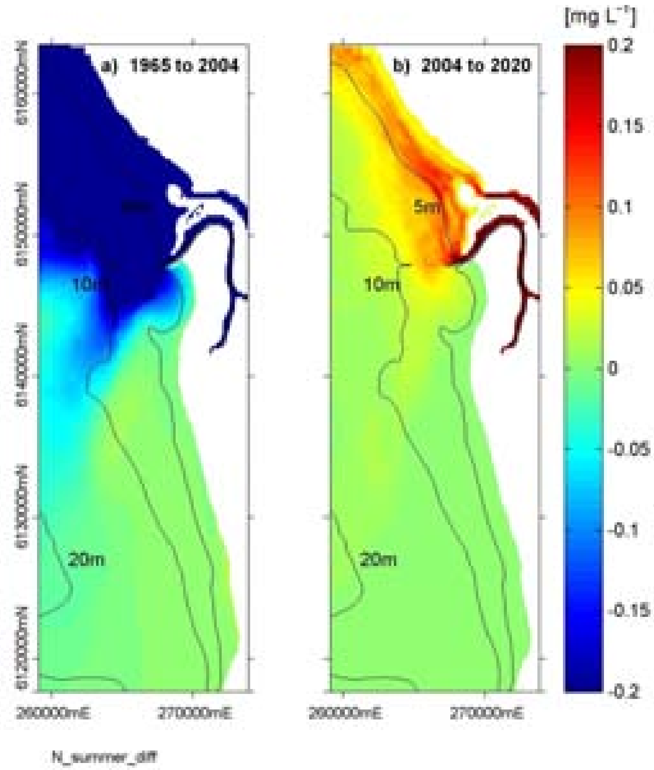

Figure 5.13: Predicted mean summer nitrogen concentration distribution differences for (a) between 1965 and 2004; (b) between 2004 and 2020.

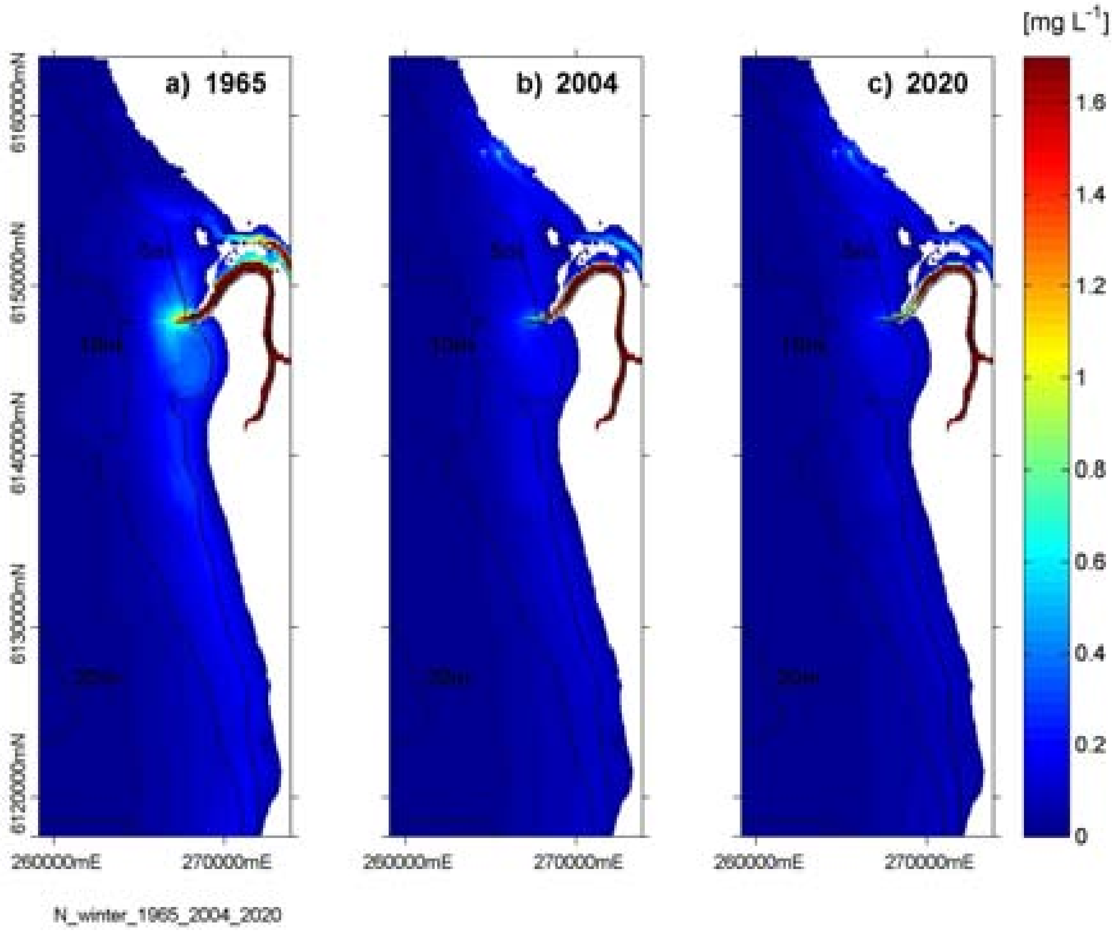

Figure 5.14: Predicted mean winter nitrogen concentrations for (a) 1965; (b) 2004; and, (c) 2020.

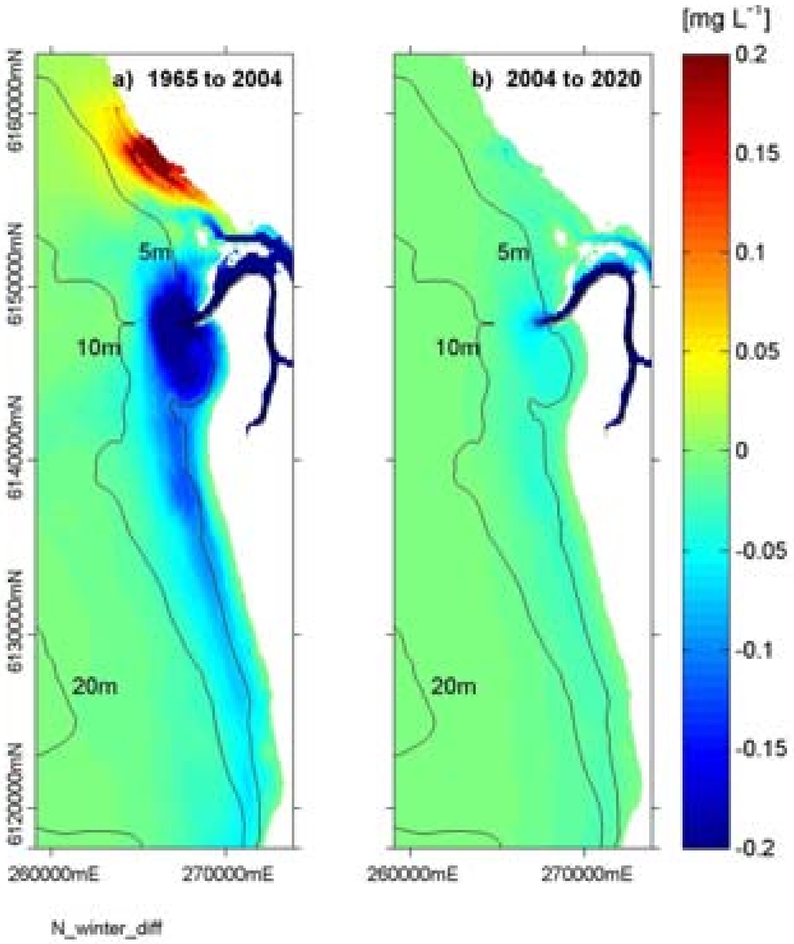

Figure 5.15: Predicted mean winter nitrogen concentration distribution differences for (a) between 1965 and 2004; (b) between 2004 and 2020.

5.3.4 Phosphorous concentration

Similar to nitrogen (Section 5.3.3), the distribution of phosphorous is also modelled under the assumption that it is a conservative tracer—there is no uptake by biological processes. The Port River plume dominated the predicted distribution of phosphorous concentration during the summer, which was transported northward under prevailing summer conditions (Figure 5.16). The high phosphorous concentration in Port River is due to the Port Adelaide WWTP. The decrease in phosphorous discharge from Port River (Port Adelaide WWTP) dominated the differences in phosphorous concentration between 1965 and 2004 (Figure 5.17a), which covered the entire northern region. Increased phosphorous concentrations were also present in the nearshore region off Glenelg and extending northwards along the entire coastal strip to the Port River entrance (Figure 5.17a). The differences in phosphorous concentration between 2004 and 2020 (Figure 5.17b) indicated no changes except in the northern section (north of Port River), where an increase in the phosphorous concentration was predicted.

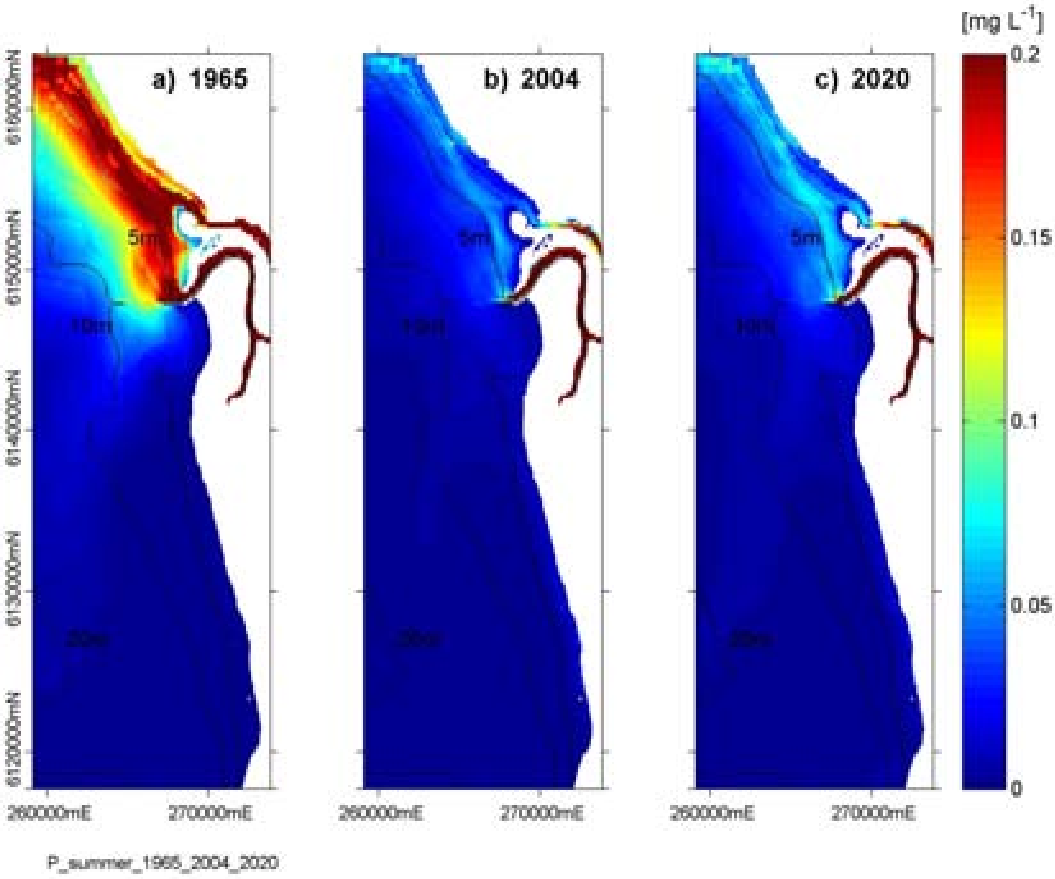

Figure 5.16: Predicted mean summer phosphorous concentrations for (a) 1965; (b) 2004; and, (c) 2020.

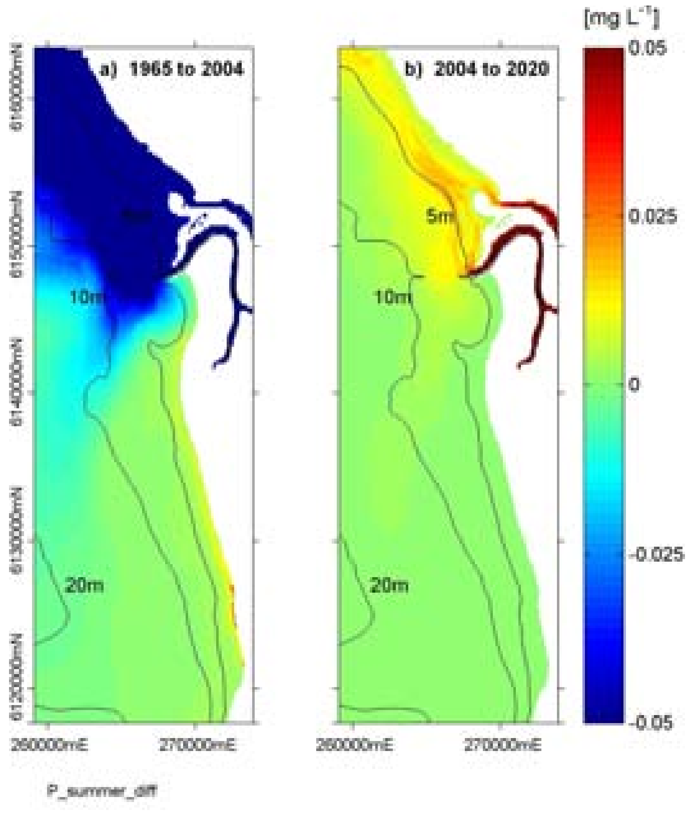

Figure 5.17: Predicted mean summer phosphorous concentration distribution differences for (a) between 1965 and 2004; (b) between 2004 and 2020.

The predicted distribution of phosphorous concentration, during the winter, also showed the plume of high phosphorous concentration discharging from Port River, but under winter conditions, the higher concentrations remained close to the river mouth, with some advection southwards (Figure 5.18).

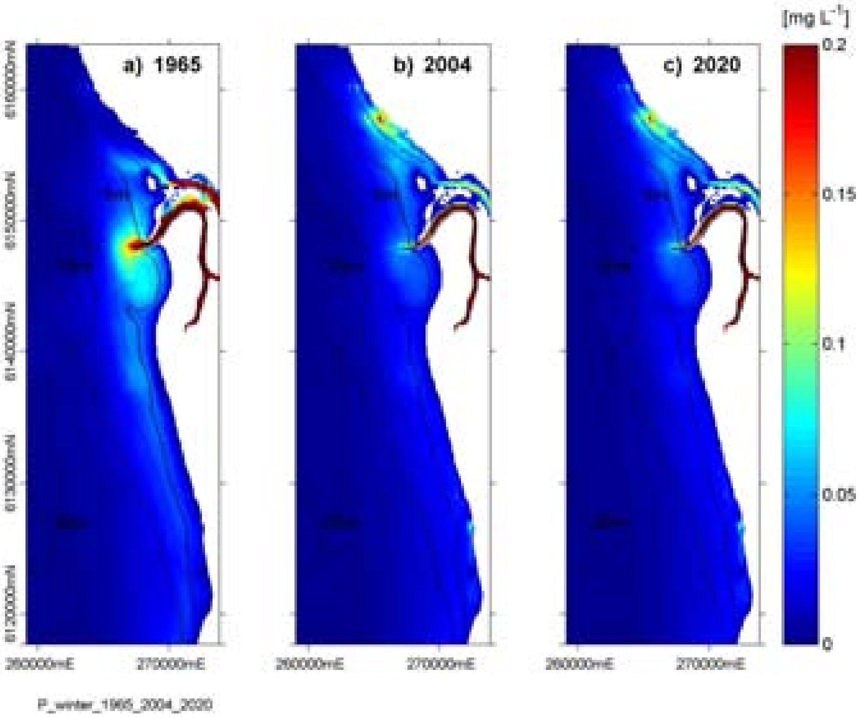

Figure 5.18: Predicted mean winter phosphorous concentrations for (a) 1965; (b) 2004; and, (c) 2020.

The influences of the Bolivar discharge in the northern region and the Glenelg wastewater discharge in the southern region were also prominent. The decrease in the discharge from Port River dominated the differences in phosphorous concentration between 1965 and 2004 (Figure 5.19a), which covered the entire region south of the Port River mouth centred on the 5 m depth contour. In the northern region there was an increase in phosphorous concentration due to the increased discharge from Bolivar. Increased phosphorous concentrations were also present in the nearshore region off Glenelg and extending northwards along the entire coastal strip to the Port River entrance (Figure 5.19a). The differences in phosphorous between 2004 and 2020 (Figure 5.19b) indicated no changes except a decrease in the vicinity of Bolivar.

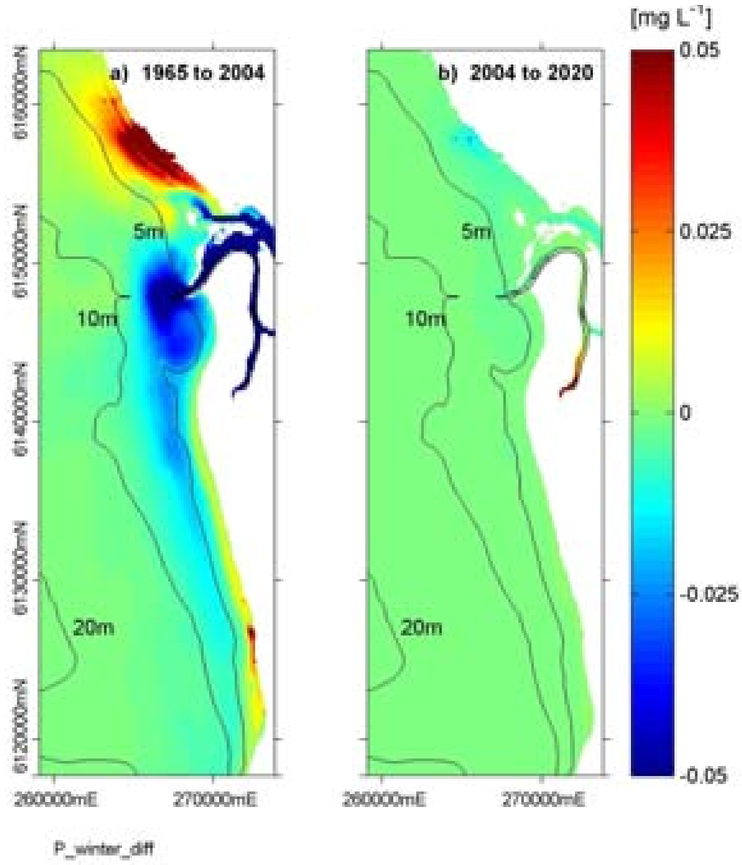

Figure 5.19: Predicted mean winter phosphorous concentration distribution differences for (a) between 1965 and 2004; (b) between 2004 and 2020.

5.3.5 Dilution

Salinity distribution was used to predict the mean dilution contours within the study area with the resulting dilution isopleths overlaid on a habitat map for summer and winter (Figures 5.20 and 5.21). The results for summer indicated that in 1965 there were high dilution rates along the metropolitan coastal strip, with the 1:1000 dilution isopleth close to the shoreline (Figure 5.20a). In the north the 1:100 dilution isopleth is shown reflecting the discharges from the Port River system. The dilution isopleths are similar for the present (2004) and in 2020, with an additional 1:250 isopleth present offshore of the metropolitan coastal strip (Figures 5.20b and 5.20c). A 1:250 dilution isopleth is also present to the north of the Port River mouth.

The dilution contours for winter are very similar for 1965, 2004, and 2020, with the dilution increasing progressively offshore (Figure 5.21). Between 1965 and 2004 the dilution contours migrated offshore, i.e. the dilution in the nearshore region decreased with time (cf Figures 5.21a and 5.21b).

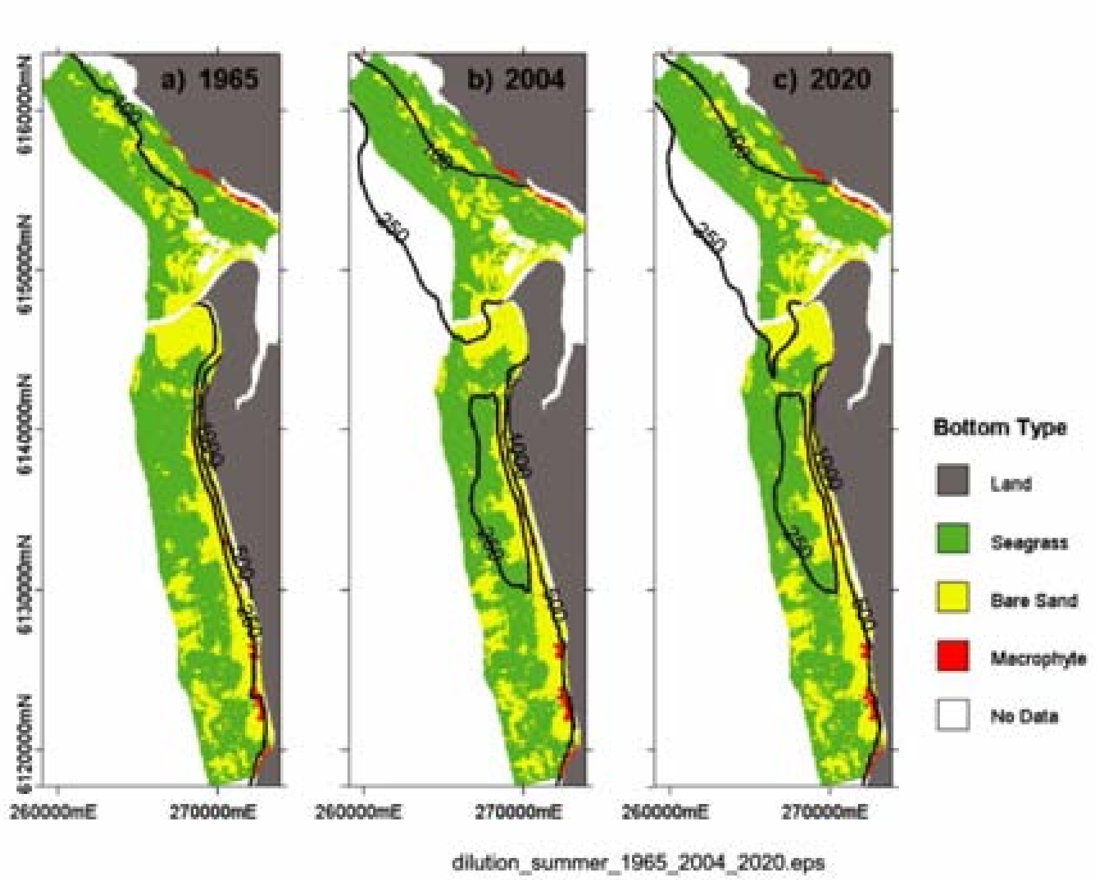

Figure 5.20: Predicted mean summer dilution contours for (a) 1965; (b) 2004; and, (c) 2020.

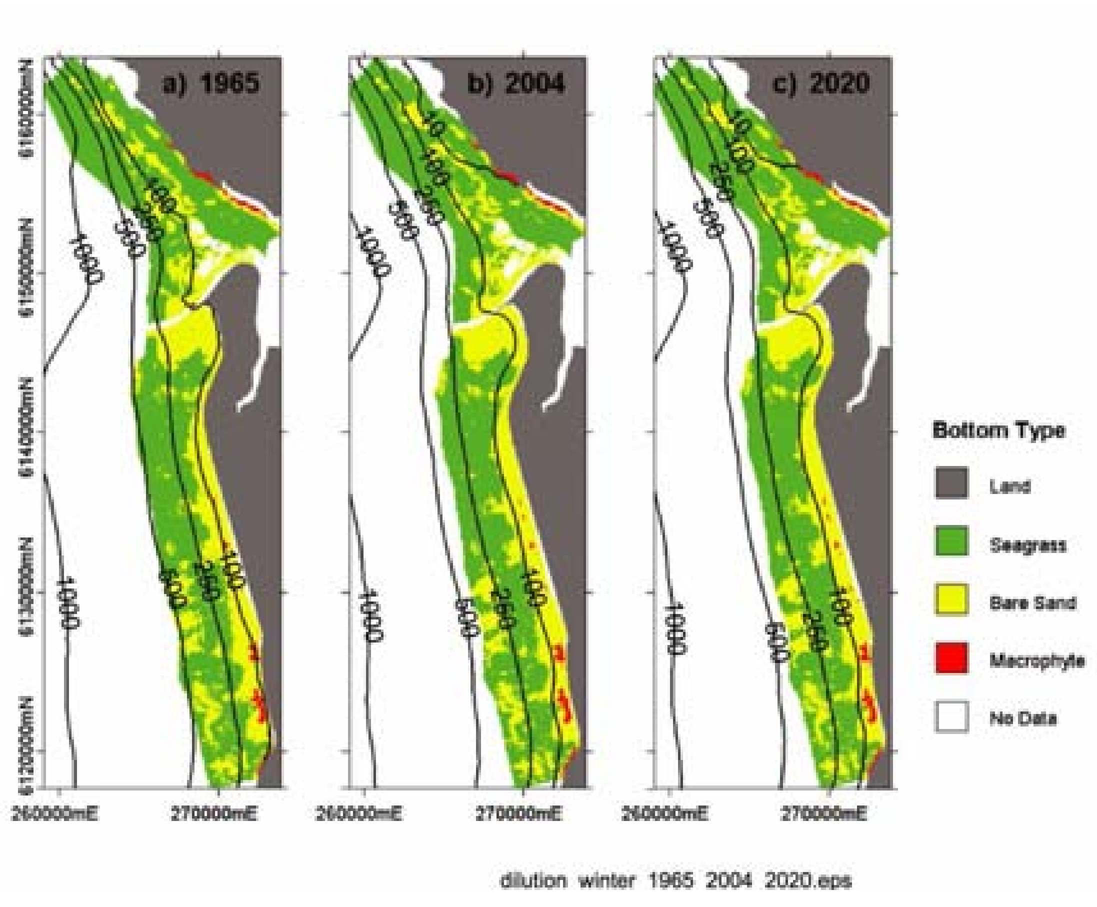

Figure 5.21: Predicted mean winter dilution contours for (a) 1965; (b) 2004; and, (c) 2020.

5.4 Distribution of conservative properties: wastewater and stormwater discharges

To investigate the relative importance of the discharges from wastewater outfalls (including discharges from all the municipal wastewater outfalls: Bolivar, Glenelg, Christies Beach as well as from Penrice) and stormwater discharges (including rivers and storm drains), model runs were undertaken where either only wastewater discharges or stormwater discharges were specified (see run 2, Table 5.1). The present-day (2004) discharges were specified, and model runs for both summer and winter were undertaken.

The suspended sediment concentrations (SSC) for summer indicated the wastewater discharges (from Bolivar and Penrice) had the largest influence when compared with stormwater discharges (Figures 5.22a and 5.23a). This was mainly due to the fact that during the summer the stormwater discharges were almost negligible. In contrast, the stormwater discharges, particularly those derived from the Port River and Gawler River system, had a dominating effect on the distribution of SSC throughout the model domain during winter (Figures 5.22b and 5.23b).

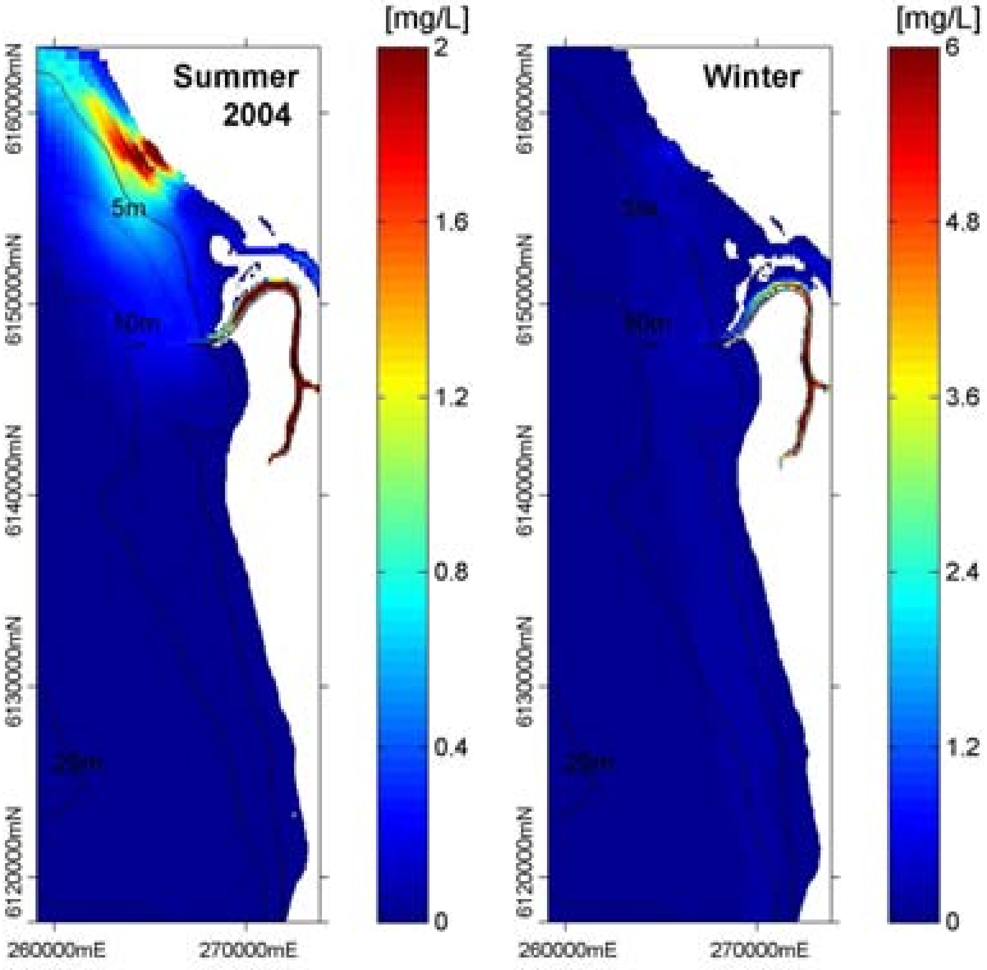

Figure 5.22: Predicted mean suspended sediment concentrations from wastewater discharges during 2004.

The nitrogen concentrations for summer indicated the wastewater discharges from Bolivar, Penrice, and Glenelg had the largest influence (Figure 5.24a). However, the stormwater discharges originating from Port River resulted in slightly higher concentrations in the region of the Port River mouth (Figure 5.25a). There were localised elevations in nitrogen concentrations in the region of the stormwater drains to the south of Glenelg (Figure 5.25a). In contrast, during the winter, the wastewater discharges, particularly from Bolivar and Port River (Penrice), dominated the nitrogen concentrations when compared with those discharged through stormwater (Figures 5.24b and 5.25b).

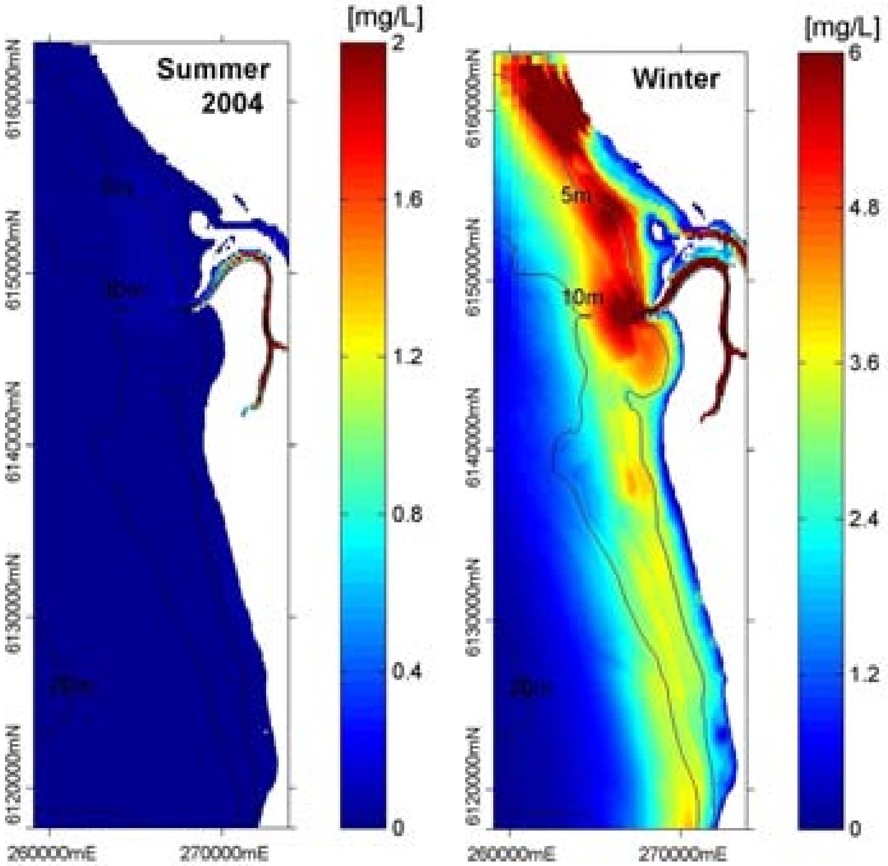

Figure 5.23: Predicted mean suspended sediment concentrations for storm water discharges during 2004.

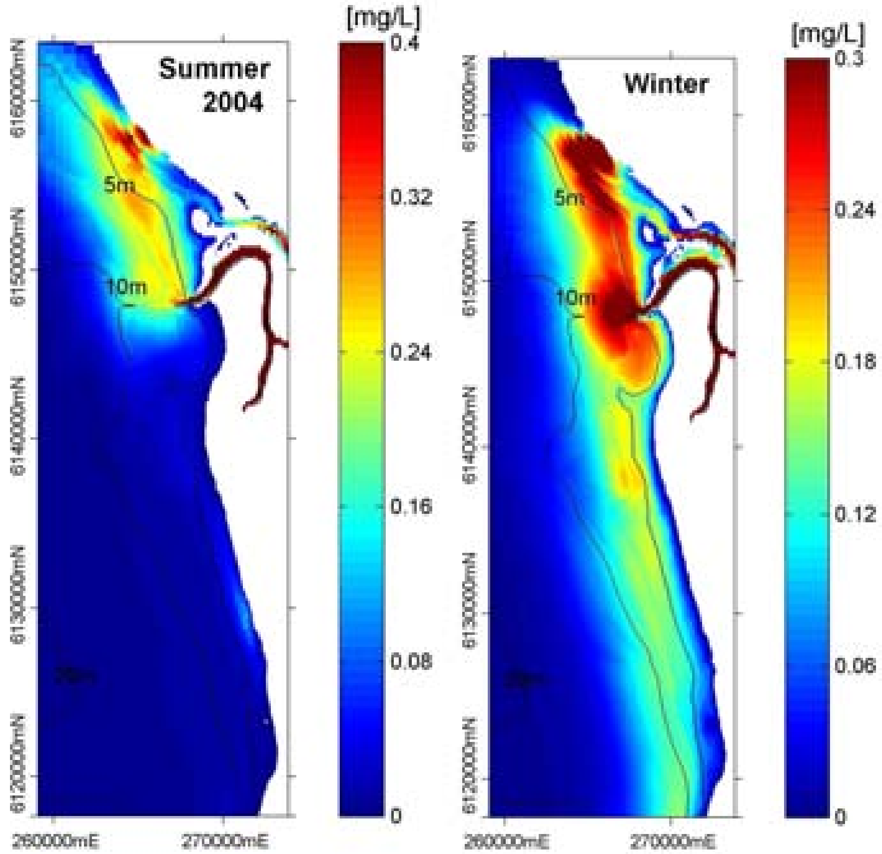

Figure 5.24: Predicted mean nitrogen concentrations from wastewater discharges during 2004.

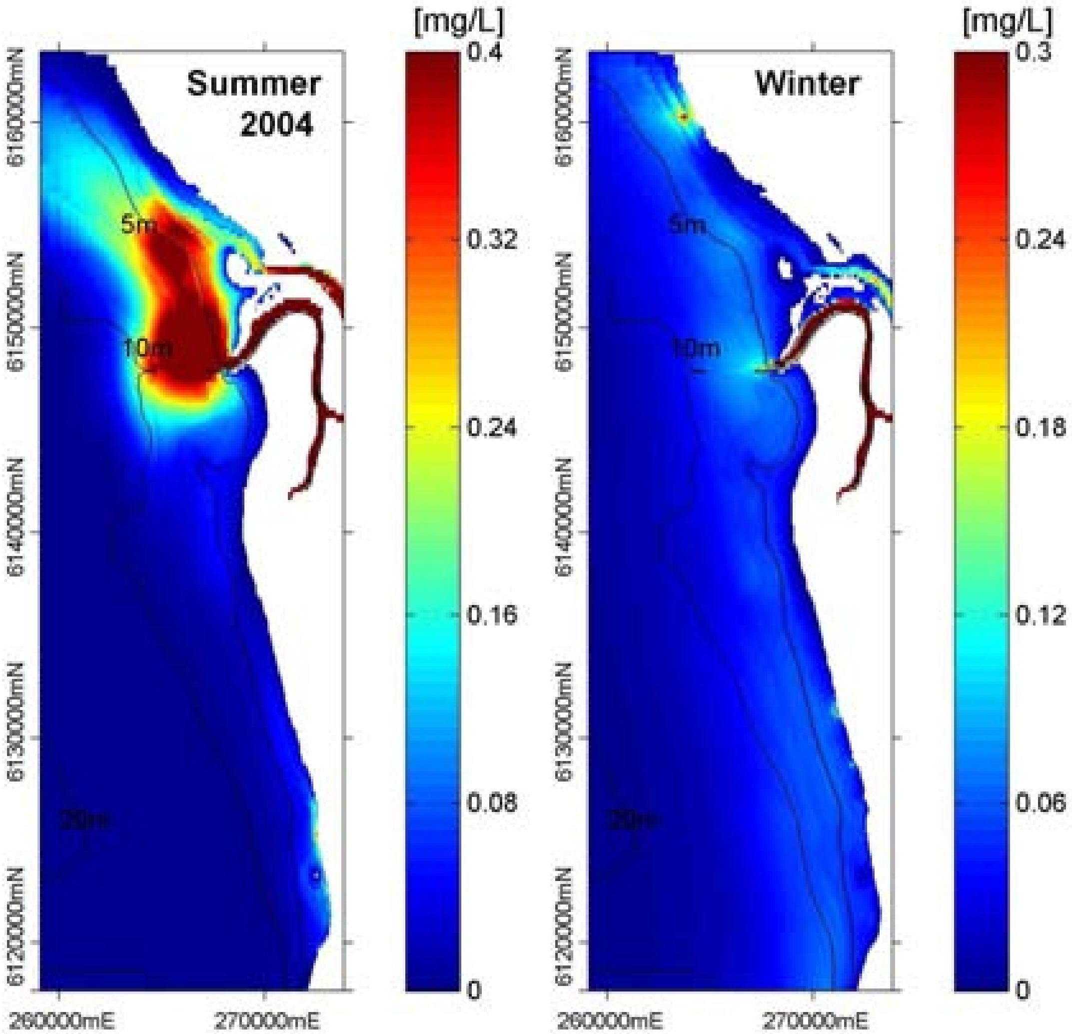

Figure 5.25: Predicted mean nitrogen concentrations for storm water discharges during 2004.

The phosphorous concentrations for summer indicated the wastewater discharges from Bolivar, Penrice, and Glenelg had a large influence (Figure 5.26a). However, the stormwater discharges originating from the stormwater drains to the south of Glenelg had a more pronounced influence on the phosphorous concentrations along the metropolitan coastal strip (Figure 5.27a). In the winter, phosphorous concentrations along the metropolitan coastal strip were still elevated, but because of the winter regime the plumes were transported southwards (Figure 5.27b). In the northern region, wastewater discharge from Bolivar dominated the phosphorous concentrations locally when compared with those discharged through stormwater (Figures 5.26b and 5.27b).

In summary, the three main properties examined—suspended sediment concentration (SSC), nitrogen, and phosphorous concentrations—exhibited variations between summer and winter for the two discharges. During summer, the discharges from wastewater outfalls (which included Penrice) had more influence on the SSC concentrations, whereas in winter the stormwater discharges had a larger influence. For nitrogen concentration, stormwater discharges had a higher influence during the summer, whereas wastewater discharges were dominant in winter. For phosphorous concentration, stormwater discharges had a higher influence along the metropolitan coastal strip during both summer and winter, whereas the wastewater discharge from Bolivar was dominant in the northern section.

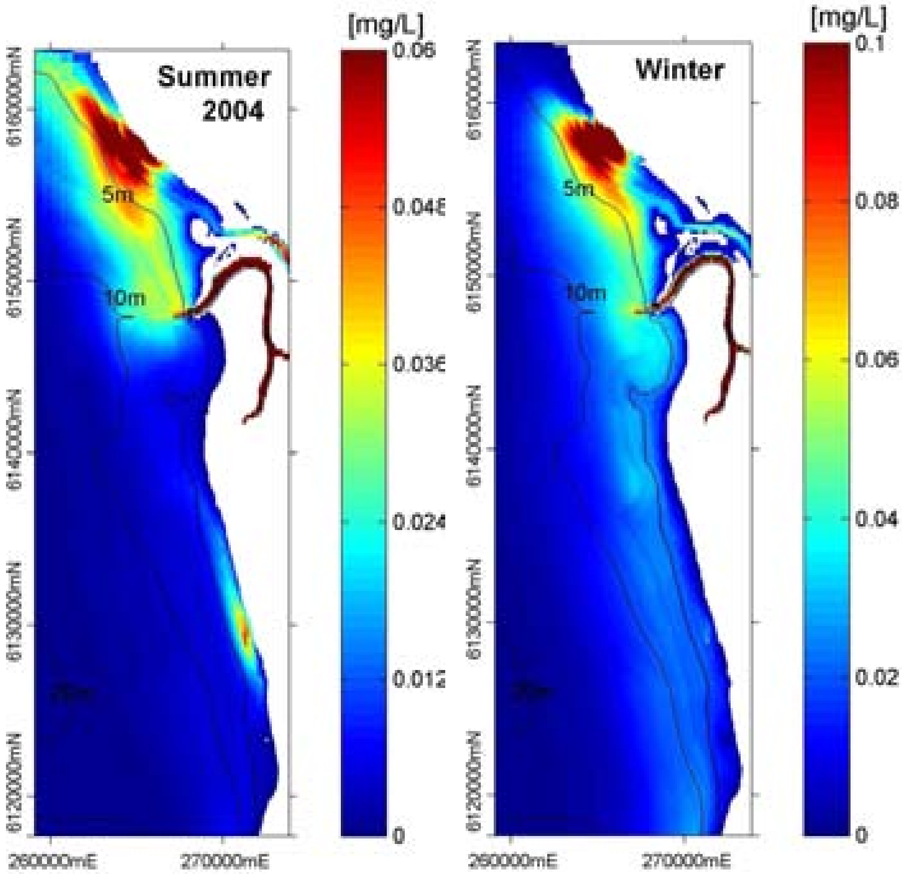

Figure 5.26: Predicted mean phosphorus concentrations for wastewater discharges during 2004.

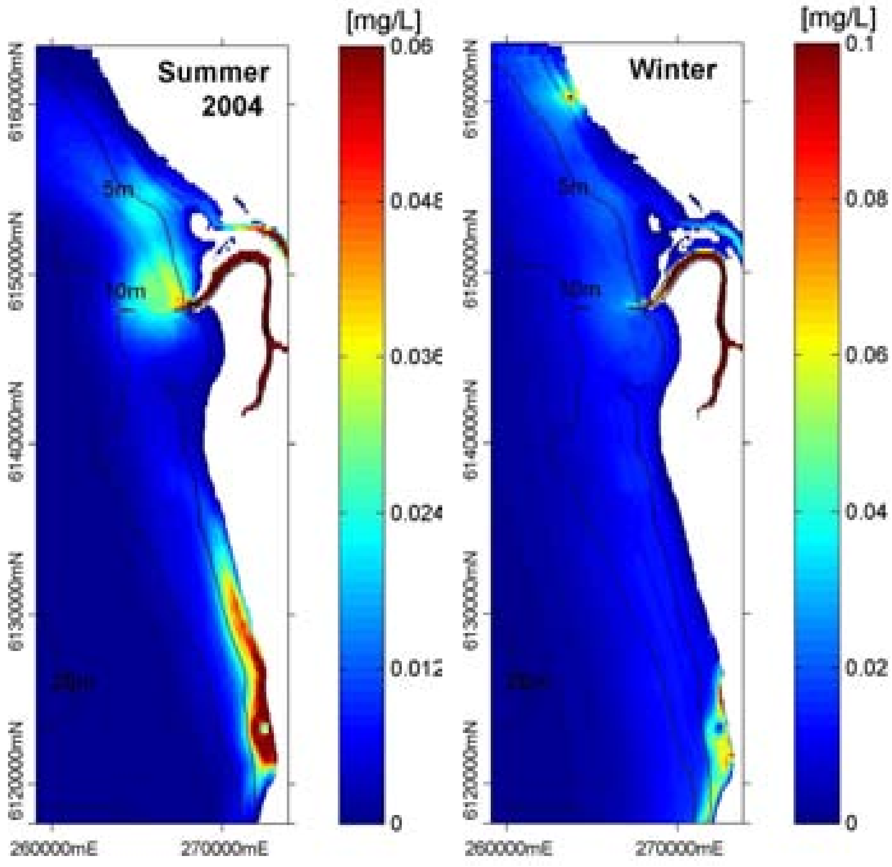

Figure 5.27: Predicted mean phosphorus concentrations for storm water discharges during 2004.

6. Conclusions

The Adelaide Coastal Waters Study (ACWS), a multi-disciplinary study, was developed to examine factors contributing to the loss of more than 4000 hectares of shallow, sub-tidal seagrass along the metropolitan Adelaide coastline since the late 1940s. The objective of the ACWS was to develop knowledge and tools to enable sustainable management of Adelaide's coastal waters by identifying causes of ecosystem modifications and the actions required to halt and reverse the degradation. As part of the ACWS, a numerical modelling system that included three separate modules was developed. In this report, each of the modules were described together with the model validation and results of the model application to the ACWS region to examine the past, present, and future discharge scenarios.

The circulation and wave models were validated with comparison of field data (waves, tides, currents, and aerial imagery) obtained from the study region.

The main conclusions of this study, based on the numerical modelling results, may be summarised as follows:

- The mean annual significant wave height decreased from south to north along the study region; the directions changed from a predominantly westerly direction in the south to south-westerly in the north. The wave climate is relatively energetic, with the wave-induced near bed currents capable of mobilising fine to medium-sized sand most of the time.

- Within the Adelaide coastal waters, tidal currents dominated the circulation pattern and the wind was a secondary effect, which influenced the mean (or net) circulation pattern, particularly at the surface. The current patterns were oriented parallel to the coastline and flowed northward during the flood stage of the tide and southward during the ebb. The seasonally varying wind climate results in a reversal in the mean circulation pattern. In summer, the net movement of water is northward, whereas during winter the direction is reversed towards the south; however, as the southerly and south-westerly winds are stronger and more prevalent, the annual movement of water is northward. In the nearshore zone, because of the dominance of wave-induced currents, the net flow is mainly towards the north.

- An anti-clockwise eddy was present offshore of the Port River mouth during the flood tide. The interaction between the strong outflow from the river and the southward flowing coastal currents were responsible for the generation of the eddy. The numerical model reproduced this eddy, which was previously identified in aerial imagery.

- Numerical modelling of shore-based discharges and ocean outfalls indicated that, in general, because of the predominantly alongshore movement (north-south) of water, the offshore extent was limited to waters where the water depth was < 10 m. Thus the land-based discharges were mainly transported in a north-south direction, parallel to the coastline, with minimal offshore extent.

- The flushing or residence time within the study region, estimated through particle tracking, depended on both location and season. The nearshore waters had higher residence times than those farther offshore. Along the Adelaide metropolitan waters, inshore of the 5 m depth contour, the flushing time can vary between 1 and 10 days depending on weather conditions. The higher limit of the flushing times may be reached under periods of neap (dodge) tides and calm winds. During summer, the mean residence times were lower (up to 1.5 days), whereas during winter the mean residence times were slightly higher (up to 2.5 days).

- The Port River/Barker Inlet system has a major influence on nutrient and suspended sediment concentrations within the study region. This is through a combination of industrial (Penrice), wastewater (Port Adelaide outfall—now discontinued), and stormwater discharges to the system. In summer, the discharges were transported northward from the Port River entrance, whereas during winter there was southerly transport with discernable impact along the Adelaide coastal strip.

- Wastewater discharge from the Bolivar outfall was generally advected northwards (and thus out of the study region) during summer and into Barker Inlet during winter. Discharges from the Bolivar outfall did not appear to have a direct influence on the Adelaide coastal strip.

- The discharges from Glenelg wastewater outfall resulted in a localised increase in suspended sediment and nutrient concentrations.

- The relative importance of stormwater and wastewater (industrial and municipal) discharges depended on the nutrient (nitrogen or phosphorous) and season. During summer, the discharges from wastewater outfalls (which included Penrice) had more influence on the magnitude and extent of SSC concentrations, whereas in winter the stormwater discharges had a larger influence. For nitrogen concentrations, stormwater discharges resulted in higher concentrations during the summer, whereas wastewater discharges were dominant in winter. For phosphorous concentrations, stormwater discharges had higher concentrations along the metropolitan coastal strip during both summer and winter, whereas the wastewater discharge from Bolivar was dominant along the northern section.

References

Battjes, J.A. and Janssen, J.P.F.M. 1978. Energy loss and set-up due to breaking of random waves. *Proc. 16th int. conf. on coastal eng.*, ASCE, 569–587.

Blumberg A., and Mellor, G.L. 1987. A description of a three-dimensional coastal ocean circulation model. In N.S. Heaps (ed.) *Three-dimensional coastal ocean models*, pp. 1–16, American Geophysical Union, Washington, DC.

Bone, Y., Deer, L., Edwards, S. and E. Campbell (2006). *Adelaide Coastal Waters Study Sediment Budget.* ACWS Technical Report No. 16. Prepared for the Adelaide Coastal Waters Study Steering Committee. University of Adelaide, October 2006.

Booij, N., Ris, R.C., Haagsma, I.J.G, Holthuijsen, L.H., Kieftenburg, A.T.M.M., van der Westhuysen, A.J. and Zijlema, M. 2004. *SWAN Cycle III version 40.41 user manual*. Available: http://fluidmechnaics.tudelft.nl/swan.html.

Booij, N., Ris, R.C. and Holthuijsen, L.H. 1999. A third-generation wave model for coastal regions I. Model description and validation. *Journal of Geophysical Research*, 104, 7649–7666.

Bouws, E. and Komen, G.J. 1983. On the balance between growth and dissipation in an extreme depth-limited wind–sea in the southern North Sea. *Journal of Physical Oceanography*, 13, 1653–1658.

Casulli, V. and Cheng, R.T. 1992. Semi-implicit finite difference methods for three-dimensional shallow water flow. *Int. J. Numer. Methods Fluids*, 15, 629–648.

CERC. 2002. *Shore protection manual: part III, chapter 6, Sediment transport outside the surf zone*.

Cobb, M. and Blain, C.A. 2003. A coupled hydrodynamic-wave model for simulating wave and tidally-driven 2D circulation in inlets. In Malcolm L. Spaulding (ed.) *Estuarine and coastal modeling, proceedings of the 7th international conference*, ASCE, Reston, VA, pp. 725–744.

Dingemans, M.W., Radder, A.C. and de Vriend, H.J. 1987. Computation of the driving forces of wave-induced currents. *Coastal Engineering*, 11, 539–563.

Grant, W.D. and Madsen, O.S. 1986. The continental-shelf bottom boundary layer. *Annual Review of Fluid Mechanics*, 18, 265–305.

Grant, W.D. and Madsen, O.S. 1979. Combined wave and current interaction correction for combined wave and current flows. *Journal of Geophysical Research*, 84, 1797–1808.

Grzechnik, M. and Noye, J. 1996. *A tidal model of Gulf St Vincent, South Australia, with fine grid submodels of the Outer Harbor and Port Stanvac regions*. Report TM1. Department of Applied Mathematics, University of Adelaide.

Hodges, B.R., Imberger, J., Saggio, A. and Winters, K. 2000. Modeling basin-scale internal waves in a stratified lake. *Limnol. Oceanogr.*, 45, 1603–1620.

Holthuijsen, L.H., Herman, A. and Booij, N. 2003. Phase-decoupled refraction-diffraction for spectral wave models. *Coastal Engineering*, 49, 291–305.

Kaempf, J. 2006. *In-situ field measurements for Adelaide Coastal Waters Study. Final technical report*. ACWS technical report no. 7 prepared for the Adelaide Coastal Waters Study Steering Committee. School of Chemistry, Physics and Earth Sciences, Flinders University of South Australia, Adelaide.

Laval, B., Imberger, J. and Findikakis, A.N. 2003. Mass transport between a semi-enclosed basin and the ocean: Maracaibo System. *Journal of Geophysical Research (Oceans)*, 108, 3234.

Longuet-Higgins, M.S. and Stewart, R.W. 1964. Radiation stress and mass transport in water waves; a physical discussion, with applications. *Deep-Sea Research*, 11, 529–562.

Madsen, A.J. and Plant, N.G. 2001. Intertidal beach slope predictions compared to field data. *Marine Geology*, 173, 121–139.

Jones, R.A. and Pattiaratchi, C.B. 2005. Nearshore currents and surf zone dispersion on Adelaide metropolitan beaches. *Coasts and Ports "Coastal Living—Living Coast". Proceedings of the 17th Australasian Coastal and Ocean Engineering Conference and the 10th Australasian Port and Harbour Conference*, 20–23 September, Adelaide, South Australia, pp. 625–630.

Petrusevics, P. 2005. *Distribution of suspended matter using SeaWiFS data. Final technical report.* ACWS technical report no. 5 prepared for the Adelaide Coastal Waters Study Steering Committee. Oceanique Perspectives, Adelaide.

Robson, B.J. and Hamilton, D.P. 2004. Three-dimensional modelling of a Microcystis bloom event in the Swan River estuary, Western Australia. *Ecological Modelling* (special issue), 174, 203–222.

SPM (Shore protection manual). 1983. American Army Corps of Engineers.

Spillman, C.M., Imberger, J., Hamilton, D.P., Hipsey, M.H. and Romero, J.R. 2006. Modelling the effects of Po River discharge, internal nutrient cycling and hydrodynamics on biogeochemistry of the Northern Adriatic Sea. Submitted to *Journal of Marine Systems*.

van Rijn, L.C. 1989. *Handbook on sediment transport by current and waves*. Report H461, Delft Hydraulics.

van Rijn, L.C. 1986. Applications of sediment pick-up functions. *Journal of Hydraulic Engineering*, ASCE, 112, 867–874.

van Rijn, L.C. 1984a. Sediment transport, part I: Bed load transport. *Journal of Hydraulic Engineering, ASCE*, 110, 1431–1456.

van Rijn, L.C. 1984b. Sediment transport, part II: Suspended load transport. *Journal of Hydraulic Engineering*, ASCE, 110, 1613–1641.

Wilkinson, J. 2005. *Reconstruction of historical stormwater flows in the Adelaide metropolitan area.* ACWS technical report no. 10 prepared for the Adelaide Coastal Waters Study Steering Committee, September 2005. Department of Environmental Health, Flinders University of SA.

Wilkinson, J., Pearce, M., Cromar, N., and Fallowfield, H. 2003. *Audit of the quality and quantity of treated wastewater discharging from wastewater treatment plants (WWTPs) to the marine environment.* ACWS technical report no.1 prepared for the Adelaide Coastal Waters Study Steering Committee, November 2003. Department of Environmental Health, Flinders University of South Australia.

Yeates, P.S., Dallimore, C.J., Antenucci, J.P. and Imberger, J. 2004. *ELCOM modelling of the Venice Lagoon*, CWR, UWA final report. The University of Western Australia.

Appendix A - Stakeholder issues

As part of the overall study task, several issues were to be addressed by the PPM2 research task, in addition to the numerical modelling task including the field measurements and remotely sensed data analysis (see Section 1); these issues are listed below. Here, only the stakeholder issues that can be addressed directly from the results of this task are addressed.

Stakeholder issue 3.2.1.1
What is the fate of nutrients and what are their respective impacts on receiving marine environment and ecosystem functions?

Nutrients are input into the Adelaide coastal waters through rivers, stormwater drains, and industrial and municipal wastewater treatment outfalls. The results of the modelling, assuming that nutrients behaved conservatively (i.e. no uptake or regeneration due to biological or chemical processes), revealed that because of the hydrodynamic regime, the nutrients remained within the coastal region and were advected north and south, parallel to the coastline. The seasonally varying wind climate results in a reversal in the net circulation pattern and thus the direction of nutrient transport. In summer, the net movement of water due to the action of wind is northwards, whereas during winter, the direction is reversed towards the south; however, as the southerly and south-westerly winds are stronger and more prevalent during the summer, the annual movement of water (and nutrients) is northward. In the nearshore zone, because of the dominance of wave-induced currents, the net flow is towards the north, interspaced by southward movement under strong north to north-westerly winds.

Wastewater discharge from the Bolivar outfall is advected northwards (and thus out of the study region) during summer and into Barker Inlet during winter. Discharges from the Bolivar outfall did not appear to have a direct influence on the Adelaide coastal strip.

The largest nutrient input to the Adelaide coastal waters is through Port River through a combination of industrial (Penrice), wastewater (Port Adelaide outfall—now discontinued), and stormwater discharges. In summer, the discharges were transported northwards from Port River, whereas during winter there was southerly transport. This was confirmed through stable isotope analysis, which identified the Penrice discharges being present along the Adelaide coastal water strip.

The discharges from Glenelg wastewater treatment plant resulted in a localised increase in nutrient concentrations.

Stakeholder issue 3.2.1.3
How does stormwater's contribution to nutrients in the Gulf compare in significance with discharges from the wastewater treatment plants? Is nitrogen the only nutrient input of concern?

The transport of nutrients as a conservative tracer was modelled, with the inputs from stormwater and wastewater treatment plants examined separately. Note that the stormwater inputs included both rivers and stormwater drains, whereas the wastewater included the municipal wastewater outfalls and the Penrice plant. The relative importance of the two types of discharges depended on the nutrient and season. During summer, the discharges from wastewater outfalls (which included Penrice) had more influence on the SSC concentrations, whereas in winter the stormwater discharges had a larger influence. For nitrogen concentration, stormwater discharges had a higher influence during the summer, whereas wastewater discharges were dominant in winter. For phosphorous concentration, stormwater discharges had a higher influence along the metropolitan coastal strip during both summer and winter, whereas the wastewater discharge from Bolivar was dominant in the northern section.

Stakeholder issue 3.2.4.3
What are the interactions with the larger body of water in the Gulf St Vincent and do these have any effect on the coastal waters?

Within the Adelaide coastal waters, tidal currents dominate the circulation and the wind is a secondary effect, which affects the mean circulation pattern, particularly at the surface. The current patterns are oriented parallel to the coastline and flow northwards during the flood stage of the tide and southward during the ebb stage. The seasonally varying wind climate results in a reversal in the mean circulation pattern. In summer, the net movement of water due to the action of wind is northwards, whereas during winter the direction is reversed towards the south; however, as the southerly and south-westerly winds are stronger and more prevalent during the summer, the annual movement of water is northward. In the nearshore zone, because of the dominance of wave-induced currents, the net flow is towards the north. Numerical modelling of the different discharges indicated that, in general, because of the predominantly alongshore movement (north-south) of water, the offshore extent was limited to waters where the water depth was < 10 m (the distance to the 10 m contour ranges from 2 km in the south to 8 km in the north). Petrusevics (2005), through the analysis of satellite data (SeaWiFS), also concluded that the impact of land-based discharges could not be identified a distance of about 2 km offshore in the southern and central region and about 5 km offshore in the northern region of the study region. Thus the land-based discharges are mainly transported in a north-south direction, parallel to the coastline, with minimal offshore extent. The Adelaide coastal waters are dependent on the Gulf St Vincent for hydrodynamic forcing (waves, tides, and the wind-induced circulation). However, as the land-based discharges are limited to the shallow water adjacent to the coastline, there is only a limited influence of the offshore waters in the cross-shore mixing processes.

Stakeholder issue 3.2.7.4
What are the relative impacts of the different outfalls along the coast in terms of assimilative capacity? Are discharges in deeper, fast flowing water less detrimental than those in shallow, slow moving water? Is relocating discharges from Port River to Bolivar a good idea?

The modelling results indicated that, for the study region, the discharges into the Adelaide waters from the Port River/Barker Inlet system had a major influence and that discharges from Bolivar advected northwards (and thus out of the study region) during summer and into Barker Inlet during winter. Discharges from Bolivar did not appear to have a direct influence on the Adelaide coastal strip.

Stakeholder issue 3.2.10.2
Are there any suitable areas for the dumping of dredge spoil within the study area?

This was not specifically modelled. It is possible that deeper regions of the Gulf of St Vincent, where wave influence is minimal, may be suitable, but further studies are required.

Stakeholder issue 3.2.11.2
What will be the likely cumulative impacts of the current and proposed power-generating plants along the Port River? Are there likely to be incremental increases in ambient Port River temperatures and, if so, what effects will these have on algal dynamics and survival of other marine organisms (including undesirable introduced marine pests)?

This was not specifically modelled. The Port River system has strong tidal currents and a clockwise residual circulation system: inflow of water from Barker Inlet and exiting through Port River. This results in the continuous outflow of the thermal discharges into the Adelaide coastal waters. Most likely there are no cumulative effects, except in the immediate vicinity of the outfalls.

The following stakeholder issues, although listed for this task, have already been addressed elsewhere:

3.2.1.2,	3.2.1.4,	3.2.3.2,	3.2.4.1,	3.2.4.2,	3.2.5.1,	3.2.5.2,
3.2.5.3,	3.2.5.4,	3.2.5.7,	3.2.5.13,	3.2.6.5,	3.2.7.7,	3.2.10.1.